Dissertation

submitted to the
Combined Faculties for the Natural Sciences and for Mathematics
of the Ruperto-Carola University of Heidelberg, Germany
for the degree of
Doctor of Natural Sciences

presented by

Diplom-Biologe Malte Wittmann

born in: Braunschweig

Oral examination: .....

Title

Synaptic and extrasynaptic NMDA receptors in hippocampal neurons: regulation of nuclear shape and cell fate

Referees: Prof. Dr. Hilmar Bading

Prof. Dr. Christoph Schuster

Acknowledgements

I would like to thank my referee Professor Hilmar Bading for the opportunity to prepare my PhD thesis in his laboratory. I am very grateful for the many ideas and discussions we had and his supervision throughout the projects.

I would further like to thank my second referee Professor Christoph Schuster for his good advice and the discussions we had.

Many thanks to Gillian Queisser for his wonderful 3D reconstructions and mathematical calculations.

Many thanks to Andrea Helwig for the sharp electron microscopic images.

Further I would like to thank C. Peter Bengtson and Simon Wiegert for carrying out the electrophysiological recordings as well as Frank Hofmann for recordings on Multi Electrode Arrays.

Many thanks to Ruth Jelinek for general support in the lab and assistance during biochemical experiments.

I would also like to thank Matthias Klugmann for the brain sections as well as the lively discussions and technical advice.

Thanks to all other members of the Bading laboratory for close interactions, support and the friendly atmosphere created.

Special thanks to the Boehringer Ingelheim Fonds (B.I.F.) for the generous financial support granted for the thesis

1. Summary

Neuronal activity induces processes important for memory formation and cell survival by inducing calcium influx through synaptic NMDA receptors. Calcium subsequently activates the ERK-MAP kinase cascades that transmits the signal from the synapse to the nucleus. A second mode for synapse-to-nucleus communication involves a propagating calcium signal that invades the cell nucleus. Nuclear calcium is a key regulator of gene expression mediated by the transcription factor CREB. The nuclear architecture contains intranuclear structures that have been shown to facilitate calcium influx into the nucleus.

This thesis describes a novel mechanism in which calcium influx through NMDA receptors induces morphological changes in the majority of hippocampal neurons by forming infoldings of the nuclear membrane. These infoldings are generated by an increase in the surface area of the nuclear membrane and require activation of the ERK-MAP kinase cascade as well as a nuclear calcium signal. Infoldings are formed rapidly within one hour and can be reversed by silencing of synaptic activity. The stability of infoldings increases within days after activation of synaptic NMDA receptors, suggesting the involvement of gene transcription in the stabilization process.

Synaptic activity is counteracted by overactivation of extrasynaptic NMDA receptors. Calcium influx through these receptors leads to a rapid loss of nuclear infoldings. It also activates pathways leading to the shut-off of CREB and to cell death. I attempted to dissect the intracellular pathways downstream of synaptic and extrasynaptic NMDA receptors by designing a specific antagonist for extrasynaptic NMDA receptors. This should be achieved by coupling of Conantokin-G, a peptide antagonist against the NR2B subunit of NMDA receptors, to beads of a specific size. The peptide coupled to beads should allow blockade of extrasynaptic NMDA receptors and thereby block cell death pathways, leaving synaptic NMDA receptors unaffected.

2. Zusammenfassung

Synaptische und extrasynaptische NMDA Rezeptoren in Neuronen des Hippokampus: Regulierung der Kernform und des Zellschicksals

Neuronale Aktivität induziert durch Kalzium-Einstrom durch synaptische NMDA Rezeptoren intrazelluläre Prozesse die bei der Gedächtnisbildung und für das Überleben der Zelle eine entscheidende Rolle spielen. Das einströmende Kalzium aktiviert die ERK-MAP Kinase Kaskade die das Signal von der Synapse zum Kern weiterleitet. Eine zweiter Weg der Kommunikation von der Synapse zum Kern besteht in einem Kalziumsignal, das in den Zellkern eindringt. Kernkalzium ist ein zentraler Regulator der Genexpression die durch den Transkriptionsfaktor CREB gesteuert wird. Die Architektur des Zellkerns weist Strukturen im Inneren auf, die mit dem Kalzium-Einstrom in den Kern in Zusammenhang stehen.

Diese Dissertation beschreibt einen neuen Mechanismus, bei dem in der Mehrzahl der Neuronen des Hippokampus durch Kalzium-Einstrom durch NMDA Rezeptoren morphologische Veränderungen in Form von Einfaltungen der Kernmembran induziert werden. Diese Einfaltungen werden durch eine Vergrößerung der Membranoberfläche erzeugt, wozu sowohl die Aktivierung der ERK-MAP Kinasekaskade als auch ein nukleäres Kalziumsignal nötig sind. Diese Einfaltungen werden innerhalb einer Stunde gebildet und können durch Ausschalten der synaptischen Aktivität rückgängig gemacht werden. Die Stabilität der Einfaltungen nimmt innerhalb mehrerer Tage nach Aktivierung der synaptischen NMDA Rezeptoren zu, was auf eine Beteiligung von Gentranskription am Prozess der Stabilisierung schließen läßt.

Der Funktion synaptischer NMDA Rezeptoren wird durch eine Überaktivierung extrasynaptischer NMDA Rezeptoren entgegengewirkt. Kalzium-Einstrom durch diese Rezeptoren führt zu einem schnellen Verschwinden von Kerneinfaltungen. Außerdem aktiviert der Einstrom intrazelluläre Signalkaskaden die zum Ausschalten von CREB und zum Zelltod führen. Beschrieben wird hier zusätzlich der Versuch, diese intrazellulären Kaskaden, die durch synaptische und extrasynaptische NMDA Rezeptoren gesteuert werden, durch die Entwicklung eines spezifischen Antagonisten für extrasynaptische NMDA Rezeptoren zu analysieren. Dies sollte durch die Kopplung von Conantokin-G, einem Peptid das antagonistisch gegen die NR2B Untereinheit des

NMDA Rezeptors wirkt, an Beads einer spezifischen Größe erreicht werden. Dieses an Beads gekoppelte Peptid sollte zu einer Inaktivierung der extrasynaptischen NMDA Rezeptoren und somit zur Blockade von Zelltod-Kaskaden führen, ohne die Funktion der synaptischen NMDA Rezeptoren zu beeinträchtigen.

3. Introduction

3.1. Nuclear lamina

The human nucleus is approximately 10 μm in diameter and organizes 1m of chromosomal DNA. It is surrounded by the nuclear envelope consisting of two membranes, each being about 7 nm thick. The envelope is fenestrated by numerous circular pores, which are about 90 nm in diameter. Between the inner nuclear membrane and chromatin exists a proteinaceous layer called the nuclear lamina (Fawcett, 1966). The lamina network of polymeric filaments consists of lamin proteins and associated binding proteins.

The lamins were originally supposed to support the stability of the nuclear envelope and provide anchorage sites for chromatin. Recent evidence suggests that lamins are involved in a number of functions, including nuclear envelope assembly, DNA synthesis, transcription and apoptosis.

Two groups of proteins interact with lamins: integral proteins of the inner nuclear membrane and proteins that are not integral membrane components but are concentrated in the area of the nuclear lamina (Goldman et al., 2002).

Lamins also form nucleoplasmic structures as shown by immunoelectron microscopy (Hozak et al., 1995) and can appear as distinct foci or as a veil that fills the nucleoplasm (Liu et al., 2000; Moir et al., 2000a). During interphase lamins are continously incorporated into the nuclear lamina, especially during growth phase in G1, indicating a role in nuclear growth (Yang et al., 1997b). In G1 phase of cycling cells photobleached regions of the lamina recovers within 2 h (Moir et al., 2000a), while in non-cycling G0 cells little recovery was observed even after 45 h (Daigle et al., 2001).

In addition to their stabilizing function, nuclear lamins and lamin-associated proteins contain nuclear binding domains, suggesting an involvement in chromatin organization. During S phase of dividing cells they colocalize with PCNA, an elongation factor required during DNA replication, at sites of nucleotide incorporation (Moir et al., 2000b; Wilson et al., 2001). In vitro lamins directly bind chromatin (Taniura et al., 1995) and DNA sequences known as matrix-attachment regions (MARs) and scaffold-attachment regions (SARs) (Luderus et al., 1992; Zhao et al., 1996).

The observation that the lamina binds regions of chromatin led to the suggestion that it might be involved in the regulation of transcription (Moir et al., 1995). In Xenopus an

increase of lamin B1 during the mid-blastula transition coincides with the induction of RNA polymerase II-dependent transcriptional activity (Benavente et al., 1985; Stick and Hausen, 1985). In BHK21 cells the disruption of normal lamin organization with a dominant negative lamin mutant inhibits RNA polymerase II activity (Spann et al., 2002). Furthermore, a lamin-binding protein, lamin-associated protein 2B, has been reported to mediate transcriptional repression (Nili et al., 2001).

3.1.1. Lamins and apoptosis

During apoptosis lamins are cleaved by caspases (Lazebnik et al., 1995; Takahashi et al., 1996) and the nuclear lamins were among of the first proteins identified as caspase targets. The cleavage of lamins during apoptosis might serve to disassemble the nuclear lamina, thereby shutting down vital nuclear processes. Expression of a caspase-uncleavable mutant and subsequent induction of apoptosis resulted in slower progression of apoptosis, including slower nuclear shrinkage and chromatin condensation (Rao et al., 1996).

Certain viruses like HIV-1 possess a preintegration complex that probably enters the nucleus by expression of a protein called Vpr, which induces blebs in the nuclear envelope (de Noronha et al., 2001). These cells arrest in the G2, allowing extended periods of viral transcription. The nuclear lamina is locally disassembled and the blebs frequently burst, allowing inflow of cytoplasmic constituents and resealing within short time periods. These transient openings suggest a direct link between viral proteins and nuclear lamins.

3.1.2. Nuclear morphology

The typical cell nucleus is commonly described as being spherical, ellipsoidal or polyhedral with rounded edges, but many neurons do actually have nuclei with a more complex shape. For example, in Purkinje cells the nucleus nearly always has deep folds on its external aspect facing the origin of the main stem dendrite and deep folds have also been reported in nuclei of the visual cortex of primates (Chan-Palay et al., 1974).

Extensions of the intranuclear membrane into the nucleus were reported previously and have been described as invaginations of both single and double membranes (Bourgeois et al., 1979; Stevens and Trogadis, 1986). Some of the intranuclear membrane channels are derived from the ER and form deep, narrow and branching invaginations of both

membranes of the nuclear envelope and can undergo dynamic changes in morphology in Hela cells over a time scale of 35 minutes (Fricker et al., 1997). This distinguishes these channels from the structures observed in Drosophila nuclei, which are invaginating only from the inner nuclear membrane to produce a continous structure with the ER (Hochstrasser and Sedat, 1987). Furthermore, these invaginations are filled with electron-dense granules and are associated with an adjacent double membrane evagination into the cytoplasm (Park and De Boni, 1992), which distinguishes them from those seen in mammalian cells. Double-membrane invaginations in plant cells (Dickinson and Bell, 1972) are developmentally restricted to a short interval in gymnosperm microspores and are very short and numerous, as well as composed of membranes devoid of nuclear pores (Li and Dickinson, 1987). Recently, a nucleoplasmic reticulum was described in epithelial cells that serves as a calcium store from which nuclear calcium signals can be evoked after local uncaging of inositol 1,4,5-trisphosphate (Echevarria et al., 2003). The proliferation of this nucleoplasmic reticulum has been reported to be regulated by CTP:phosphocholine cytidylyltransferase-α (CCTα) in CHO cells (Lagace 2005). CCT-α is a nuclear enzyme that translocates to the nuclear envelope upon various stimuli, including fatty acids (Wang et al., 1993), phosphatidylcholine degradation and by PLC (Watkins and Kent, 1992) and isoprenoids (Lagace et al., 2002).

3.1.3. Lamins in genetic deseases

Several genetic deseases exist that are caused by mutations in lamin genes and that lead to severe alterations in the stability and shape of the cell nucleus. These changes have a major impact on the organization of the components of the nuclear envelope and can impair processes like gene transcription and survival.

Mutations in the lamin A gene have been shown to lead to laminopathies and result in increased fragility and disorganization of the nuclear envelope (Vigouroux et al., 2001). Hutchison-Gilford progeria syndrome (HGPS) is a premature aging disorder caused by a point mutation in the lamin A gene that leads to constitutive activation of a cryptic splice site and results in a truncated gain-of-function isoform of lamin A. It is associated with significant changes in nuclear shape and an abnormally thick lamina (Goldman et al., 2004). Nuclear pore complexes show an abnormal distribution in late passages of fibroblasts of HGPS patients which correlates with the idea that lamins anchor nuclear pores by binding to NUP153 (Smythe et al., 2000). Just recently the mutation in the

lamin A gene that causes HGPS has been shown to be involved in normal physiological aging leading to morphological defects similar to those of HGPS patients. Blockade of the cryptic splice site by antisense oligonucleotides in cells of old individuals reversed the age-related nuclear defects (Scaffidi and Misteli, 2006).

Mice in which the lamin A gene has been knocked out appear normal at birth but exhibit an abnormal gait after 3 to 4 weeks, leading to death by week 8. These mice suffer from skeletal and cardiac muscle wasting and loss of white fat. Cultured fibroblasts show abnormal nuclear blebs with significantly reduced levels of lamins, LAP2 and the nuclear pore component NUP153. Furthermore the membrane in the blebbed regions does not colocalize with condensed heterochromatin (Sullivan et al., 1999).

A major finding of this thesis is the regulation of nuclear infoldings by NMDA receptors. It turned out that there were striking differences of the effects mediated by synaptic and extrasynaptic NMDA receptors on nuclear infoldings, a phenomenon that has been described for the induction of survival and death pathways before (Hardingham et al., 2002).

3.2. The Involvement of NMDA Receptors in Neuron Death

NMDA receptor antagonists have long been known to reduce the early phase of post-ischemic neuron death in rats (Simon et al., 1984; Minematsu et al., 1993b; Minematsu et al., 1993a). Brain ischemia causes elevated glutamate levels in the extracellular space (Benveniste et al., 1984; Stoffel et al., 2002) largely due to the reverse function of glutamate transporters (Rossi et al., 2000). Ischemia can also cause astrocyte dysfunction, necrosis and apoptosis, compromising the neuroprotective buffering of glutamate via the astrocyte specific glutamate transporter, GLT-1, and the conversion of glutamate to inactive glutamine in glial cells (Tanaka et al., 1997; Schubert et al., 2000; Chen and Swanson, 2003; Takuma et al., 2004). Excess extracellular glutamate and the resultant stimulation of ionotropic glutamate receptors is believed to be involved in subsequent excitotoxicity and active cell death (commonly termed apoptosis) leading to a penumbra of secondary neuron loss surrounding the focal lesion site (Lipton, 1999a; Bramlett and Dietrich, 2004).

Intervention with alpha-amino-3-hydroxy-5-methyl-4-isoxazolepropionic acid (AMPA) or NMDA receptor antagonists is problematic because they also block normal and vital glutamate-mediated neurotransmission between non-injured neurons, inducing behavioral (psychotomimetic) side-effects, sedation, and amnesia (Morris, 1989; Davis et al., 1997; Lees, 2000; Ikonomidou and Turski, 2002). More importantly, NMDA receptor antagonists are known to induce or exacerbate apoptosis and neurotoxicity (Brenneman et al., 1990; Ciani et al., 1997; Ikonomidou et al., 1999; Ikonomidou et al., 2000; Snider et al., 2002; Low and Roland, 2004). This cell death caused by NMDA receptor antagonists may be due to the inhibition of cell survival pathways (Hardingham et al., 2002; Yoon et al., 2003).

NMDA receptors have not been abandoned, however, in current clinical strategies against excitotoxicity as evidenced by the recent approval in the USA of memantine, an NMDA open channel blocker, for the treatment of advanced Alzheimer's disease (Farlow, 2004). More specific and efficacious pharmaceutical tools are needed, however, to prevent second-stage damage following stroke, to dampen glutamate-mediated excitation in epilepsy, and to interfere with the complex biochemical pathways that lead to cell death in certain neurodegenerative diseases including Alzheimer's disease, Huntington disease and AIDS (Lipton and Rosenberg, 1994; Lancelot et al., 1998; Kaul et al., 2001). Selective intervention in the role of NMDA receptors in these pathologies must distinguish between the aspects of NMDA receptors mediating neurotoxicity and those which protect against it.

3.2.1. NMDA receptor overview

NMDA receptors are glutamate-gated cation channels whose activation contributes to depolarization by allowing sodium and calcium influx. The presence of both NR1 and NR2 subunits are required to form functional channels due to the presence of the glutamate binding domain at their junction. Four distinct subtypes (NR2A-D) of the NR2 subunit exist. A binding site for glycine is found on the NR1 subunit while the NR2B subunit possesses a polyamine binding site where regulatory molecules can modulate the activity of the NMDA receptor.

At resting membrane potentials, NMDA receptors are normally inactive due to a voltage-dependent block of the channel pore by magnesium ions. Activation of the NMDA channel occurs during simultaneous depolarization of the post-synaptic cell and

the binding of glutamate and glycine. Bursting activity in a presynaptic glutamatergic cell can satisfy these conditions through co-activation of postsynaptic excitatory AMPA receptors. Alternatively, accumulation of extracellular glutamate following ischemia is expected to activate both synaptic and extrasynaptic NMDA receptors.

NMDA and other glutamate receptors cluster together in dendritic spines where they mediate synaptic transmission, with an adaptive nature evident in long-term potentiation (LTP) or long-term depression (LTD) involved in memory formation and learning (Bear and Malenka, 1994; Paulsen and Sejnowski, 2000). NMDA receptors are also found at extrasynaptic sites (Rosenmund et al., 1995; Clark et al., 1997; Rao and Craig, 1997; Rao et al., 1998; Tovar and Westbrook, 2002). NMDA receptor clusters have been detected colocalized (ie. synaptic) and non-colocalized (ie. extrasynaptic) with presynaptic markers using immunocytochemical methods in hippocampal and cortical neurons (Aoki et al., 1994; Liao et al., 1999; Pickard et al., 2000).

The distinguishing features responsible for the striking differences in the biological responses induced by extrasynaptic and synaptic NMDA receptors remain unclear. NMDA receptor activation in both cases leads to a calcium influx into post-synaptic cells, a signal crucial for the induction of NMDA-receptor dependent plasticity and learning on the one hand and excitotoxic cell death on the other (Bading, 2000; Hardingham and Bading, 2003). Such contrasting actions of NMDA receptors may be due to differences in the downstream signaling complexes linked to synaptic and extrasynaptic NMDA receptors.

3.2.2. The Prevalence of NR2B Subunits in Extrasynaptic NMDA Receptors

The subunit composition of NMDA receptors varies with their location. While NR2A containing receptors are predominantly confined to synapses, NR2B containing receptors are preferentially distributed extrasynaptically in rats (Charton et al., 1999; Tovar and Westbrook, 1999; Lopez de Armentia and Sah, 2003). Current evidence indicates that native NR2C subunit containing receptors are only present in cerebellum and NR2D containing receptors are not present within synapses in the brain (Momiyama et al., 1996; Cull-Candy et al., 1998; Cull-Candy et al., 2001; Brickley et al., 2003).

Electrophysiological evidence using NR2B selective antagonists and the kinetic characteristics of NMDA receptor currents has indicated that NR2B and not NR2A-containing receptors dominate NMDA receptor mediated synaptic transmission in young rats. However, as NR2A mRNA expression begins from around postnatal day 7, they begin contributing to, and by postnatal day 30, dominating synaptic NMDA currents. This developmental regulation of NR2 subunit distribution is qualitatively common to most brain regions examined to date including the hippocampus, cortex, cerebellum and lateral (but not central) amygdala (Monyer et al., 1994; Zhong et al., 1995; Flint et al., 1997; Stocca and Vicini, 1998; Lopez de Armentia and Sah, 2003). Immunohistochemical and electrophysiological evidence has shown a similar redistribution of NR2 containing receptors also occurs during the second and third weeks in cultured cortical neurons (Li et al., 1998; Tovar and Westbrook, 1999). This development of NR2A and NR2B subunit distribution parallels the contribution of each receptor subtype to LTP induction (Kohr et al., 2003) and to the emergence of synchronous neuronal activity in cortical cultures (Opitz et al., 2002).

3.2.3. NR2B-containing Receptors and Neuronal Death

Although NMDA receptor antagonists are known to induce neuronal apoptosis, antagonists selective for NR2B subunit containing receptors provide a degree of neuroprotection against cell death in ischemic and glutamate excitotoxicity models (Reyes et al., 1998; Williams et al., 2003; Kundrotiene et al., 2004). NMDA-induced apoptotic cell death appears to increase in cells transfected with mutant huntington and the NR1/NR2B but not the NR1/NR2A subunits (Zeron et al., 2001). In line with this evidence, NR2B subunits are highly expressed in medium spiny neurons of the striatum, the neuronal population selectively lost in Huntington disease. Not surprisingly, a potential therapeutic role of NR2B antagonists is currently emerging (Chazot, 2004).
It remains unclear whether the involvement of NR2B-containing NMDA receptors in neuron death relates to their localization, conductance characteristics or intracellular signaling mechanisms. NR2B-containing receptors have higher calcium permeability than NR2A (Dingledine et al., 1999), show less desensitization (Krupp et al., 1996) and produce slower post-synaptic potentials (Carmignoto and Vicini, 1992; Flint et al., 1997; Vicini et al., 1998) than NR2A-containing receptors. The deactivation time constant for currents mediated by NR1/NR2A assemblies comprises tens of milliseconds, compared to hundreds of milliseconds for NR1/NR2B and several

seconds for NR1/NR2D receptors (Monyer et al., 1994; Vicini et al., 1998; Wyllie et al., 1998; Cull-Candy et al., 2001). Thus the activation of NR2B-containing receptors will carry substantially more calcium into the neuron than would the activation of NR2A-containing receptors. Increased calcium entry via predominantly extrasynaptic NR2B-containing receptors may generate high calcium concentrations in specific micro-domains that may initiate death processes.

3.2.4. Extrasynaptic NMDA receptor activation leads to death

Several conditions including the exposure of neurons to hypoxic/low glucose media or the stimulation of extrasynaptic NMDA receptors with bath-applied glutamate causes rapid CREB dephosphorylation of its activator site serine 133 (Hardingham and Bading, 2002). A similar CREB dephosphorylation has also been observed following stroke *in vivo* (Tanaka et al., 1999; Walton and Dragunow, 2000). One possible mechanism through which extrasynaptic NMDA receptors lead to CREB-shut off involves direct interaction with HDAC1 (histone deacetylase 1, a class I HDAC), and protein phosphatase 1 (PP1) (Canettieri et al., 2003). PP1 is also part of a signaling complex consisting of Yotiao, a scaffolding protein beneath the NMDA receptor, and PKA (protein kinase A), that is involved in regulating NMDA receptor activity (Westphal et al., 1999). Although direct evidence for PP1-induced cell death exists, blockade of PP1 has also been shown to promote cell death *in vitro (Jiang et al., 2000)*. This points to a complex role of PP1 the precise action of which may depend on cofactors and the association with particular signaling complexes.

3.2.5. Signaling cascades regulating survival and death

Calcium influx through NMDA receptors can trigger LTP or LTD of synaptic connections, and can send signals to the nucleus to activate gene expression (Bading et al., 1993; Bito et al., 1996; Hardingham et al., 1997; Hardingham et al., 1999; Malenka and Nicoll, 1999; Fink and Meyer, 2002). These processes are thought to play a role in memory and learning as well as promoting cell survival (Figure 1). Calcium acts as a second messenger to induce post-translational modifications including the activation of calcium calmodulin-dependent (CaM) kinases and the Ras–extracellular signal-regulated protein kinases (Ras-ERK1/2) pathway which phosphorylate and inactivate the pro-apoptotic protein BAD (Yano et al., 1998; Bonni et al., 1999). ERK1/2 activation is linked to both survival (Hetman and Gozdz, 2004) and death pathway

activation (Chu et al., 2004). Synaptic NMDA receptor activation *in vivo* also results in the transcription of several immediate early genes (Cole et al., 1989; Wisden et al., 1990; Schulz et al., 1999; Cammarota et al., 2000) many of which are controlled, at least in part, by the transcription factor cAMP-response element- binding-protein (CREB).

3.2.6. CREB: A Calcium Regulated Transcription Factor

Synaptic NMDA receptor-mediated calcium signals activate DNA regulatory elements including the serum response element (SRE), which functions as a cytoplasmic calcium response element, and the cAMP responsive element (CRE) which responds to nuclear calcium signals (Hardingham et al., 1997). The CRE interacts with CREB to regulate the expression of several genes including brain-derived neurotrophic factor (BDNF) involved in cell survival (Ghosh et al., 1994; Bonni et al., 1999; Finkbeiner, 2000; Hardingham et al., 2002; Lonze et al., 2002; Mantamadiotis et al., 2002). Mice lacking CREB and its relative, the cAMP response-element modulator (CREM), show extensive neuronal apoptosis and progressive neurodegeneration (Mantamadiotis et al., 2002). CREB may also be important for long-term synaptic plasticity, learning and memory (Cho et al., 1998; Barco et al., 2002).

There are two principal calcium signaling pathways which can lead to CREB phosphorylation at its activator site, serine 133 (Figure 2). One pathway involves the propagation of a calcium signal from the synapse to the nucleus. Nuclear calcium then activates a calcium-calmodulin (CaM) kinase IV, a potent CREB kinase (Finkbeiner and Greenberg, 1996; Hardingham et al., 2001a) . The second signaling pathway is slower and involves ERK1/2 and RSK2 activation (Bading and Greenberg, 1991; Bading et al., 1993; Ginty et al., 1993; Hardingham et al., 1999; Hardingham et al., 2001b; Impey and Goodman, 2001; Wu et al., 2001).

ERK1/2 is therefore shuttling to the nucleus to phosphorylate RSK2. The nuclear accumulation of ERKs is regulated by nuclear anchoring proteins, whose synthesis is regulated by the ERK1/2 pathway. DUSP5 (hVH-3/B23), an inducible nuclear phosphatase, has been proposed as a candidate for the inducible nuclear anchor of ERK1/2 (Mandl et al., 2005). Nuclear export of ERK1/2 is regulated in a MEK1/2 dependent manner, which transiently shuttles from the cytoplasm to the nucleus and exports ERK1/2 to the cytoplasm (Adachi et al., 2000).

Sef (similar expression of fgf genes) is induced downstream of Ras/MAPK signaling and acts as a negative regulator for Ras/MAPK (Furthauer et al., 2002; Kovalenko et al., 2003; Xiong et al., 2003; Preger et al., 2004). Spatial regulation of Ras/MAPK is controlled by Sef by binding the ERK/MEK complex and preventing dissociation of ERK1/2 from MEK and nuclear translocation of ERK1/2 without inhibiting its activity in the cytosol (Torii et al., 2004). Consequently, the phosphorylation of nuclear targets like Elk-1 is inhibited by presence of Sef while the activation of cytoplasmic targets like RSK2 is not impaired. A cytoplasmic hold of activated ERK1/2 is also observed during differentiation of embryonic carcinoma cells, where ERK1/2 activity is uncoupled from activation of Elk-1, while phosphorylation of RSK is not changed during differentiation (Smith et al., 2004).

Therefore it is believed that the spatial regulation of activated ERK1/2 plays an essential role in developmental processes.

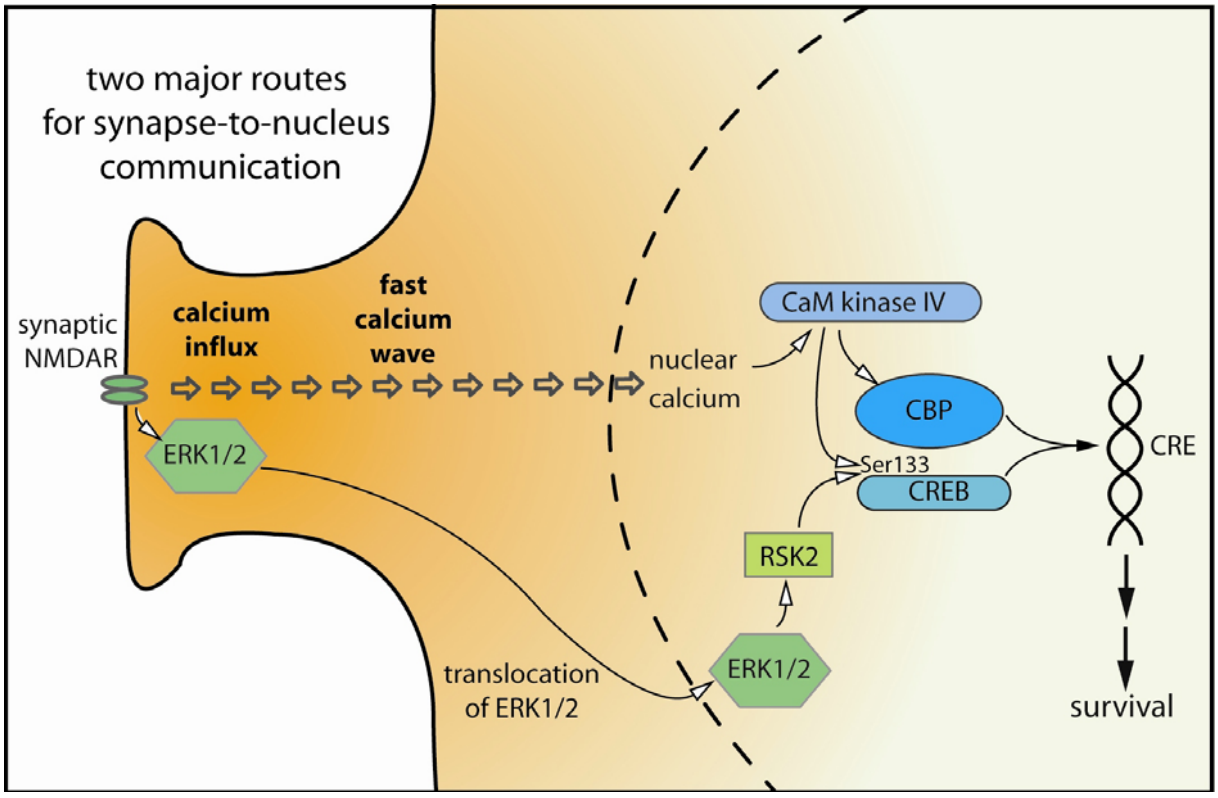

(Wittmann et al., 2004)

Figure 1. Synaptic NMDA receptors signal to the nucleus to regulate neuronal survival via two major communication routes: a fast propagating calcium transient and a somewhat slower transduction mechanism involving ERK1/2 that translocate to the nucleus following their activation by calcium signals in the immediate vicinity of synaptic NMDA receptors (Hardingham et al., 2001a). Nuclear calcium activates CaM kinase IV, which leads to phosphorylation of CREB on Ser133, activation of CBP, and stimulation of CREB/CBP-mediated transcription (Hardingham et al., 1997; Chawla et al., 1998; Impey et al., 2002). ERK1/2 stimulate RSK2 (ribosomal S6 kinase 2) that can phosphorylate CREB on serine 133. The ERK1/2-RSK2 cascade is not sufficient for inducing CREB-dependent gene transcription, however, it can prolong CREB phosphorylation on serine 133 and thus serves as an auxiliary CREB activity-promoting pathway.

3.2.7. MAP kinases and cell death

Many of the effects of NMDA receptor activation on gene transcription, survival and death are mediated by protein kinases including CaM kinases, ERK1/2 and the p38 MAP kinase (Figure 3). The ERK1/2-pathway as well as the JNK (c-Jun N-terminal kinase) pathway have been shown to mediate pro-survival events (Xia et al., 1995; Dougherty et al., 2002; Li et al., 2003), while the induction of apoptosis correlated with the activation of the p38 MAP kinase (Xia et al., 1995; Kawasaki et al., 1997; Cheng et al., 2001). ERK1/2 may achieve this by phosphorylating and inactivating the pro-apoptotic factor BAD (Jin et al., 2002), while JNK phosphorylates Bcl-2 (Deng et al., 2001), which is able to inhibit efflux of cytochrome C from mitochondria, thereby preventing apoptosis (Yang et al., 1997a). The actions of ERK1/2 on survival/death, however, remain controversial. Evidence from animal models indicates that the ERK1/2 pathway is activated during focal cerebral ischemia and that its pharmacological blockade could significantly reduce the focal infarct volume following a transient middle cerebral artery occlusion (Alessandrini et al., 1999; Mori et al., 2002). There is evidence for the involvement p38 MAP kinase in apoptosis (Xia et al., 1995; Bossy-Wetzel et al., 2004; Cao et al., 2004). Apoptosis could be attenuated in a dose-dependent manner in cerebellar granule neurons using the p38 MAP kinase inhibitors SB203580 and PD169316 (Nath et al., 2001). P38 MAP kinase is a downstream target of Fas-mediated apoptosis in cerebellar granule neurons (Hou et al., 2002) and is capable of activating nuclear factors, including the pro-apoptotic factor Rb (Wang et al., 1999b). Hyper-phosphorylation of Rb leads to dissociation from E2F1, a potent activator of apoptosis (Hou et al., 2000; O'Hare et al., 2000; Hou et al., 2001). P38 MAP kinase is also activated in response to neuronal stresses like glutamate toxicity (Kawasaki et al., 1997) and cerebral ischemia (Sugino et al., 2000; Barone et al., 2001).

3.2.8. The “Source Specificity” vs “Calcium Load” Hypotheses

Although calcium influx clearly is an initiator of neurotoxicity, conflict exists as to the dependence of toxicity on a particular route of entry (the “source specificity” model) or whether the calcium source is irrelevant and toxicity relates simply to the intracellular calcium concentration (the “calcium load” hypothesis) (Eimerl and Schramm, 1994; Lu et al., 1996). The degree of cell death evoked by persistent glutamate or NMDA application is clearly related to the duration and concentration of intracellular calcium

increases and the overload of mitochondria and their release of pro-apoptotic proteins such as cytochrome C (Hartley et al., 1993; Lu et al., 1996; Luetjens et al., 2000; Pivovarova et al., 2004). However equivalent calcium loads through L-type calcium channels are not (or much less) toxic (Tymianski et al., 1993; Sattler et al., 1998; Hardingham and Bading, 2003). Furthermore, calcium influx evoked by intense activation of synaptic NMDA receptors *in vitro* is not toxic whereas similar calcium loads following extrasynaptic NMDA receptor stimulation promote breakdown of the mitochondrial membrane potential and cell death (Hardingham et al., 2002).

3.2.9. Mitochondria

The close relationship between NMDA receptors and mitochondria has been proposed to explain the source specificity model (Peng and Greenamyre, 1998). Calcium entry through NMDA receptors is more rapidly absorbed by mitochondria than calcium entry from kainate activated or voltage dependent channels (Peng and Greenamyre, 1998) and has a lower threshold than that of L-type calcium channels for inducing mitochondrial depolarization (Keelan et al., 1999).

Mitochondria are closely linked to neurotoxicity (Nicholls and Budd, 2000). Focal ischemic lesions *in vivo* are associated with calcium dysregulation and mitochondrial collapse (Dirnagl et al., 1999) and the inhibition of mitochondrial calcium uptake greatly attenuates glutamate-induced cell death (Stout et al., 1998). Calcium entering the cell through NMDA receptors is absorbed by mitochondria through a uniporter whose function depends on the mitochondrial membrane potential. Collapse of this potential results in calcium and cytochrome C release, production of superoxides and finally cell death (Luetjens et al., 2000). Cell viability is also critically dependent on mitochondrial respiration and maintenance of glucose levels, achieved by glucokinase, which is regulated by BAD, and dephosphorylation of BAD during glucose-deprivation induces BAD-dependent cell death (Danial et al., 2003). BAD is also dephosphorylated by calcineurin (protein phosphatase 2B) after glutamate-induced calcium influx (Wang et al., 1999a).

3.2.10. PSD-95 and the Coupling of NMDA Receptors to Mitochondria and nNOS Production

NMDA receptors couple directly via their intracellular carboxyl terminus of either the NR1 or NR2 subunits to large complexes of cytoplasmic proteins including scaffolding, adaptor, cell adhesion and cytoskeletal proteins, as well as components of signal transduction pathways, some of which are calcium regulated (Pawson and Scott, 1997; Husi et al., 2000; Sheng and Pak, 2000). A structure in the postsynaptic membrane called the postsynaptic density (PSD) binds several scaffolding proteins including PSD-95, thereby linking NMDA receptors to signaling molecules important for synaptic plasticity (Migaud et al., 1998; Sheng and Kim, 2002). PSD-95 also links NMDA receptors to nitric oxide (NO) production that plays a role in NMDA-induced excitotoxicity (Sattler et al., 1999). The toxic effects of NMDA receptor activation may be mediated by a specific coupling between PSD-95 and neuronal NO synthase (nNOS) (Brenman et al., 1996) which catalyzes NO production (Dawson et al., 1991) leading to neurotoxicity (Lipton, 1999b). In addition, the coupling of NMDA receptors to the molecular machinery of the PSD may facilitate uptake of calcium into the mitochondria (Peng and Greenamyre, 1998) which can also lead to cell death (see above).

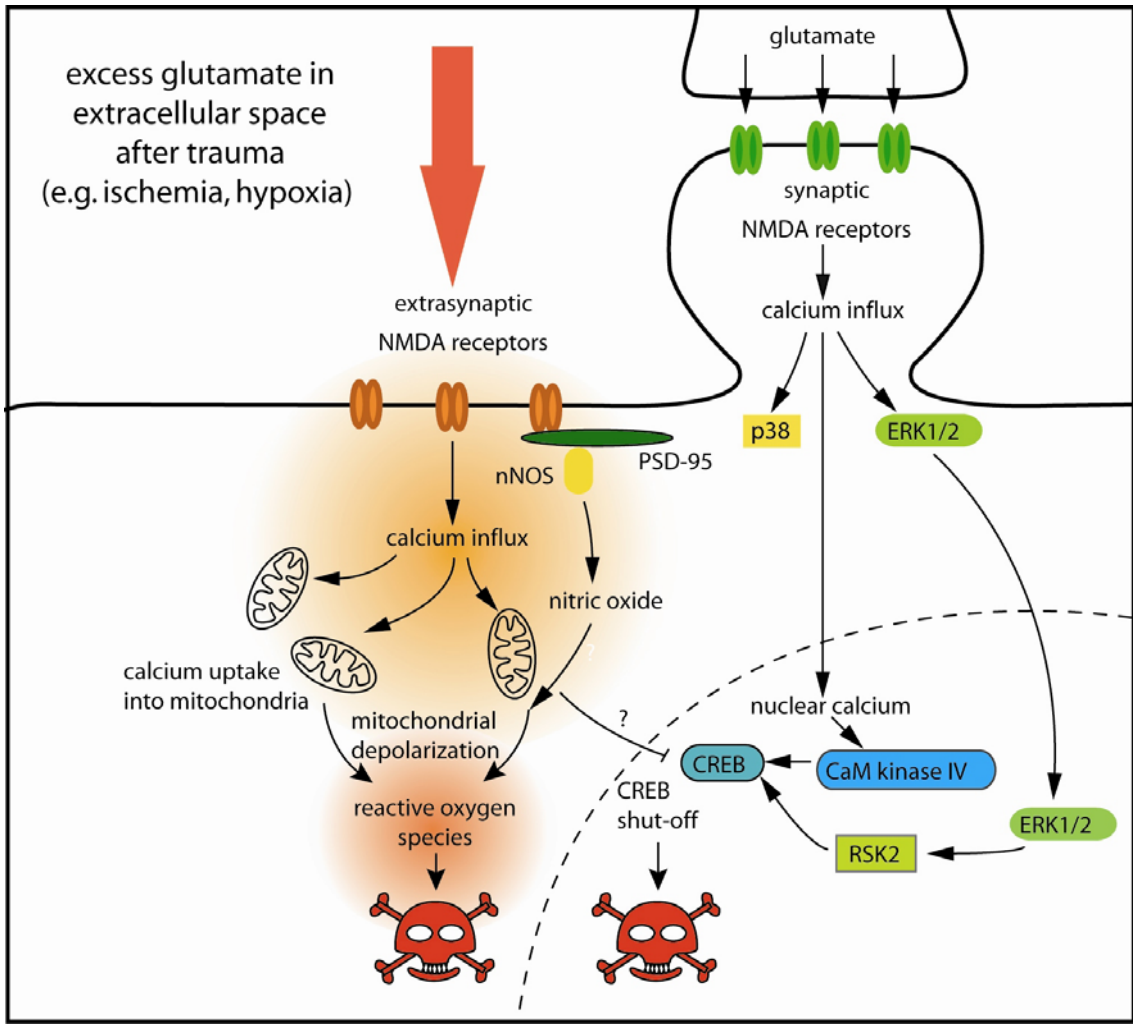

(Wittmann et al., 2004)

Figure 2. *Extrasynaptic NMDA receptors are thought to be activated by increases in glutamate concentrations in the extracellular (non-synaptic) space, which occur following hypoxic/ischemic insults. Calcium entry though extrasynaptic NMDA receptors leads to calcium uptake into mitochondria and to their depolarization; it also activates nNOS, and through an unknown mechanism, leads to the shut-off of CREB function. Mitochondrial dysfunction and NO synthesis lead to the production of reactive oxygen species that promote cell death.*

3.2.11. Conantokins

Conantokins are small peptides produced in the venom of the predatory deep sea snail conus. They allosterically inhibit calcium flow through the NMDA receptor by non-competitively inhibiting polyamine stimulatory effects in these receptors. They are extensively processed by post-translational modifications, the most common one being gamma-carboxylation of glutamyl residues.

Conantokin-G (conG) is also referred to as “sleeper peptide”, as it induces a sleep-like state in young mice, while creating a hyperactive state in older mice (Rivier et al., 1987). ConG decreased the NMDAR-mediated excitatory postsynaptic potential in hippocampal cultures (Klein et al., 1999) and has been shown to be selective for the NR2B subunit of the NMDA receptor (Donevan and McCabe, 2000). ConG is stabilized by undergoing a conformational change in the presence of certain metal ions that bind to its gamma-carboxyglutamate residues, leading to an α-helical conformation which is believed to increase its stability (Castellino and Prorok, 2000). Replacement of the gamma-carboxy glutamates resulted in inactivation or decreased potency, while replacement of the carboxy-terminal 4 amino acids had no effect on its activity (Castellino and Prorok, 2000).

4. Results

4.1. Nuclear infoldings

Synaptic activity elicits a calcium signal that translocates from the cytoplasm into the nucleus where it participates in the induction of gene transcription. The regulation of calcium flow is most likely not only dependent on passive diffusion of calcium ions but may involve facilitation of calcium flow by pumps like serca ATPases. Hippocampal neurons were therefore analysed for the localization of serca pumps in the nuclear membrane.

4.1.1. Localizations by fluorescence microscopy

Live confocal imaging was used to localize SERCA pumps with fluorescently labelled thapsigargin, an irreversible blocker of these pumps (Figure 3). The fluorescent signal revealed fine tubular structures projecting into the nucleus in neurons and occasionally also in glial cells. The same structures were observed after fixation with an α-SERCA antibody (Figure 4), although the signal to noise ration with this antibody was suboptimal in the majority of cells.

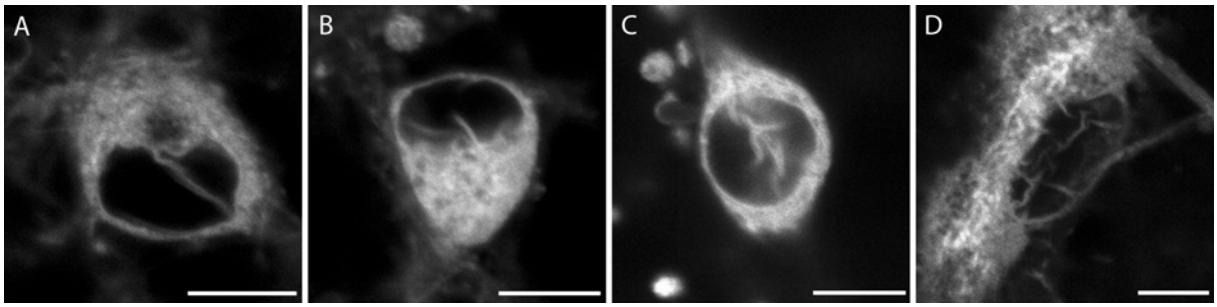

Figure 3. *Confocal images of live neurons (A-C) and a glial cell (D) stained with thapsigargin-bodipy. Shown are tubular structures projecting into the nucleus. Scale bars: 10 µm.*

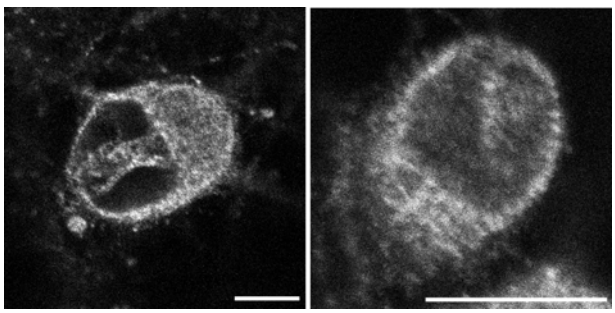

Figure 4. *Confocal images of fixed neurons stained for the serca 2 ATPase. Nuclear infoldings appear positive for α-SERCA 2 staining. Scale bars: 10 µm.*

To obtain more insights into the nature of these structures they were analysed for the colocalization of Endoplasmic Reticulum by using ER-Tracker. Live neurons were stained with thapsigargin-bodipy and ER-Tracker and analysed by confocal microscopy (Figure 5). The overlay of both channels revealed an almost complete colocalization, indicating that the structures observed are indeed continous with the intermembrane space of the nucleus. The question remained if these structures are invaginations of a single nuclear membrane or if they contain both membranes.

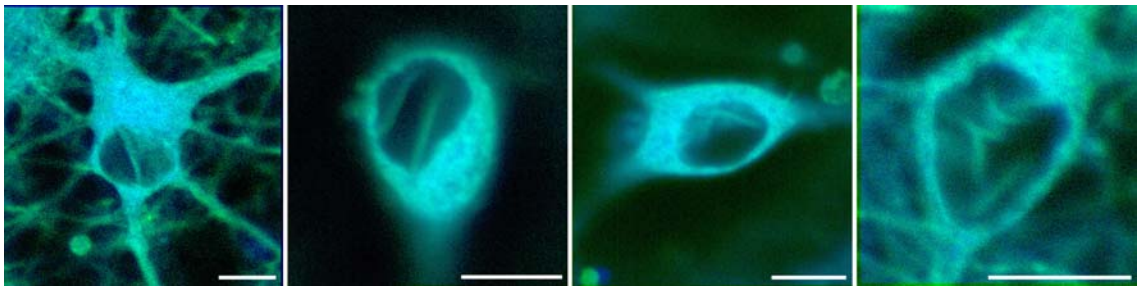

Figure 5. *Overlay of confocal images of live neurons stained for thapsigargin-bodipy (green) and ER-Tracker (blue). Scale bars: 10 µm.*

4.1.2. Electron microscopy

Cryo sections from primary neurons in culture at 12 days in vitro (DIV) were contrasted with uranyl acetate (1 %) and the nuclei screened for the presence of membranes reaching into the nucleoplasm by electron microscopy. Figure 6a shows that there were major invaginations of the nuclear membranes that infolded into the nucleus. Further magnification revealed that indeed both nuclear membranes are involved in this infolding process (Figure 6b). This shows that not a single membrane is infolded giving rise to a nucleoplasmic reticulum, but that neuronal nuclei seem to contain invaginations of both nuclear membranes. To verify that this occurrence was not a cell culture artefact, cryo sections from adult rats were contrasted with uranyl acetate (1 %) and analysed for the presence of infoldings. Figure 7a shows that there are no major morphological differences between the infoldings observed in cell culture and animals. In both cases the invaginations traverse deeply into the nucleoplasm and are composed of both outer and inner nuclear membrane (Figure 7b).

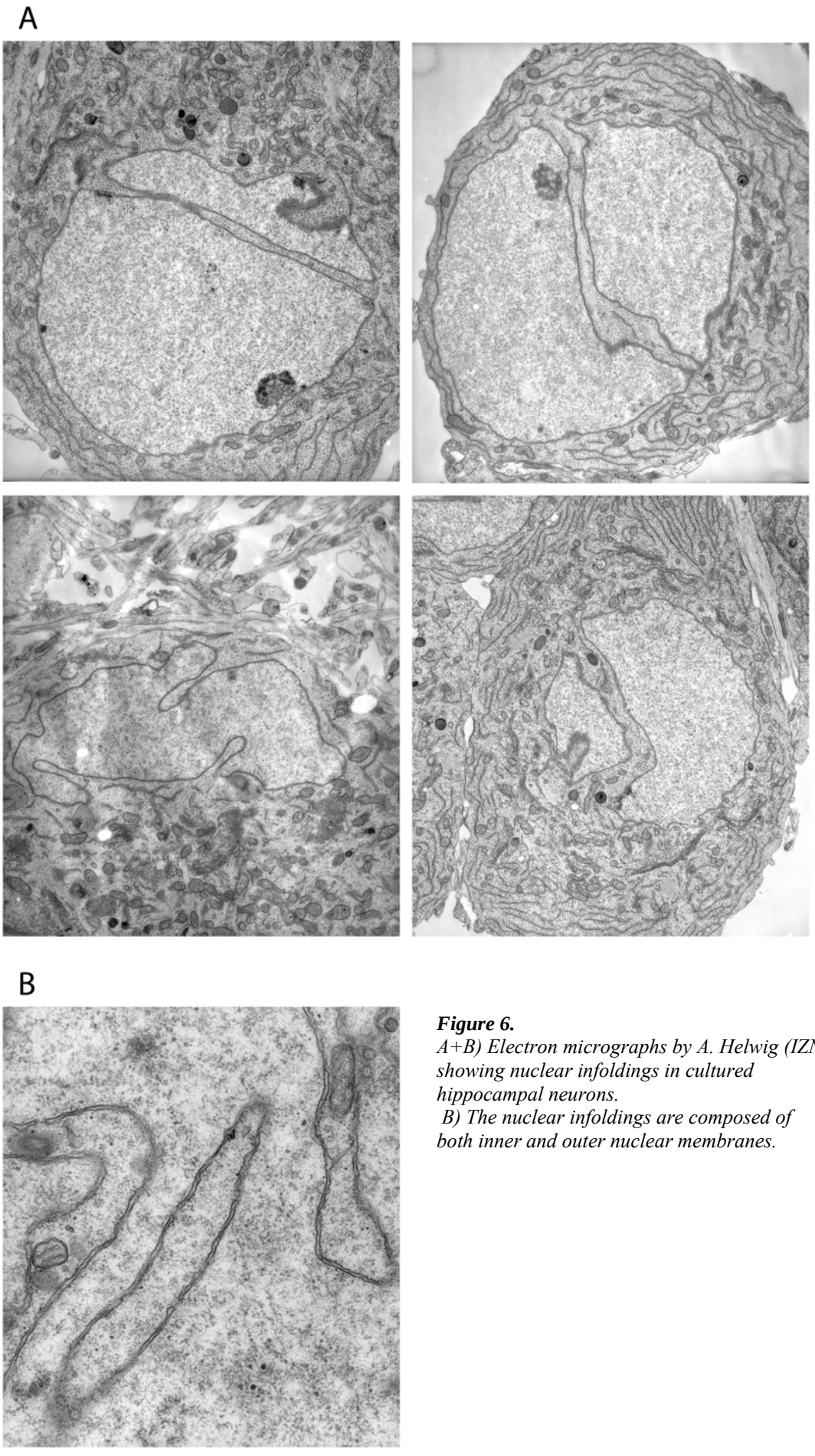

Figure 6.
A+B) Electron micrographs by A. Helwig (IZN) showing nuclear infoldings in cultured hippocampal neurons.
B) The nuclear infoldings are composed of both inner and outer nuclear membranes.

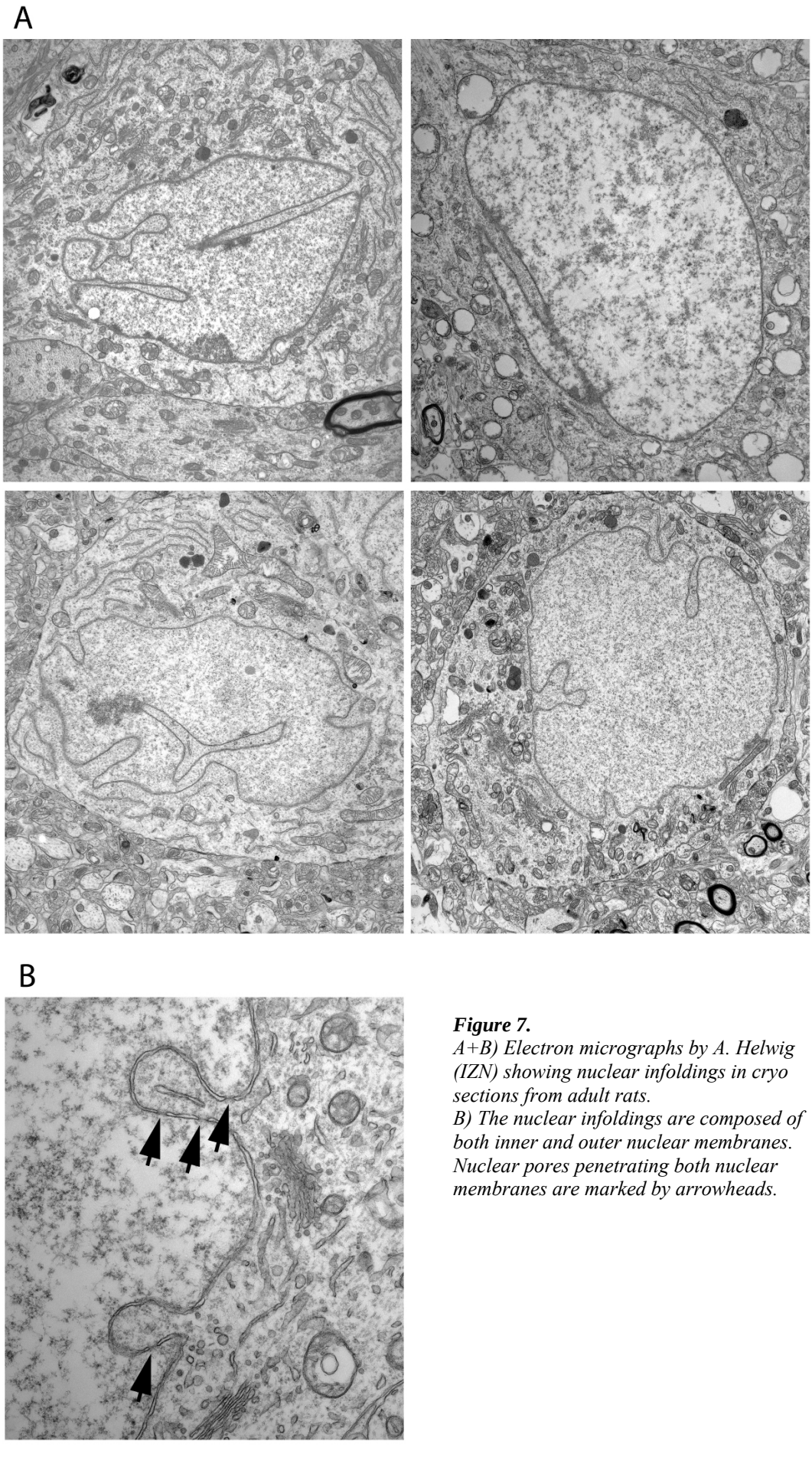

Figure 7.
A+B) Electron micrographs by A. Helwig (IZN) showing nuclear infoldings in cryo sections from adult rats.
B) The nuclear infoldings are composed of both inner and outer nuclear membranes. Nuclear pores penetrating both nuclear membranes are marked by arrowheads.

4.1.3. 3D reconstructions of nuclear infoldings

Three dimensional reconstructions were carried out to characterize the morphology of the nuclear structures. To be able to reconstruct the confocal images into a 3-dimensional model a marker had to be found that would allow imaging of the nuclear membranes and that creates a good signal to noise ration. Instead of detecting the membrane itself, which turned out to be technically difficult, it appeared suitable to label proteins of the nuclear lamina underlying the inner nuclear membrane by immunofluorescence.

I used a monoclonal α-lamin B antibody (kind gift of the laboratory of Herrmann, DKFZ) that gave little to no background in the cytoplasm while perfectly staining the nuclear lamina (Figure 8).

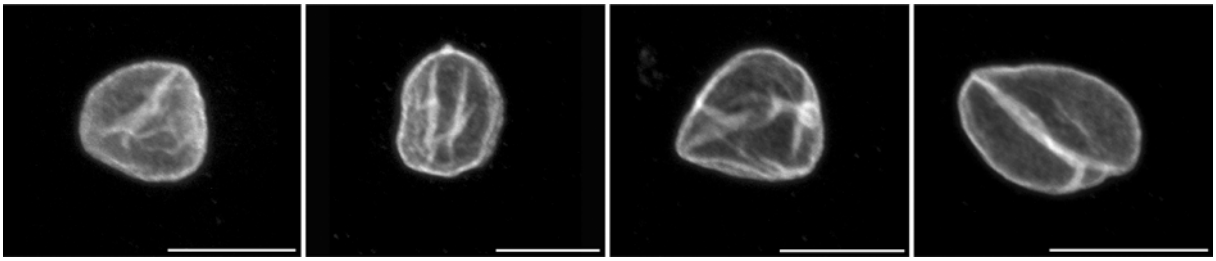

Figure 8. *Deep infoldings traversing the entire nucleus are decorated with lamin B. Fixed neurons were stained for lamin B and confocal z stacks were taken spanning the dimensions of the entire nucleus. These were then projected into a single plane using ImageJ. Scale bars: 10 µm.*

Unfortunately the same antibody gave only weak signals in free-floating brain sections from rats of different ages and a suboptimal signal to noise ratio (Figure 9), therefore all 3D reconstructions had to be based on confocal images from cultured cells.

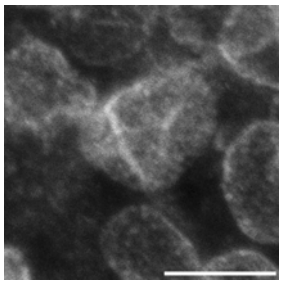

Figure 9. *Lamin B staining in free-floating brain sections of adult rats. Sagital brain slices of adult rats were obtained from Matthias Klugmann (IZN) and stained for lamin B. The image shows a nuclear infolding in a hippocampal neuron. Scale bar: 10 µm.*

The confocal images of cultured neurons were reconstructed using anisotropic filtering, image segmentation by Otsu and calculation of the surface using a Dijkstra graph search algorithm in collaborative effort by Gillian Queisser from the Interdisciplinary Center for Scientific Computing (IWR) in Heidelberg.

Figure 10 A shows the 3D model of a typical non-infolded nucleus. All neurons were comparatively flat in z dimension as neurons in culture grow on a substrate instead of a three-dimensional mesh, which results in relatively flat nuclei. Typical examples of infolded nuclei after 3D reconstruction are shown in Figure 10 B. From these images it is obvious that the structures identified by thapsigargin staining are true infoldings of both nuclear membranes instead of tubular structures, as has been reported for certain cell lines (Fricker et al., 1997). These infoldings have a major impact on the shape of the nucleus and it remained to be determined if this induced a change of any mechanisms functioning within the nucleus.

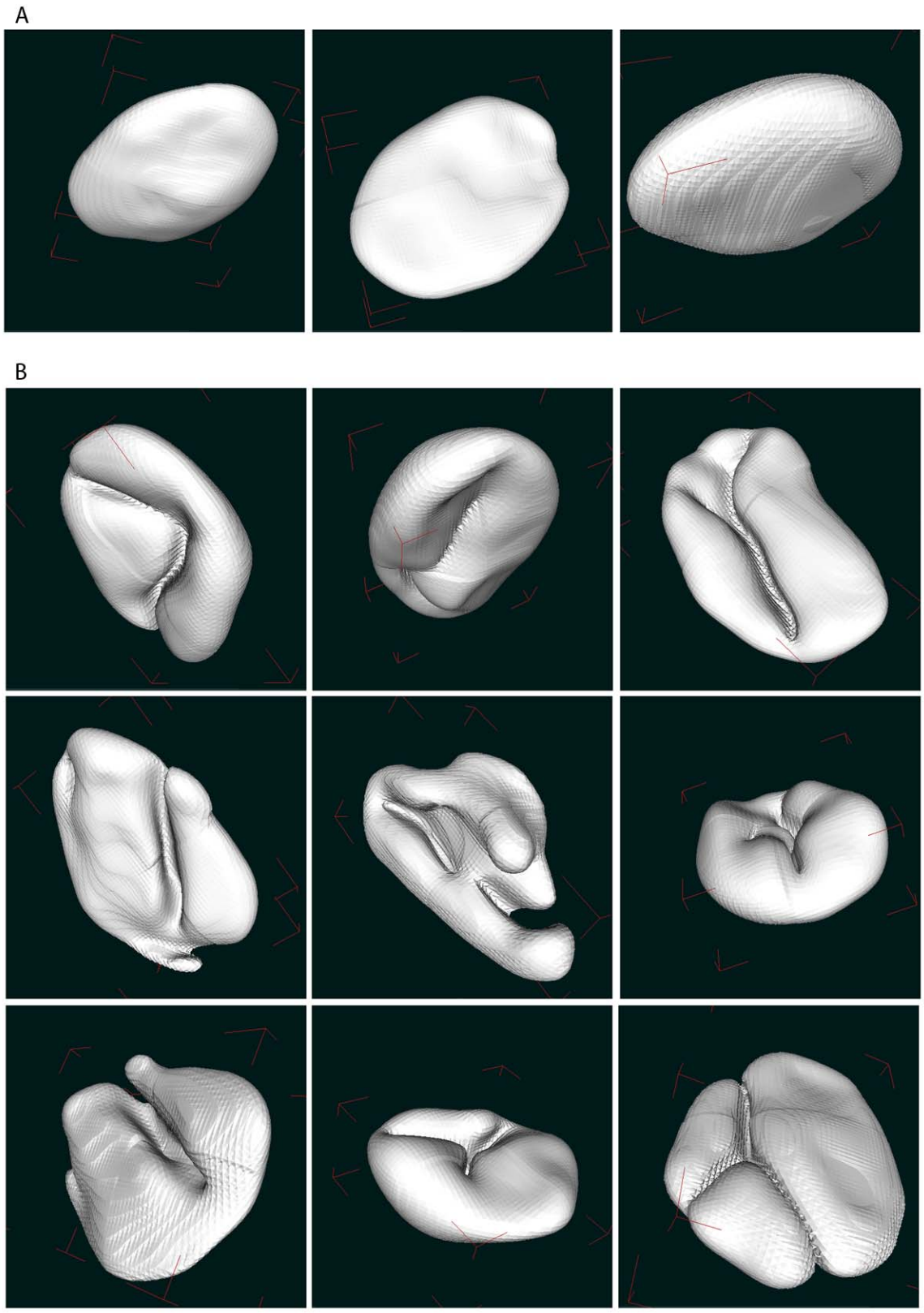

Figure 10. *3D reconstructions were done by Gillian Queisser (IWR) using an anisotropic diffusion filter and the NEUron Reconstruction Algorithm.*
A) 3D models of non-infolded neuronal nuclei.
B) 3D models of neuronal nuclei possessing infoldings of different shapes.
The models depicted here represent the inner part of each nucleus, not incuding both nuclear membranes.

As a consequence of deep nuclear infoldings it is more than likely that at least one of two parameters comprising the nucleus must change: the volume or the surface area. As it is unknown exactly how an infolding of the neuronal nuclear membrane is achieved, two hypothetical models can be regarded:

1. an infolding of the nucleus by reduction of the volume, leaving the surface area unchanged. This could possibly occur by loss of liquid from the nucleoplasmic space and would subsequently result in a concentration of nuclear proteins, thereby affecting enzymatic events like gene transcription.
2. creation of infoldings by synthesis or recruitment of new nuclear membranes. This would leave the volume unchanged but create a requirement either for the synthesis of new membrane components, most likely by enzymes at the inner nuclear membrane or perinuclear space, or recruitment from another source. As both nuclear membranes compose the infoldings, a possible source for new membrane lipids could be the Endoplasmic Reticulum.

To assess this question, fixed cultured neurons were stained for lamin B and confocal stacks spanning the entire nucleus were generated. These were then reconstructed and the surface area of the inner nuclear membrane calculated using a mathematical algorithm called “Marching-Front-operation” (Gillian Queisser, IWR).

The volume and surface area of each nucleus were measured in relative values. The average volume of infolded nuclei was not significantly larger than the volume of control nuclei. On the other hand there was a large difference in surface area between infolded and control nuclei (Figure 11 A). The average surface area from 31 nuclei analysed was significantly larger ($p = 0{,}002$; two-tailed, unpaired T-Test) than the average surface area from 21 nuclei that did not possess infoldings. Calculation of the volume-to-surface ratio of each infolded and non-infolded nucleus resulted in an average ratio that was significantly smaller in infolded nuclei than in non-infolded nuclei (Figure 11 B). This directly shows that in average the infolded nucleus does have a larger surface area than a nucleus that does not have any infolding, indicating that either generation or recruitment of membranes are necessary for the structural rearrangements.

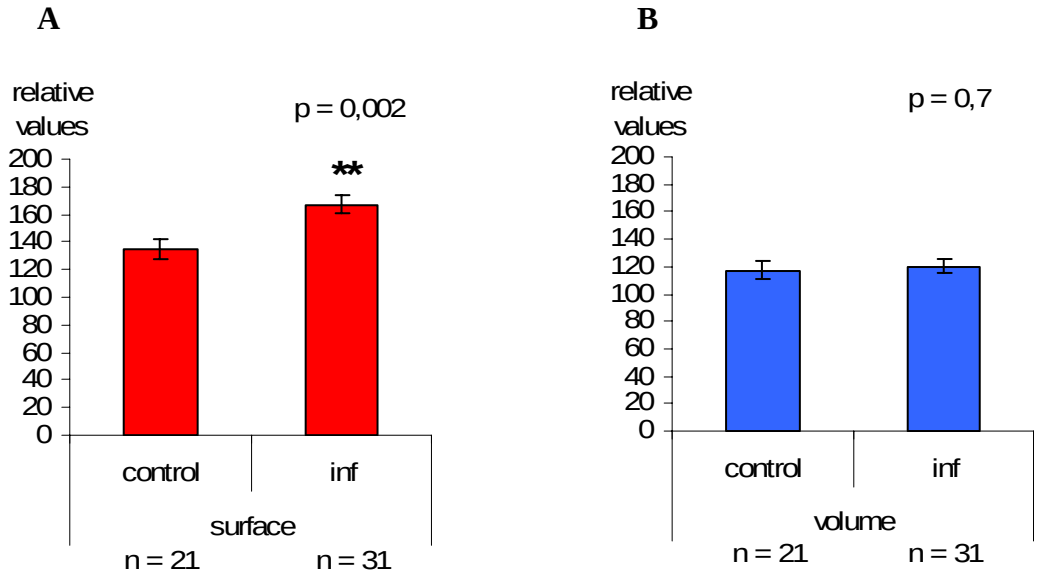

Figure 11. *The average surface area (A, red) of infolded nuclei (inf) is significantly larger than that of non-infolded nuclei (control)(p = 0,002), while the average volume (B, blue) does not differ between both groups (p = 0,7). Statistical significant differences (two-tailed unpaired T-Test) compared to control nuclei are indicated with asterisks (** p < 0,005). Error bars: SEM.*

4.1.4. Destabilization of nuclear infoldings by activation of extrasynaptic NMDA receptors

It has been described before that nuclear channels observed in different cell lines undergo changes in morphology within minutes (Fricker et al., 1997). To test if this also holds true for the infoldings observed in hippocampal neurons these were transfected with a lamin B-GFP construct and observed by confocal time lapse microscopy. Although lamin B decorated the nuclear infoldings, no change in morphology could be observed within a time period of 1 h (data not shown).

However, the morphology of infoldings did change after application of toxic levels of NMDA (50 µM), activating both synaptic and extrasynaptic NMDA receptors. When cells transfected with lamin B-GFP were transfered into CO_2-independent medium and a stack spanning the entire nucleus recorded every 90 sec, the nuclear infoldings completely disappeared within 15 min after NMDA bath application (Figure 12). The loss of intensity is primarily taking place in the area of the infolding while the nuclear rim stays constant in fluorescence. This indicates that the fluorescence loss is not due to bleaching but merely to a redistribution and spreading of the compacted signal within the infolding to the entity of the nuclear membrane.

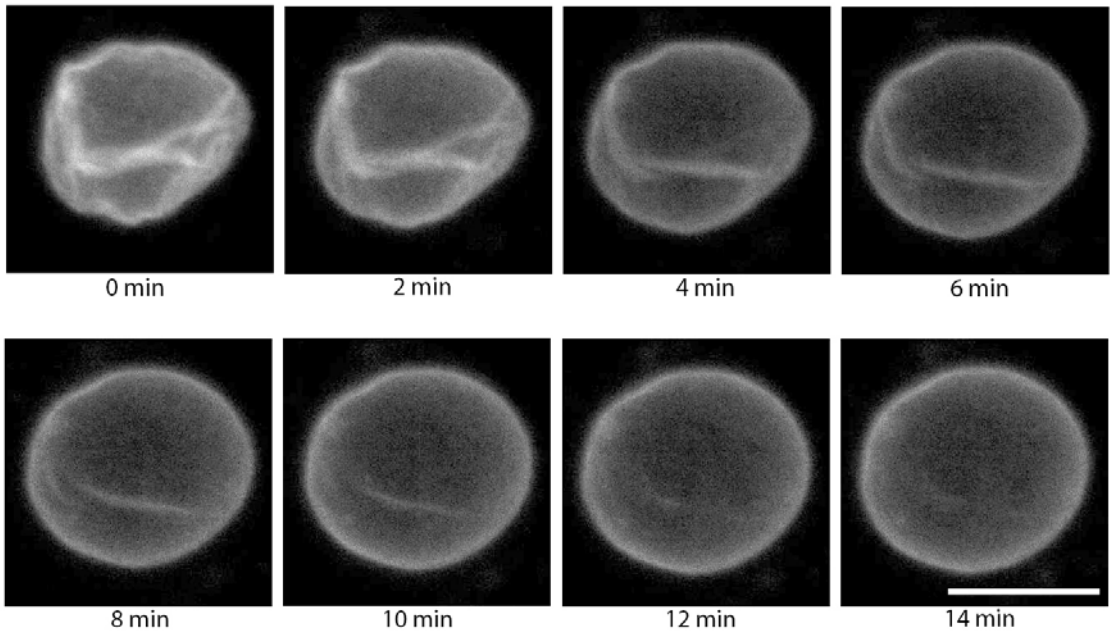

Figure 12. *Confocal time lapse imaging of lamin B-GFP after NMDA bath application. Neurons were transfected with lamin B-GFP and 30 confocal z stacks spanning the entire nucleus were recorded every 2 min (xyzt). Addition of NMDA (50 µM) lead to a rapid disappearance of nuclear infoldings. Images of each time point were projected into one plane and converted into a time lapse using ImageJ. Scale bar: 10 µm.*

It appeared as if a nuclear swelling would occur, thereby pushing its infoldings to the outside. The duration and kinetics did however appeared to be dependent on the amount of lamin B-GFP that was expressed in the nucleus examined. In severe cases in which a large excess of lamin B-GFP was present, the nuclear morphology differed from the normal morphology of infoldings observed by immunostaining (Figure 13). Instead of having few distinct infoldings partially or completely traversing the nucleus, these overexpressing nuclei showed massive slope-like alterations of the nuclear lamina, visualized with lamin B-GFP. NMDA bath application did not lead to any change or destruction of these structures, indicating that an excess of lamin B seems to somehow stabilize the nucleus and prevent its swelling upon excitotoxic insults (Figure 14). It should however be noted that no statement can be made about the viability of the lamin B-overexpressing cell, as severe alterations of the nuclear membrane are most likely toxic after a certain time. The prevention of nuclear swelling should be regarded purely as a mechanical stabilization of the membrane.

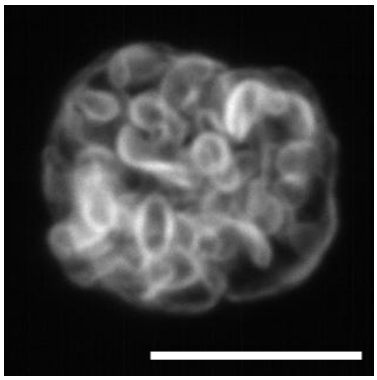

Figure 13. *Severe overexpression of lamin B-GFP in a neuron. Projection of confocal z stack using ImageJ. Scale bar: 10 μm.*

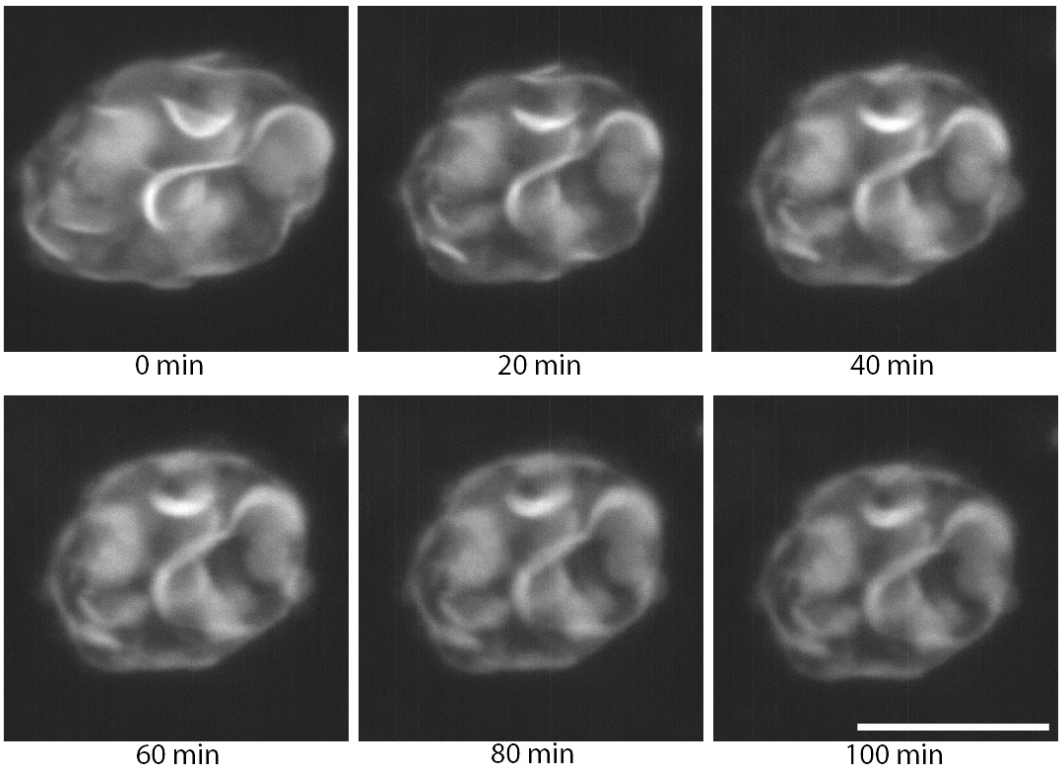

Figure 14. *Neurons severely overexpressing lamin B-GFP are less affected by NMDA-induced excitotoxicity and retain their infoldings. Neurons were transfected with lamin B-GFP and 30 confocal z stacks spanning the entire nucleus were recorded every 5 min (xyzt). Upon addition of NMDA (50 μM) the nuclear structures created by overexpression of lamin B-GFP did not change in time. Scale bar: 10 μm.*

To examine the kinetics of destabilization of infoldings in entire cultures the ratio of infolding-positive neurons to healthy neurons was quantified by immunostaining of fixed neurons lamin B after NMDA treatment (Figure 15). It appeared that already after 15 min the majority of infoldings had disappeared while after 30 min basically no infoldings could be observed.

To see if MAP kinases are involved in this toxic nuclear swelling, the ERK cascade was blocked by the pharmacological inhibitors PD98059 and UO126 respectively (Figure 16). It appeared that 30 % of untreated cells possessed nuclear infoldings which could

nearly completely be destabilized with 50 µM NMDA within 15 min. Neither incubation with PD98059 or UO126 or a combination of both could abolish this effect. Surprisingly, blockade of the ERK1/2 pathway with PD98059 alone lead to a decrease in the basal level of infolding-positive cells.

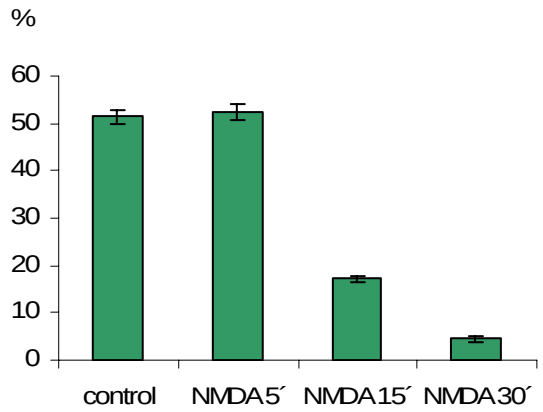

Figure 15. *The percentage of neurons having nuclear infoldings rapidly declines after addition of NMDA (50 µM). Neurons were fixed after NMDA application at indicated time points and stained for lamin B. Quantifications were carried out by fluorescence microscopy. Error bars: SEM.*

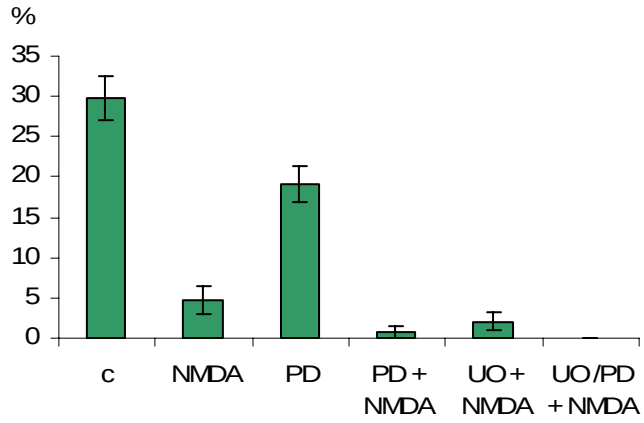

Figure 16. *Blockade of the ERK pathway did not prevent destabilization of nuclear infoldings. Neurons were treated for 1 h with the MEK1 blocker PD98059 (PD, 50 µM) or UO126 (UO, 10 µM) respectively. NMDA (50 µM) bath application lead to complete loss of infoldings within 15 min. Error bars: SEM.*

4.1.5. Induction of nuclear infoldings by stimulation of synaptic NMDA receptors

To test if nuclear infoldings might possibly show any form of reorganization over time, synaptic NMDA receptors were activated by bicuculline and infoldings quantified after immunostaining for lamin B. Surprisingly, although the general shape of infoldings did not change, their numbers did. Stimulation with bicuculline induced de-novo formation of infoldings in previously not infolded neurons, leading to an increase in the total number of infolding-positive neurons from 30 % to 70 % (Figure 17a). The increase seemed to be linear with 50 % after 30 min and slightly declined after 2 h to 60 %. However, the number of infoldings appeared to be dependent on the density of the

culture and following experiments showed that there is in fact no decline after bicuculline stimulation but a variation between different coverslips. The question remained what exactly led to the induction of infoldings as synaptic activity induced by bicuculline leads to activation of different types of receptors. It turned out that activation of L-type channels was also capable of inducing infoldings to a certain extend, but that this induction was abolished in the presence of the NMDA receptor antagonist MK-801 (Figure 17b). The NMDA receptor is prone to open upon membrane depolarization induced by opening of L-type channels. Elevation of cAMP levels with the adenylyl cyclase activator Forskolin and the phosphodiesterase inhibitor IBMX did not lead to an increase in numbers.

Therefore the synaptic NMDA receptor has to be the switch that triggers the infolding of neuronal nuclei.

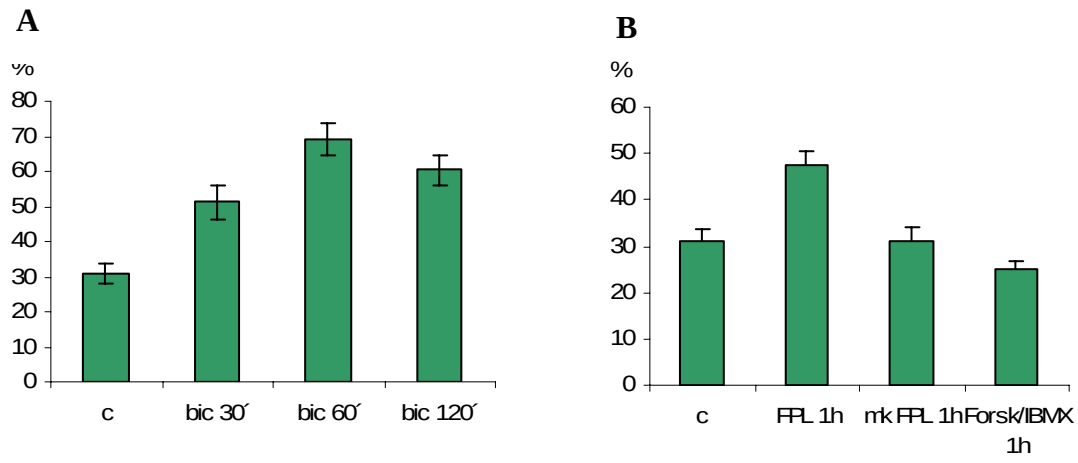

Figure 17.
A) Synaptic activity induced by bicuculline treatment leads to an increase of infolding-positive neurons from 30 % to 70 % within 1 h.
B) Activation of L-type channels cannot induce nuclear infoldings. While addition of FPL led to an induction of infoldings, this was totally abolished in the presence of MK-801 (20 µM). Elevation of cAMP levels with Forskolin (10 µM) / IBMX (500 µM) did not induce infoldings. Error bars: SEM.

4.1.6. Live imaging of the induction of infoldings

To get an insight into the kinetics of the infolding process, live neurons not possessing any infolding should be recorded during the generation of infoldings. Therefore neurons were loaded with the membrane dye DiD and time lapse recordings were performed by confocal microscopy taking z stacks that covered the entire nucleus (Figure 18). The neurons shown here undergo a slow formation of infoldings, visible as a light deformation from the side in cell A and an obvious infolding from below in cell B.

A drawback of the membrane dye used here was its toxicity, therefore the number of neurons observed during the generation of infoldings was very low.

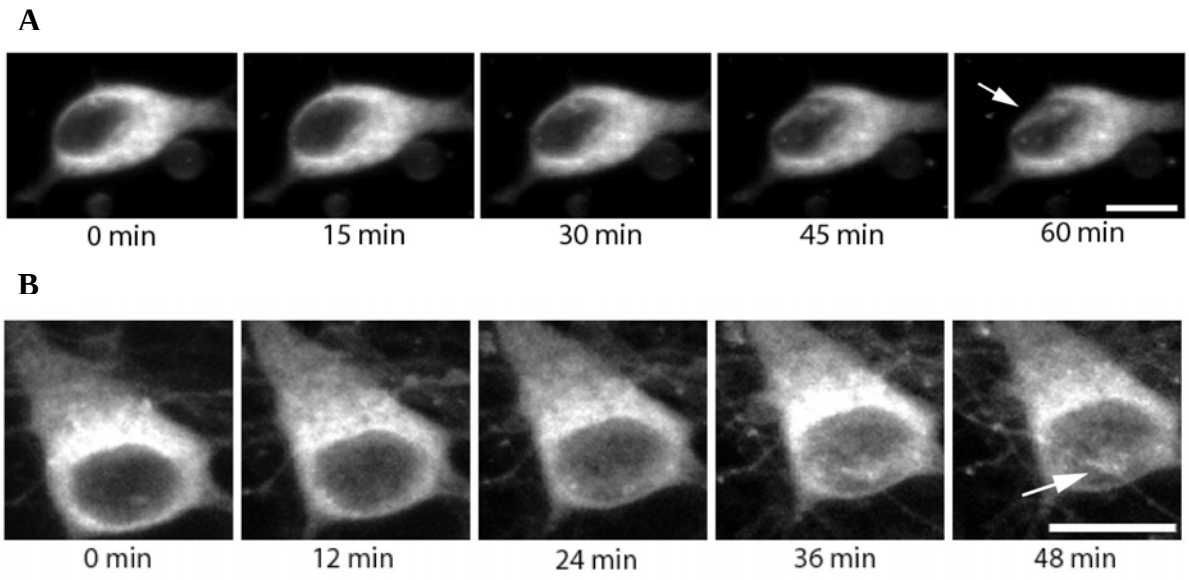

Figure 18. *Time lapse imaging of the generation of nuclear infoldings. Membranes of living neurons were stained with DiD and stimulated with bicuculline at 37°C. Infoldings are being induced from the side (A) or the bottom of the nucleus (B). Scale bars: 10µm.*

4.1.7. Intracellular signaling cascades involved in the generation of nuclear infoldings

As one of the major properties of the NMDA receptor is its permeability for calcium which leads to activation of intracellular protein cascades by binding to calmodulin, a number of pharmacological antagonists were tested for potential inhibitory effects. All inhibitors were incubated on cells for 1 h at concentrations according to the literature. Subsequently neurons were stimulated with bicuculline for 1 h and infoldings were quantified. The choice fell onto blockers of the Erk1/2 pathway as PD98059 showed a reduction of the basal level of infoldings before (see Figure 16). The substances that were effective in decreasing the number of bicuculline-induced infoldings were the MEK1 inhibitors PD98059 and UO126, which prevent phosphorylation of ERK1/2, the calmodulin antagonist calmidazolium (Figure 21) and L-NAME (Figure 19), an inhibitor of nitric oxide synthase. The latter could however not be reproduced in all repetitions of the experiment, leaving the direct involvement of nitric oxide questionable. Inhibitors that had no effect are the PI3 kinase inhibitor LY294002, the GSK3-β inhibitor SB216763, the translation inhibitor anisomycin, the transcription inhibitor actinomycin D and BDNF. Surprisingly, the inhibitor of calcium-calmodulin

dependent kinase KN-62 did not show any inhibitory effect (Figure 19), neither did Autocamtide-2 related inhibitory peptide II **(**AIP II) (Figure 20). In contrast, another calmodulin antagonist, W7, did also block the induction (Figure 22).

To test if the effects observed with calmidazolium were truely due to its affinity to calmodulin and not to unspecific action on the NMDA receptor, the bicuculline-induced phosphorylation of ERK1/2 was assessed in the presence of calmidazolium (Figure 23). PD98059 and UO126 blocked ERK1/2 phosphorylation, while calmidazolium did not, showing that it did not interfere with the MAP kinase cascade.

The bicuculline-induced calcium signals were also not affected by calmidazolium (Figure 24).

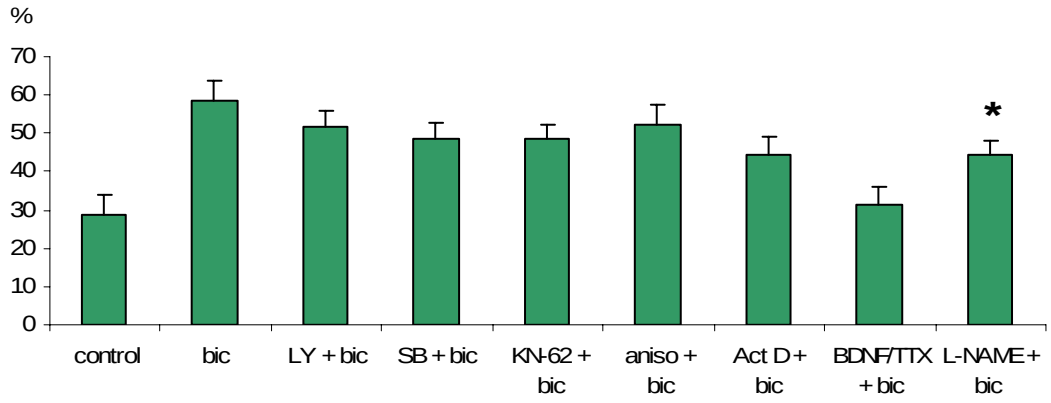

Figure 19. *Inhibition by LY294002 (LY, 10 µM), SB216763 (SB, 30 µM), KN-62 (1 µM), anisomycin (aniso, 1 µg/ml) or actinomycin D (Act D, 10 µg/ml) did not prevent induction of infoldings by bicuculline (bic, 50 µM). No induction was observed by BDNF (100ng/µl) in the presence of TTX (1 µM). L-NAME (1 µM) showed a minor inhibitory effect in the experiment shown. Statistical significant differences (two-tailed unpaired T-Test) are indicated with asterisks (* p < 0,05). Error bars: SEM.*

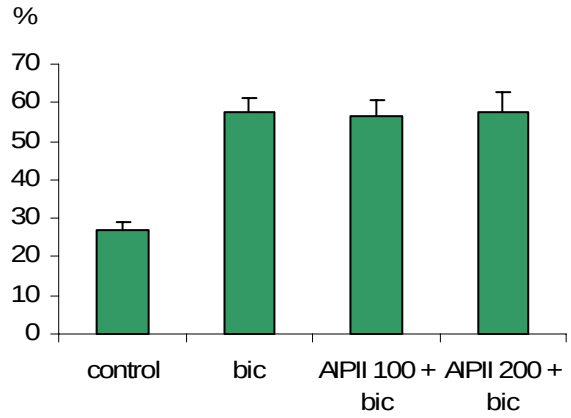

Figure 20. Autocamtide-2 related inhibitory peptide II *(AIPII) did not prevent the induction of infoldings at 100 nM or 200 nM. Error bars: SEM.*

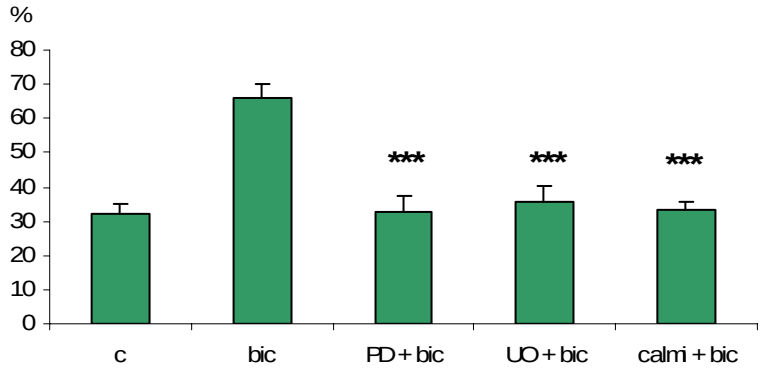

Figure 21. *Inhibition of ERK1/2 or Calmodulin prevents bicuculline-induced induction of nuclear infoldings. In neurons treated with PD98059 (50 µM), UO126 (10 µM) or calmidazolium (calmi, 1 µM) an induction of infoldings by bicuculline (50µM) was inhibited. Statistical significant differences (two-tailed unpaired T-Test) compared to control nuclei are indicated with asterisks (* p < 0,05; ** p < 0,005; *** p < 0,001). Error bars: SEM.*

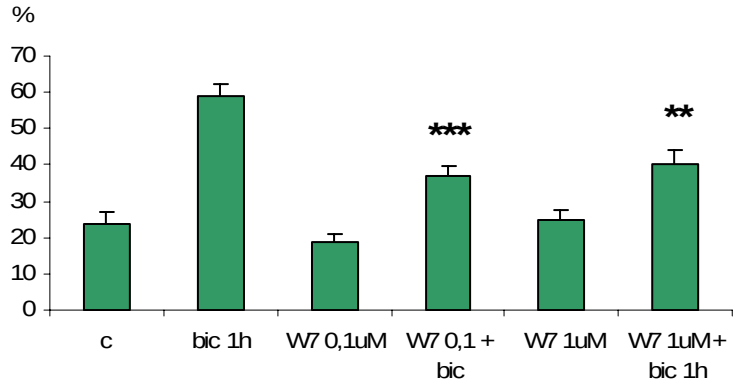

Figure 22. *The calmodulin antagonist W7 inhibited the induction of nuclear infoldings induced by bicuculline. W7 (100 nM or 1 µM) alone had no effect on the number of infoldings, while it significantly inhibited the bicuculline (bic, 50 µM)-induced induction at 100 nM or 1 µM. Statistical significant differences (two-tailed unpaired T-Test) are indicated with asterisks (** p < 0,005; *** p < 0,001). Error bars: SEM.*

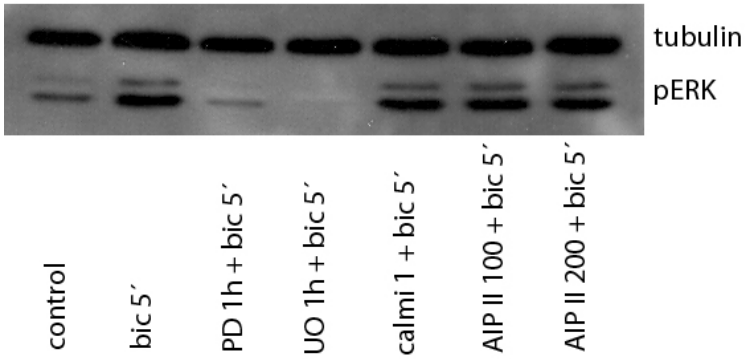

Figure 23. *Phosphorylation of Erk1/2 is not inhibited by calmidazolium. Bicuculline-induced Phospho-Erk1/2 levels (pErk) were significantly reduced by PD98059 (PD, 50 µM) and UO126 (UO, 10 µM) but not by calmidazolium (calmi, 1 µM), showing that the effects of this blocker are not mediated by unspecific effects on the MAP kinase pathway.* Autocamtide-2 related inhibitory peptide II *(AIP II, 100 nM or 200 nM) did not prevent phosphorylation of ERK1/2 either.*

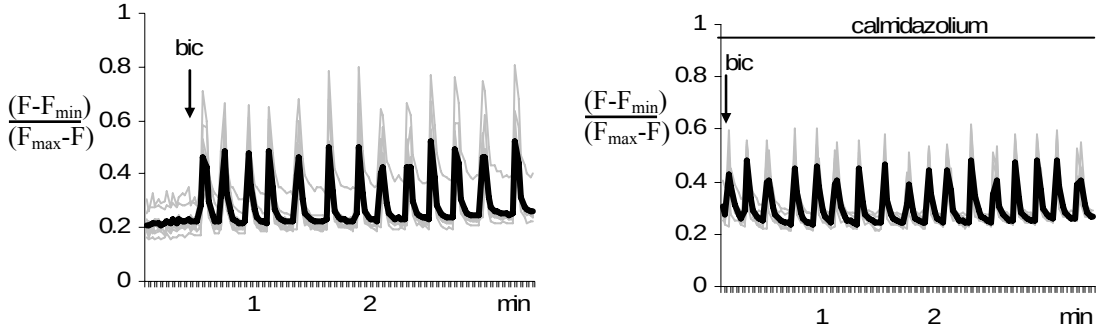

Figure 24. *Calmidazolium does not interfere with bicuculline-induced calcium oscillations. Neurons were treated with calmidazolium (1 µM) for 1 h and calcium influx via synaptic NMDA receptors was induced by bicuculline (50 µM). The presence of calmidazolium did not have any effects on the average amplitude or frequency of calcium spikes. The average calcium trace is shown in black.*

The involvement of several other signaling molecules was investigated by transient plasmid transfections. Possible candidates for nuclear reorganization were molecules of the Rho family, as these are also involved in a number of other processes controlling cell shape, including cell motility. Figure 25 shows transfection of the constitutively active form of Rho (Rho-V14), the dominant negative form Rho-N19 as well as constitutively active Rac-L61 and p190, which inactivates Rho.

Surprisingly, all transfected neurons showed a strong increase in the number of infoldings even in the absence of bicuculline. Non-transfected neurons also had slightly more often infoldings, indicating that the transfection reagent or the medium changes involved led to their induction. Despite higher basal levels of transfected cells, additional stimulation with bicuculline led to a further increase in the average number of infoldings, indicating that the molecules tested are not involved in the process of nuclear infoldings.

Further experiments involved expression of a plasmid containing four Calmodulin binding peptide sequences with a nuclear localization sequence (CamBP4), and hrGFP as negative control (Figure 26). The induction of nuclear infoldings did take place in hrGFP transfected cells as well as in surrounding cells, while in cells containing CamBP4 no induction of infoldings was observed. Expression of a dominant negative Cam kinase IV construct did however not prevent the induction by bicuculline (Figure 27).

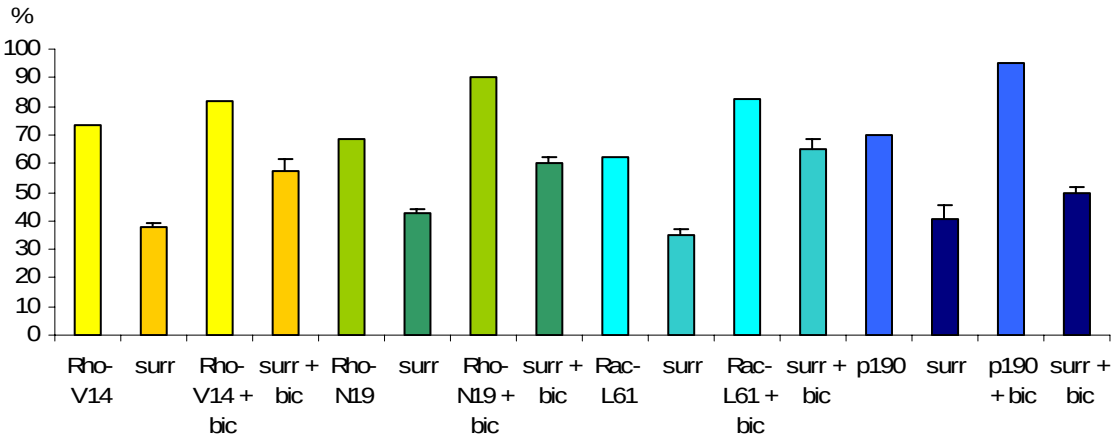

Figure 25. *Molecules of the Rho family are not involved in the induction of nuclear infoldings. Transient transfections of Rho-V14, Rho-N19, Rac-L61 and p190 did not prevent further induction of infoldings by bicuculline (bic, 50 µM). The basal levels in transfected cells were much higher than normal, non-transfected surrounding cells (surr) on the same coverslips showed slightly more infoldings. Error bars: SEM.*

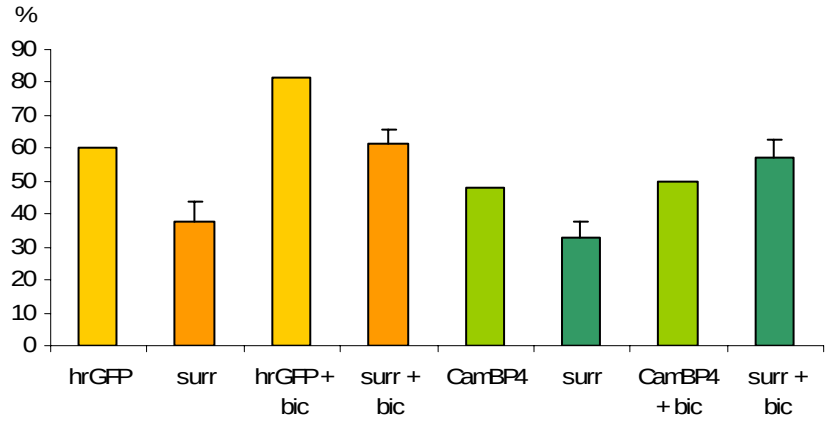

Figure 26. *Calmodulin Binding Peptide (CamBP4) prevented induction of nuclear infoldings. In neurons transfected with CamBP4 an induction by bicuculline (bic, 50 µM) did not occur, while the negative control (humanized ranilla GFP, hrGFP) had no effect. Error bars: SEM.*

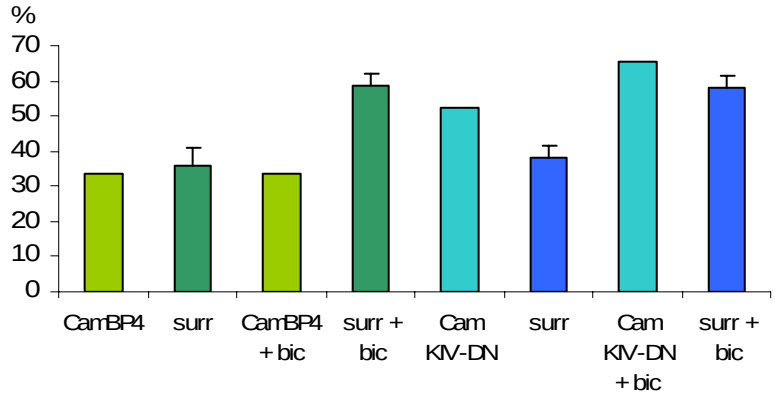

Figure 27. *Comparison of the effects of CamBP4 and CamKIV-DN. In neurons transfected with CamBP4 there was no bicuculline-induced (bic, 50 µM) induction of infoldings, while the Cam kinase IV dominant negative construct did not confer any inhibitory effect. Error bars: SEM.*

4.1.8. Decay of nuclear infoldings

Silencing the synapse overnight with tetrodotoxin (TTX) or closing NMDA receptors overnight with the NMDA receptor antagonist APV did not lead to a decrease in infoldings under control conditions (Figure 28). However, the basal level of infolded nuclei could be significantly decreased by addition of the NMDA receptor antagonist kynurenic in the presence of magnesium. These compounds were added from 4 to 8 days in vitro during the growth period of the neuronal culture and analysed for induction at 12 days in vitro. Figure 29 shows that in comparison to control cells cultured under standard conditions the presence of kynurenic significantly lowered the basal level of infoldings. An induction with bicuculline was still possible, although the level reached after 1 h was also lower than under standard conditions. This indicates that the basal level is constantly induced and maintained by the basal activity of the neuronal culture.

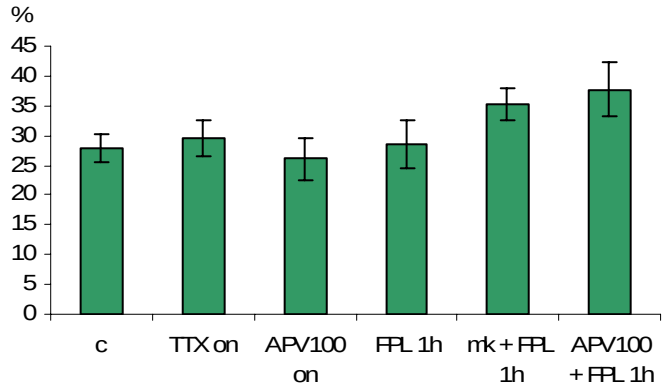

Figure 28. *The basal level of infoldings cannot be reduced by blockade of NMDA receptors. NMDA receptors were blocked over night with TTX (1 µM) or APV (100 µM). The basal level of infoldings was not reduced compared to control cultures. Error bars: SEM.*

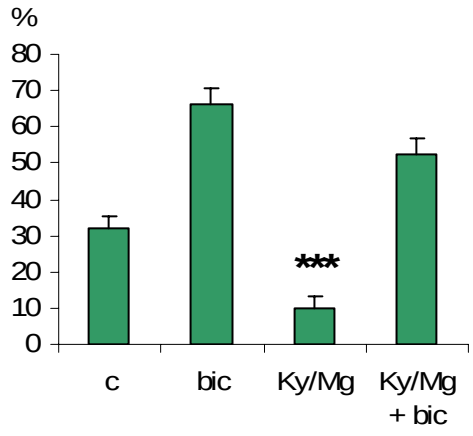

Figure 29. *Blockade of NMDA receptors by kynurenic during the growth period reduced the basal level of nuclear infoldings. Kynurenic (1mM) and Mg^{2+} (10mM) were added from 4 DIV to 8 DIV. The basal level is significantly reduced at 12 DIV. Induction with bicuculline (bic, 50 µM) for 1 h lead to a slightly lower percentage of infolding-positive neurons than under normal conditions. Statistical significant differences (two-tailed unpaired T-Test) are indicated with asterisks (*** $p < 0{,}001$). Error bars: SEM.*

Although the basal level of infoldings seemed to be stable in these cultures, it remained to be determined if the newly induced infoldings after bicuculline stimulation would also be stable. Therefore the decay kinetics were quantified in two parallel approaches: a short term decay assay composed of the induction with bicuculline for 1 h and subsequent silencing of synaptic activity with TTX. Neurons were then fixed after different time points, stained for lamin B and infoldings quantified by immunofluorescence (short decay). A "long decay" was done in parallel with the difference that these neurons had been treated for 1 h with bicuculline 40 h before addition of TTX (Figure 30).

Quantification of infoldings revealed that the addition of TTX directly after induction with bicuculline lead to a fast decay of infoldings within 1 h. In contrast, neurons that had been stimulated with bicuculline 40 h before showed a much slower decay upon silencing of synaptic activity. In addition, their basal level of infoldings remained high even 40 h after induction with bicuculline (Figure 31). This shows that neuronal activity is necessary to maintain nuclear infoldings. A stabilization can be achieved after several days, pointing to an either transcriptional or translational mechanism and therefore to the possibility of an involvement of a specific set of genes in the reorganization of nuclear morphology.

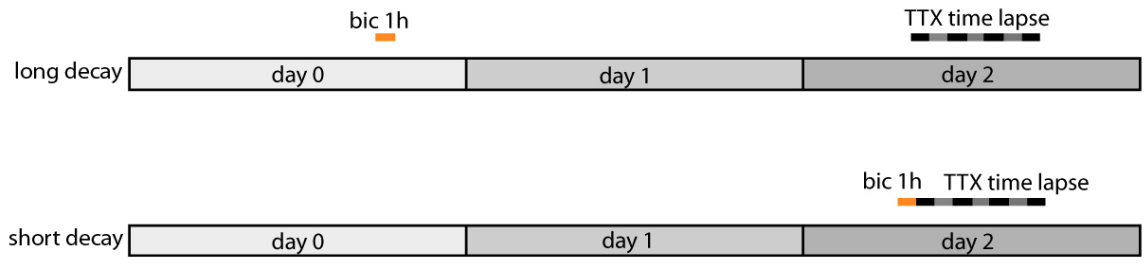

Figure 30. *Principle of decay experiment: in the "short decay" infoldings were induced on several coverslips with bicuculline (50 µM) on day 2 and synapses subsequently silenced with TTX (1 µM). The percentage of infolding-positive neurons was then analysed at different time points after silencing. In the "long decay" experiment all neurons were stimulated with bicuculline (50 µM) 2 days before silencing at day 0, followed by subsequent washout of bicuculline. The TTX treatment was done in parallel to the "short decay" experiment at day 2.*

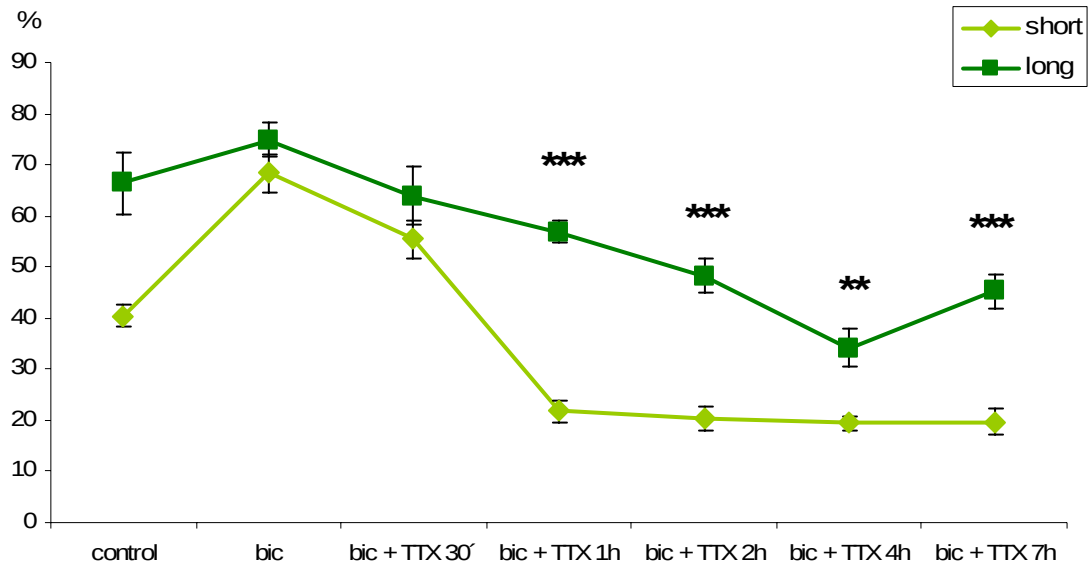

Figure 31. *Neurons of the short decay experiment had a basal level of infoldings of approximately 40 % before bicuculline and an induced level of 70 %. TTX (1 µM) lead to a rapid decay of infolding-positive neurons within 1 h. In contrast, stimulation with bicuculline (bic, 50 µM) in the long term experiment lead to an increased level of about 70 % after 2 days and much slower decay kinetics after TTX treatment, reaching a minimum of 35 % after 4 h. Statistical significant differences (two-tailed unpaired T-Test) are indicated with asterisks (** p < 0,005; *** p < 0,001). Error bars: SEM.*

4.1.9. Functional assays: bicuculline-induced calcium spikes

One possible function of nuclear infoldings might be the facilitation of calcium-dependent reactions in the nucleus by optimizing the routes of calcium influx. In a non-infolded nucleus the distance from the nuclear membrane to the inner nucleus is comparatively long, building a gradient of calcium with high calcium concentrations in the vicinity of the membrane and a lower concentration in the middle of the nucleus. In an infolded nucleus these diffusion ways would be much shorter as calcium most likely enters at the sites of infoldings like everywhere else, as nuclear pores have been observed within infolded membranes (see Figure 7).

Facilitation of calcium routes might also influence the calcium kinetics during synchronous bursting induced by bicuculline. To compare the calcium events in infolded and non-infolded control cells, these were loaded with the calcium indicator fluo-3 and ER-Tracker. The latter was used to identify infolding-positive neurons.

Z stacks of ER-Tracker were scanned by confocal microscopy and calcium signals were recorded after treatment with bicuculline. The z stacks containing information about infoldings were then overlaid with ImageJ to distinguish infolded and non-infolded cells and calcium signals of averages from both groups were compared (Figure 32). In the

first attempts the amplitude of bicuculline-induced calcium spikes was clearly smaller in non-infolded neurons than in infolded ones. Surprisingly the differences were the same in nuclei and cytoplasms, indicating that not the calcium signal itself is enhanced, but that infoldings generally lead to a higher calcium signal within the cell which would point to a possible enhancement of transcription and recruitment of calcium channels to the plasma membrane. Unfortunately a series of experiments did not reveal a significant difference between both groups, which might in part be due to high variability within cultures (Figure 33).

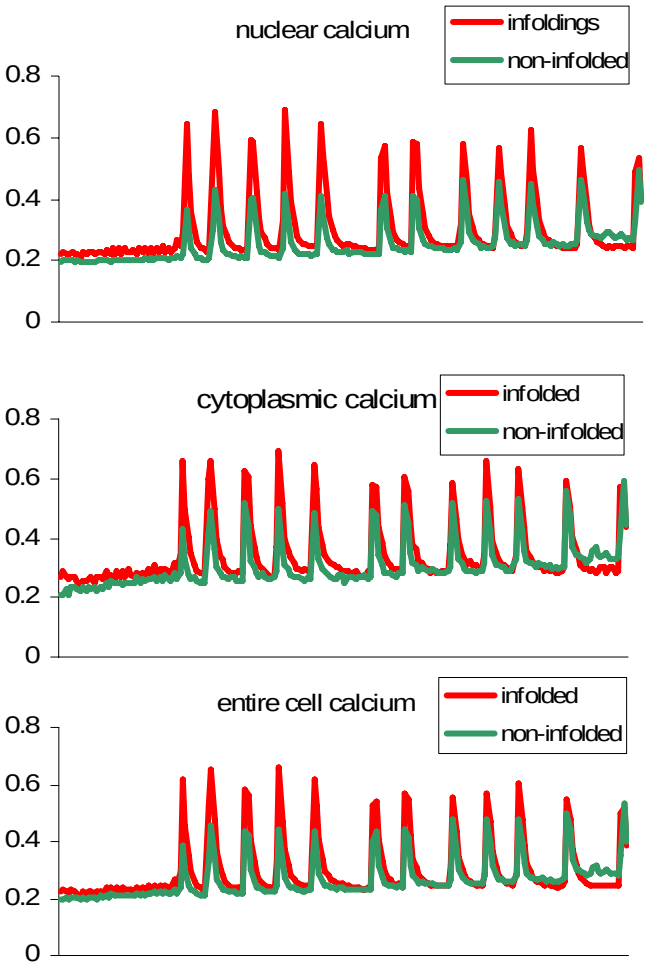

Figure 32. *Comparison of bicuculline-induced calcium spikes in infolding-negative and infolding-positive neurons. Neurons were loaded with ER-Tracker and fluo-3 and synchronous bursting was induced with bicuculline (50 µM). Infoldings were identified in projections of confocal stacks of ER-Tracker and averages of calcium signals of positive and negative neurons were compared.*

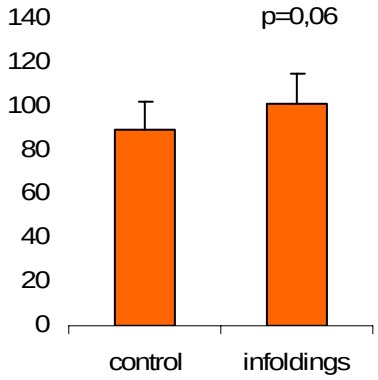

Figure 33. *The average percentage of the increase of calcium peaks was compared between infolding-positive and non-infolded neurons (control). Statistical significant differences (one-tailed paired T-Test) gave a p-value of 0,06, which is not significant (n=13). Error bars: SEM.*

4.1.10. Functional assays – Patch clamp recordings

Whole cell patch clamp recordings were carried out as a collaborative event by Simon Wiegert (IZN).

Extracellular and intracellular currents were recorded from hippocampal neurons and sorted into 3 groups of responses: neurons without spontaneous activity, with random activity and those exhibiting recurrent bursting. To be able to identify the patched neurons Biotin was included in the patch pipette. Patched neurons were stained for lamin B and the patched neuron was identified by detection with Streptavidin-FITC (Figure 34). The electrical activity was then correlated to the presence of nuclear infoldings (Figure 35). 20 % of patched cells were electrically silent and contained as often infoldings as they were devoid of such. Randomly active cells more often lacked infoldings (24% vs 19%), while neurons showing recurrent bursting activity more often were infolded (24% vs 14%).

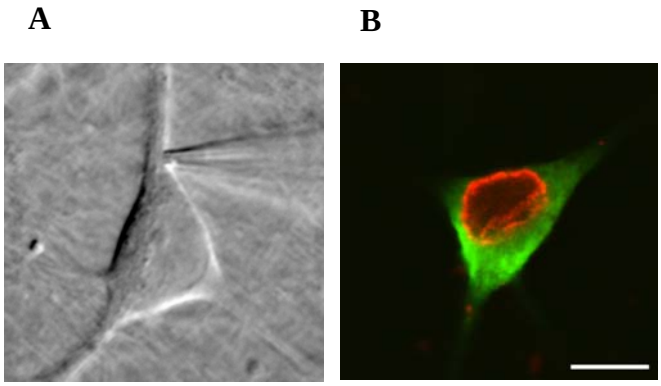

Figure 34.
A) DIC image of a neuron patched at the base of the dendrite to circumvent artefacts that would otherwise arise from patching to close to the nucleus.
B) Immunofluorescence of a patched neuron loaded with Biotin (green) and stained for lamin B (red). Scale bar: 10 µm.

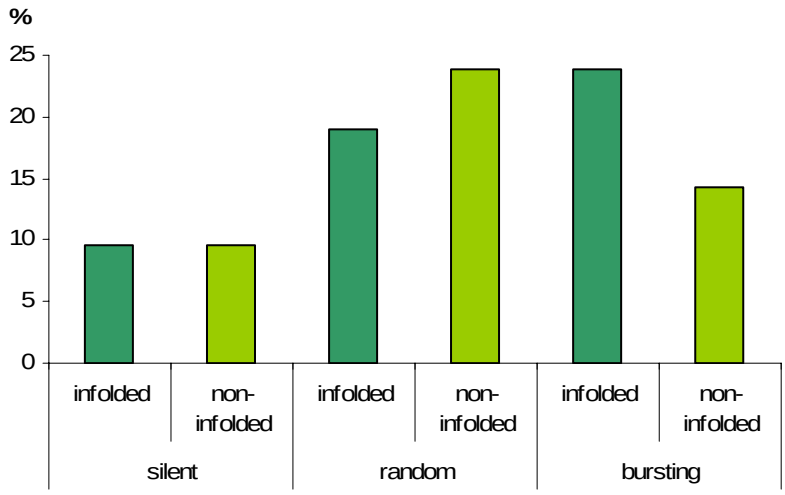

Figure 35. *Patched neurons were divided into 3 groups: neurons showing no basal activity, neurons with random activity and those with recurrent bursting activity. These data were correlated to the presence of infoldings in the neurons patched.*

4.1.11. Functional assays – the immediate early gene cfos

Although calcium imaging and EPSC recordings did not lead to any conclusion, it still remained possible that transcriptional mechanisms are enhanced by infolded nuclei. As the generation of infoldings takes approximately 1 h, a possible candidate for differential regulation was the immediate early gene cfos. Therefore neurons were stimulated with bicuculline, fixed at different time points of 1 h, 2 h and 3 h and immunostained for lamin B and cfos. Z stacks were recorded by confocal microscopy and projections of images analysed with ImageJ. The projections of lamin B were used to distinguish infolded from control cells and cfos projections were analysed densitometrically for protein upregulation. Figure 36 shows a typical example of differential cfos regulation upon bicuculline stimulation. There seemed to be a fast increase 2 h after bicuculline in infolded cells, although after 1 h as well as after 3 h no difference between both groups could be observed. This indicates that infoldings might enhance the kinetics of gene transcription within a limited time window, while non-infolded nuclei take longer to reach the same levels.

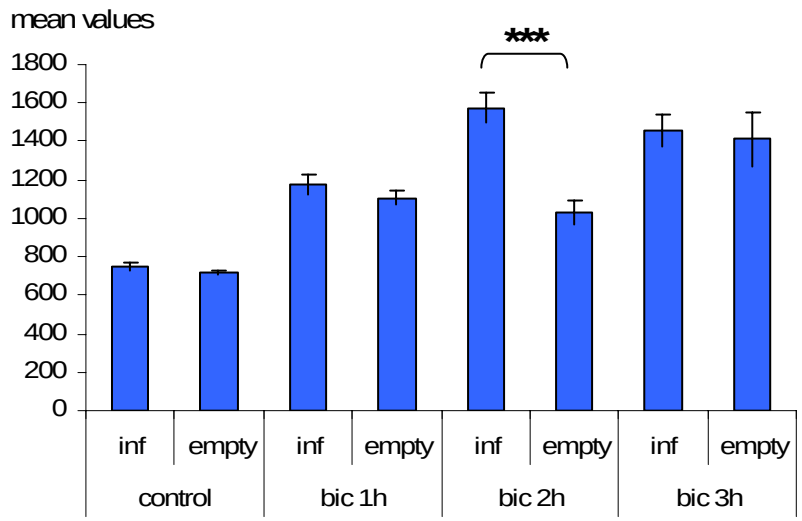

Figure 36. *Cfos is differentially regulated 2 h after bicuculline. Neurons stimulated with bicuculline (bic, 50 µM) were fixed at three distinct time points of 1 h, 2 h and 3 h. Infoldings were identified in projections of confocal stacks of lamin B stainings and protein levels of cfos quantified densitometrically in confocal projections. Cfos levels increased from control coverslips up to 3 h after bicuculline and the levels were equal in infolded and non-infolded cells at 0 h, 1 h and after 3 h. Only 2 h after bicuculline treatment the average cfos level in infolding-positive neurons was significantly higher than in non-infolded nuclei. Statistical significant differences (two-tailed unpaired T-Test) compared to control nuclei are indicated with asterisks (*** $p < 0{,}001$). Error bars: SEM.*

4.1.12. Nuclear pore complexes

Nuclear pores are essential for all processes in the nucleus, as they allow passage of large molecules by directed transport as well as diffusion of small molecules and calcium ions, thereby indirectly participating in gene transcription. As it is shown in this thesis that the surface area of the nuclear membrane increases during infolding of the nuclear membrane, the question remained what would happen to the density of nuclear pore complexes in infolded nuclei in comparison to non-infolded ones. Therefore densitometric analysis of nuclear pore complexes was performed using an antibody directed against nuclear pore complex proteins in infolded and non-infolded cells. Confocal z stacks of nuclei stained by immunofluorescence were recorded and summed into a projection and analysed densitometrically using ImageJ (NIH). A representative experiment of nuclear pore quantifications is shown in Figure 37. In unstimulated neurons the amount of nuclear pores is higher in infolded nuclei compared to non-infolded (14,7 %) due to the larger surface area of the nuclear membrane. Induction of new infoldings in previously not infolded nuclei within one hour does give rise to an enlargement of the nuclear membrane but the number of nuclear pores has not yet risen. Therefore the average number of pore complexes in infolded nuclei after 1 h bicuculline

treatment decreases compared to unstimulated neurons, resulting in a smaller difference between infolded and non-infolded nuclei (1,4%).

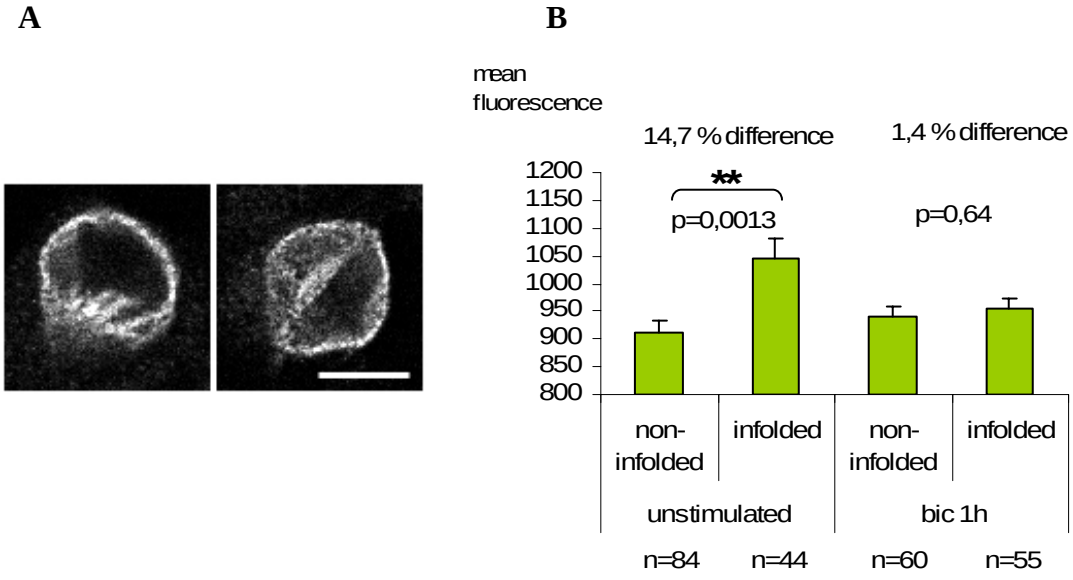

Figure 37. *Induction of nuclear infoldings precedes insertion of nuclear pore complexes. A) Confocal images of nuclei stained for nuclear pore complexes. Scale bar: 10 µm. B) Nuclear pore complexes were visualized by immunofluorescence and pore densities were quantified densitometrically by confocal microscopy. Infolded nuclei in unstimulated neurons in average contain more nuclear pore complexes than non-infolded nuclei (14,7 %). After induction of infoldings with bicuculline (bic, 50µM) the nuclear membrane has enlarged but the number of pore complexes in newly infolded nuclei is still low. This results in a decrease in average difference of pore densities between infolded and non-infolded nuclei (1,4 %). Statistical significant differences (two-tailed unpaired T-Test) are indicated with asterisks (** p < 0,005). Error bars: SEM.*

4.2. Excitotoxicity

A recent publication has shed light onto the functional difference between synaptic and extrasynaptic NMDA receptors in neuronal cell death (Hardingham et al., 2002). However, although potent inhibitors against NMDA receptors are existing, a blocker specific for extrasynaptic NMDA receptors is currently not available, due to the close homology of synaptic and extrasynaptic NMDA receptors.

The construction of such an inhibitor would allow a precise analysis of the different signaling cascades downstream of synaptic and extrasynaptic NMDA receptors in primary cultured neurons.

4.2.1. Stimulation of extrasynaptic NMDA receptors induces necrotic cell death

For the construction of a potent inhibitor several assays were set up based on a previous publication {Hardingham, 2002 #22} and kinetics of cell death characterized in our primary hippocampal neurons.

The induction of excitotoxicity, mediated by extrasynaptic NMDA receptors, was measured in a cell death assay based on a nuclear staining in fixed cells. Healthy and pyknotic cells, an early sign of necrotic cell death (Fujikawa et al., 2000) were quantified by fluorescence microscopy (Figure 38). Figure 39 shows an increasing amount of necrotic cell death starting at NMDA concentrations of 20 µM. Between 30 µM and 50 µM are sufficient to virtually kill all neurons within three to four hours. The spontaneous amount of dead cells in culture can be variable, due to the fact that the cultures used are prepared on a weekly basis and therefore may vary in density.

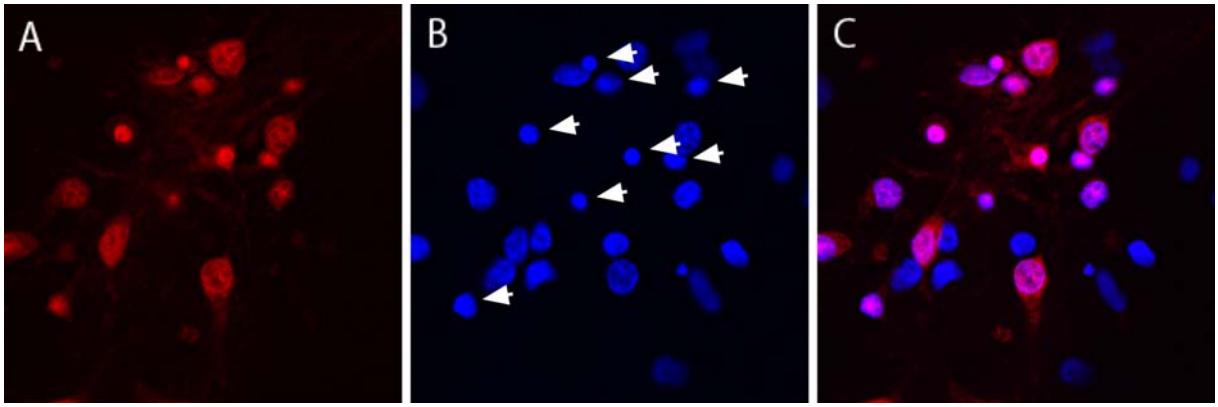

Figure 38. *Fluorescence-based cell death assay. A) Neuronal staining using a monoclonal NeuN antibody. B) DNA staining with Hoechst 33258. Necrotic nuclei are marked by arrowheads. C) Overlay of A) and B).*

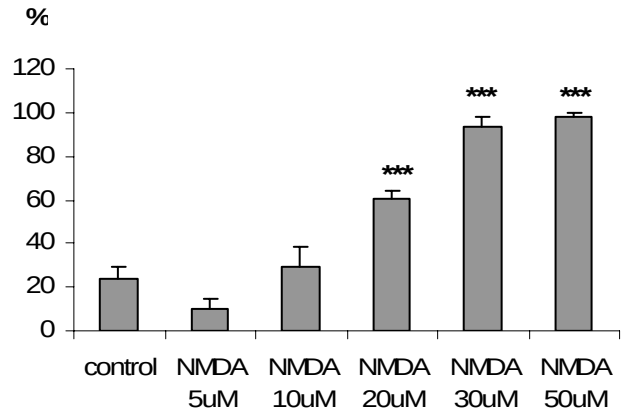

Figure 39. *The amount of cell death induced is dependent on the concentration of NMDA. Different concentrations of NMDA were applied for 5 min to activate extrasynaptic NMDA receptors in hippocampal neurons. The amount of necrotic cell death was quantified after 4 h with a fluorescence-based cell death assay by quantification of pyknotic nuclei. Statistical significant differences (two-tailed unpaired T-Test) are indicated with asterisks (*** $p < 0{,}001$). Error bars: SEM.*

Even very short incubation times with 50 µM NMDA have profound effects on the induction of necrotic cell death. Figure 40 shows NMDA treatments for 10 sec, 30 sec and 5 min and subsequent washout of NMDA and replacement with fresh medium. Incubation times as low as 10 sec are already sufficient to induce excitotoxicity in about 60 % of all neurons, while an almost maximal rate is achieved after 5 min.

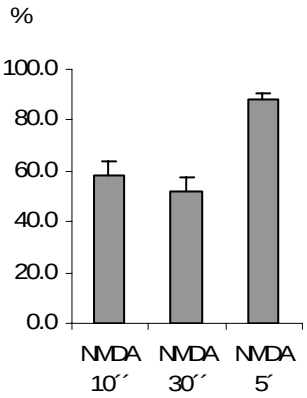

Figure 40. *Even very short bath application of NMDA induces excitotoxicity. Different durations of 50 µM NMDA application were compared and death quantified after 4 h. Error bars: SEM.*

To confirm that the type of cell death induced with NMDA is necrotic and not apoptotic, cleaved caspase-3 was used as an indicator of apoptotic cell death. Cells were treated for 3 h with 30 µM NMDA, resembling an induction of excitotoxicity, as well as for 22 h after which time a cleavage of caspase-3 should be visible if the induction of

apoptosis would occur under these conditions. The broad spectrum kinase inhibitor Staurosporine (STS) was used as a positive control for apoptotic cell death (Figure 41). The cascade leading to apoptotic cell death was not induced with toxic concentrations of NMDA at any time point, while after treatment with STS a cleavage of pro-caspase-3 is evident already after 3 h. A bicuculline treatment for 5 min was included as negative control. Bicuculline leads to activation of synaptic NMDA receptors and enhancement of cell survival (see below).

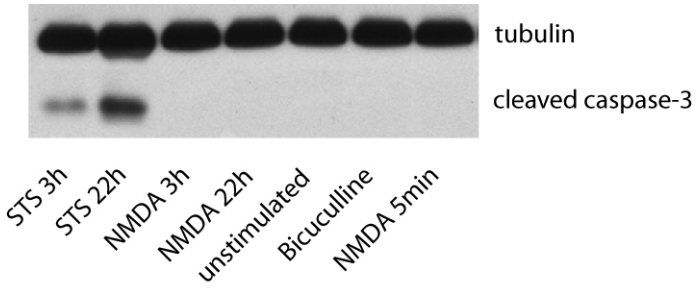

Figure 41. *Excitotoxicity is a necrotic form of cell death. Cells were treated with 30 µM NMDA for 3 h or 22 h and samples were analysed by Western Blotting. A cleavage of pro-caspase 3, an early indicator of apoptosis, could not be observed. Treatment with the broad spectrum kinase inhibitor Staurosporine (STS, 200 nM) resulted in a weak caspase 3 signal after 3 h and an stronger one after 22 h.*

Figure 42 shows a typical calcium trace after application of 50 µM NMDA. Cells immediately and irreversibly depolarize to give rise to an intracellular calcium plateau of 1 to 1,5 times the dissociation constant (kd) within the cell.

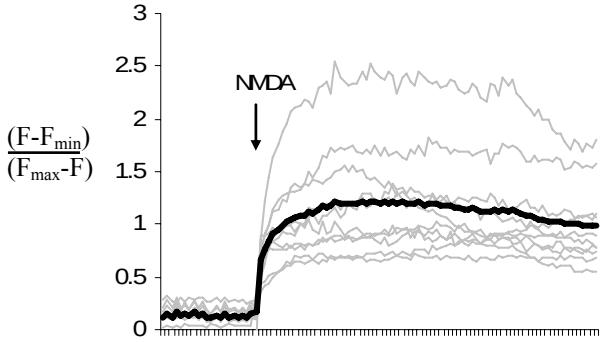

Figure 42. *NMDA bath application leads to a calcium plateau induced by opening of synaptic and extrasynaptic NMDA receptors. Neurons were loaded with the cell permeable fluorescent calcium sensor fluo-3 (Molecular Probes) and fluorescence intensities were recorded by confocal time lapse microscopy. Addition of 50 µM NMDA lead to an immediate increase from basal level to a calcium plateau of 1,2 times the dissociation constant of calcium (kd).*

Another early indicator of cell death is the loss of mitochondrial membrane potential $\Delta\Psi_m$ (Keelan et al., 1999). Therefore neurons were loaded with the mitochondrial dye Rhodamine 123 and leakage into the cytoplasm was measured during application of 50 µM NMDA (Figure 43). Toxic concentrations of NMDA induce almost maximal depolarizations of mitochondria which seem to progress slower than the influx of calcium observed with fluo-3 (see Figure 42).

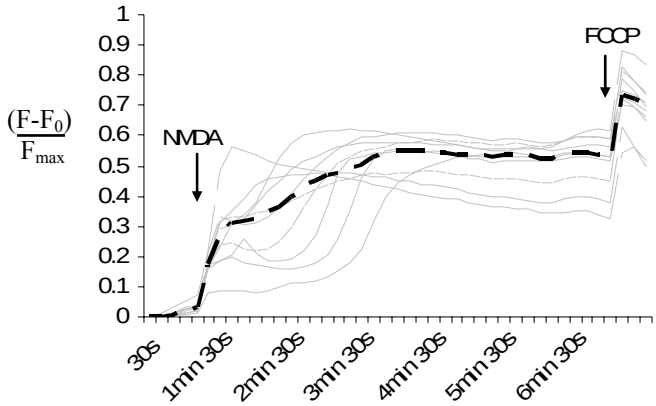

Figure 43. *NMDA bath application of 50 µM leads to depolarization of the mitochondrial membrane potential. Neurons were loaded with the cell permeant fluorescent dye Rhodamine 123 (Rh123) that is incorporated by the cell into mitochondria. 50 µM NMDA bath application lead to a depolarization of the mitochondria. Fluorescence increase by leakage of Rh123 into the cytosol was recorded by confocal microscopy.*

4.2.2. Stimulation of synaptic NMDA receptors enhances cell survival

While activation of all NMDA receptors triggers cell death, specific activation of only the synaptic NMDA receptors has an opposing effect. Synaptic NMDA receptors were activated by addition of the $GABA_A$ receptor antagonist bicuculline, which leads to a synchronous synaptic activity in the neuronal network and subsequent influx of calcium via synaptic NMDA receptors (Figure 44). Figure 45 shows that pre-incubations with bicuculline do partially protect neurons against NMDA-induced toxicity, and that this effect is time-dependent. While only a few hours of pre-treatment seem to have small or even no effects on cell death, a pre-treatment for 25 h proved to optimally protect neurons from excitotoxicity, lowering cell death from about 90 % to 60 %.

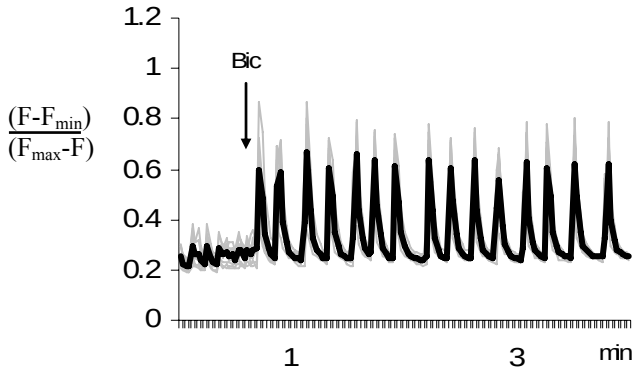

Figure 44. *Confocal time-lapse recordings of global calcium transients during exposure to bicuculline (bic, 50 µM).*

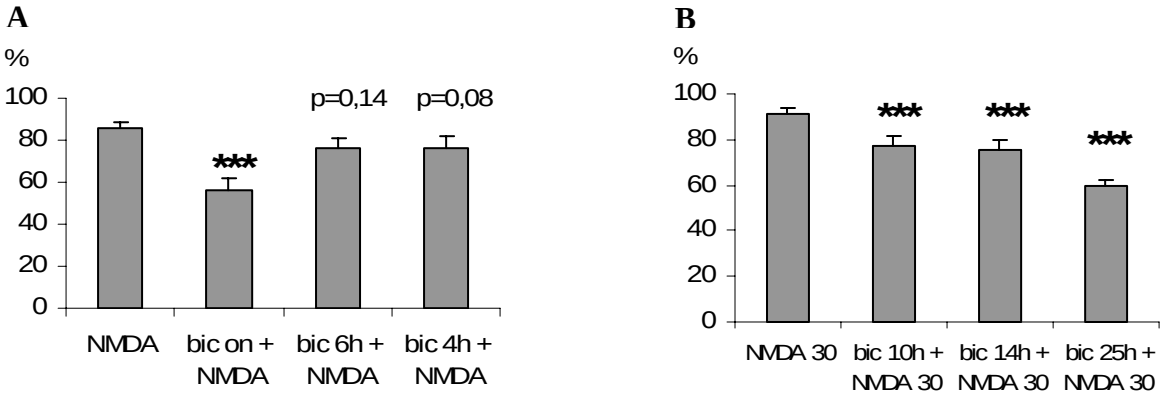

Figure 45. *Treatment with bicuculline protects against excitotoxic cell death. A) Neurons treated with bicuculline (bic, 50µM) for 4 h or 6 h showed no protection against NMDA-induced cell death, whereas treatments over night significantly protected against excitotoxicity. B) Bicuculline is protective after 10 h and the protection increases with longer incubation times up to 25 h. Statistical significant differences (two-tailed unpaired T-Test) are indicated with asterisks (*** $p < 0,001$). Error bars: SEM.*

Further enhancement of this effect was confirmed by combined application of bicuculline with 4-AP (4-Aminopyridin), a weak potassium channel blocker which leads to a slight depolarization and has been shown to increase the frequency of bicuculline-induced bursting (Pokorska et al., 2003) and confers to an increased protectivity compared to applications of bicuculline alone (Hardingham et al., 2002) (Figure 46).

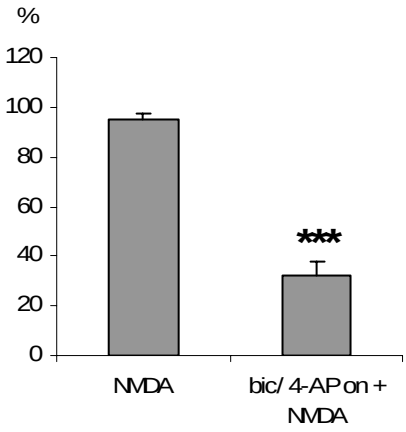

Figure 46. *Enhancement of bicuculline-induced calcium influx through synaptic NMDA receptors by 4-AP (2,5 mM) also resulted in an increased protection against excitotoxicity. Statistical significant differences (two-tailed unpaired T-Test) are indicated with asterisks (*** $p < 0,001$). Error bars: SEM.*

A minor reduction in the NMDA-induced calcium plateau compared to control cells can be seen in Figure 47 after an over night pre-incubation with bicuculline.

However, recordings of the mitochondrial membrane potential did not reveal any difference in depolarization after pre-incubation (Figure 48). Under control conditions as well as after bicuculline pre-treatment over night, mitochondria depolarize to equal levels after application of NMDA. The different kinetics of individual cells in both experiments may be due to slight differences in the density of the neuronal network and have no effect on the final level of depolarization. Differences in the kinetics of mitochondrial membrane depolarization have been regularly observed in all experiments with cultures of 11-13 days in vitro and have been reported before (Keelan et al., 1999).

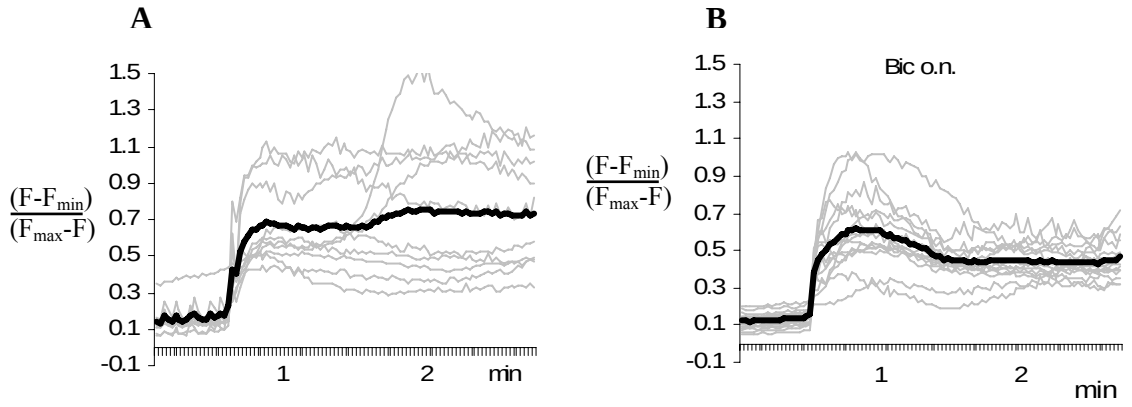

Figure 47. *NMDA-induced calcium influx after an over night incubation with bicuculline (50 µM) (B) is slightly decreased compared to a control experiment in the same culture that had not been pretreated (A). Average calcium signals are shown in bold.*

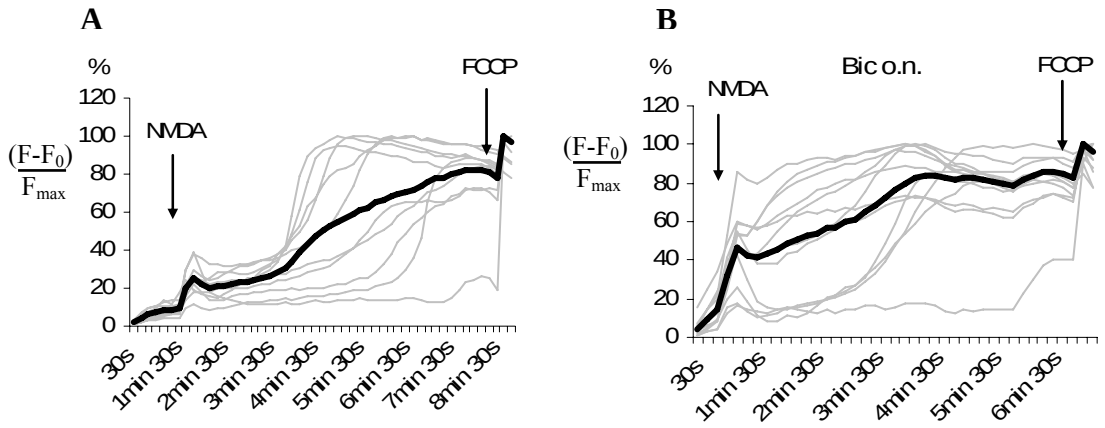

Figure 48. *Depolarization of the mitochondrial membrane potential was not different in cultures treated over night with bicuculline (50 µM) (B) compared to untreated cultures (A). Traces are normalized to maximal depolarization with the chemical uncoupler FCCP. Average traces are shown in bold.*

As expected, acute application of bicuculline during measurements of the mitochondrial membrane potential did not reveal any changes of $\Delta\Psi_m$, excluding any direct effect onto mitochondria (Figure 49).

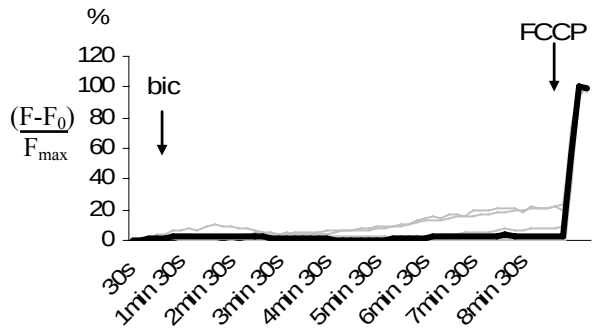

Figure 49. *Stimulation of synaptic NMDA receptors does not lead to depolarization of mitochondria. Traces are normalized to maximal depolarization with the chemical uncoupler FCCP.*

4.2.3. Extrasynaptic NMDA receptors and MAP kinases

MAP kinases like ERK1/2 or p38 can be transiently phosphorylated upon glutamate or NMDA bath application but prolonged opening of extrasynaptic NMDA receptors leads to a subsequent decay of the phosphorylation state. The MAP kinases therefore follow the deactivation kinetics of CREB, that has been shown to be dephosphorylated by a yet unidentified shut-off mechanism (Hardingham et al., 2002).

The dephosporylation of ERK1/2 is slowly progressing within the first 5 min, with a reduction almost to baseline after 15 min, while p38 is dephosphorylated much quicker with an almost 50 % reduction 5 min after NMDA bath application (Figure 50).

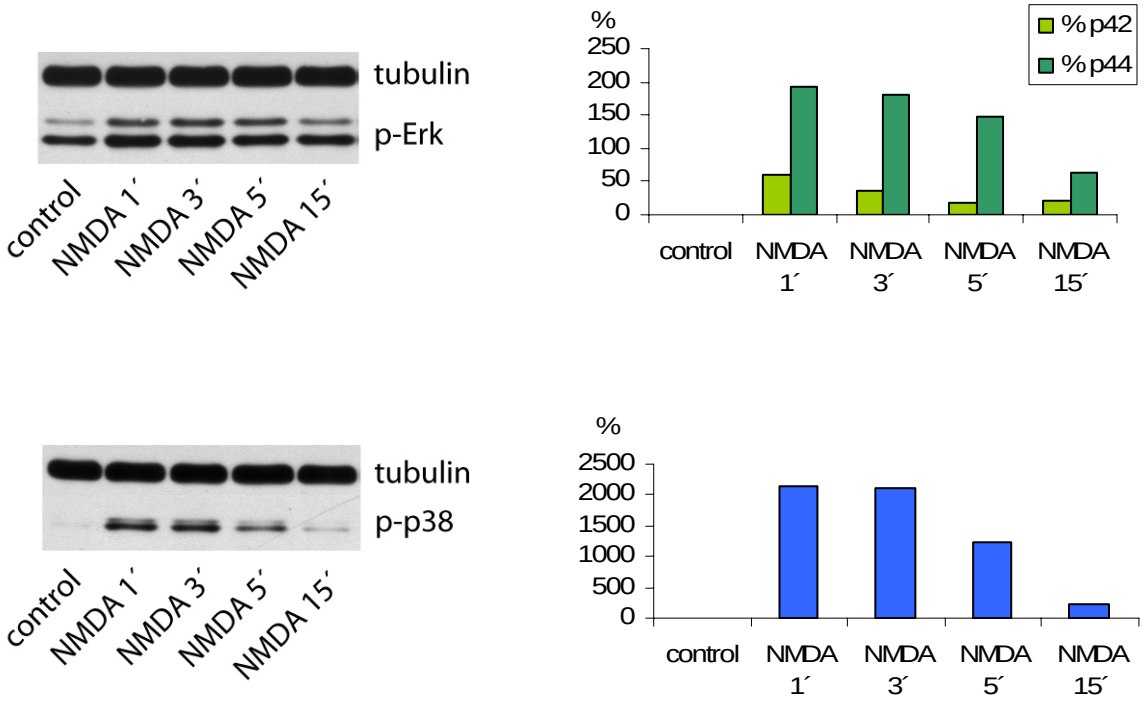

Figure 50. *Dephosphorylation of ERK1/2 (p44/p42) and p38 upon NMDA bath application. NMDA (30 µM) was applied for the times indicated. The dephosphorylation of p38 progresses much faster than the one of ERK1/2.*

4.2.4. CREB shut-off

Stimulation of synaptic NMDA receptors by bicuculline induces a robust phosphorylation of CREB, while extrasynaptic NMDA receptors initiate a general CREB shut-off mechanism that is dominant over CREB-activating pathways (Hardingham et al., 2002).

However, the intracellular pathways involved in this shut-off remain unknown. To investigate which molecules might be involved, CREB phosphorylation was induced by the L-type channel agonist FPL 64176 (5 µM). 5 min after induction by FPL, 50 µM NMDA were applied for 15 min to induce a CREB shut-off. Several inhibitors were tested by a pre-incubation of 1 h for an effect on the shut-off mechanism (Figure 51a). The inhibitors tested involved a combined inhibition of calcineurin and protein phosphatase 2B by FK506 and Cyclosporin A respectively, the nitric oxide synthase inhibitor L-NAME, the peroxynitrite scavenger MnTBAP, the free radical scavenger TEMPO in combination with the antioxidant catalase and ascorbic acid as antioxidant with Trolox, a derivative of Vitamin E (Vergun et al., 2001).

Unfortunately none of the molecules tested so far seems to be involved in the CREB shut-off pathway. However, it has to be remarked that there is presently no indicator for the proper functioning of the inhibitors used, therefore concentrations were applied according to the literature.

The MAP kinase ERK1/2 showed a similar dephosphorylation following NMDA bath application like CREB. However, treatment with available inhibitors had no effect on the shut-off mechanism (Figure 51b)

A

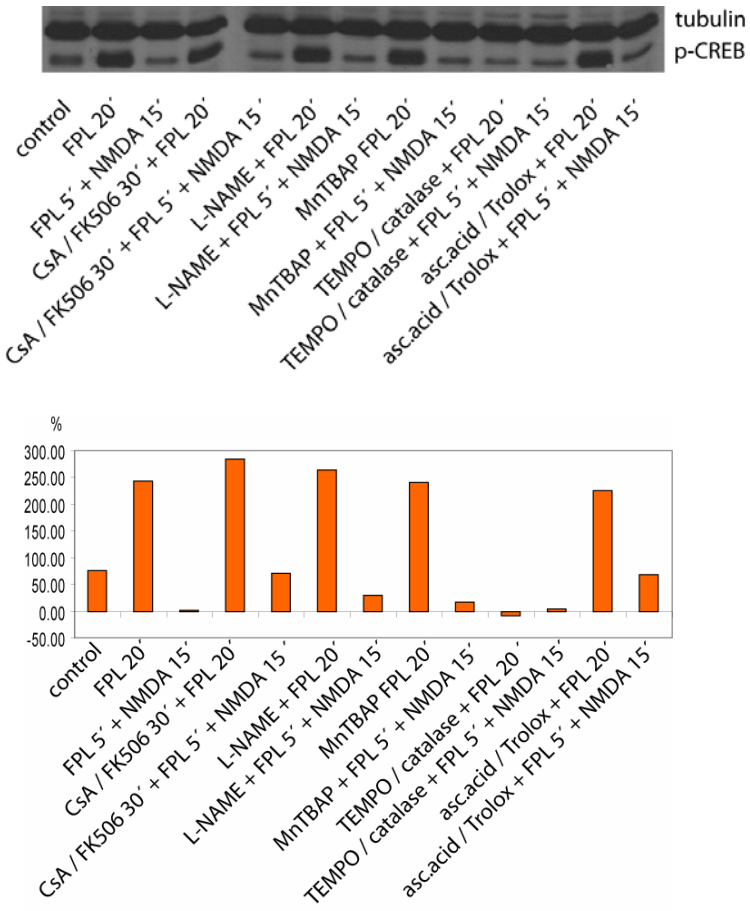

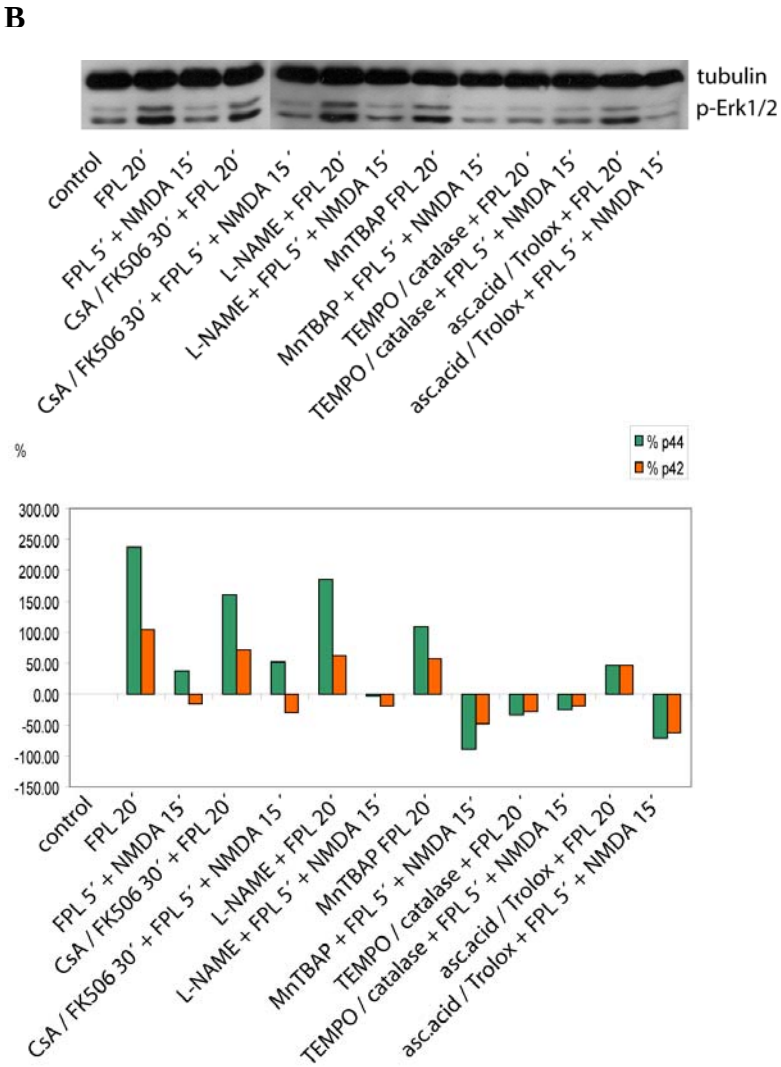

Figure 51. *A) CREB phosphorylation was achieved by opening of L-type channels with FPL 64176 (5 µM). The CREB shut-off was induced by NMDA bath application for 15 min. None of the inhibitors applied had any impact on the dephosphorylation of CREB.*
B) Phospho-ERk1/2 follows a shut-off mechanism equal to CREB, but the inhibitors tested had no effect on the Erk shut-off.

4.2.5. Specific blockade of NR2B reduces excitotoxicity

As it was reported that extrasynaptic NMDA receptors contain more NR2B than NR2A subunits (Tovar and Westbrook, 1999), the tool of choice for specific blockade of extrasynaptic NMDA receptors would be a NR2B-specific antagonist. One such antagonist is a small non-competitive inhibitory peptide derived from the deep sea snail conus, called Conantokin-G (conG) (Klein et al., 1999).

To effectively block all NR2B-containing NMDA receptors and to enable the peptide to reach all receptors by passive diffusion, cells were pre-incubated with 1 µM conG for 30 min before subsequent measurements. Figure 52 shows complete blockade of calcium influx upon addition of 50 µM NMDA in the presence of conG. A comparison of the effects of glutamate and NMDA on excitotoxic cell death shows no significant difference between both agonists and the induction is almost completely blocked in the presence of conG (Figure 53). Application of conG at 1 µM is even sufficient to prevent excitotoxic effects of NMDA concentrations as high as 1 mM (Figure 54).

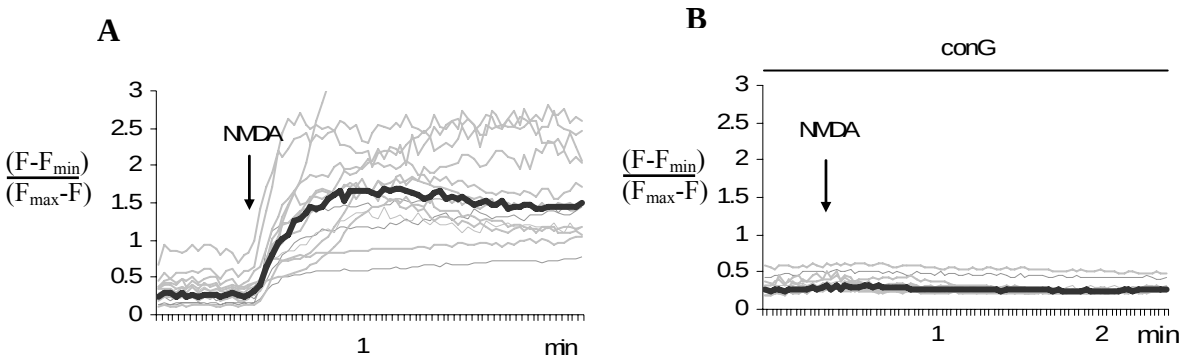

Figure 52. ***A)*** *NMDA bath application of 50 µM lead to a opening of synaptic and extrasynaptic NMDA receptors and a quick rise of calcium levels to a plateau.. B) The presence of 1 µM conG completely abolished this rise in calcium.*

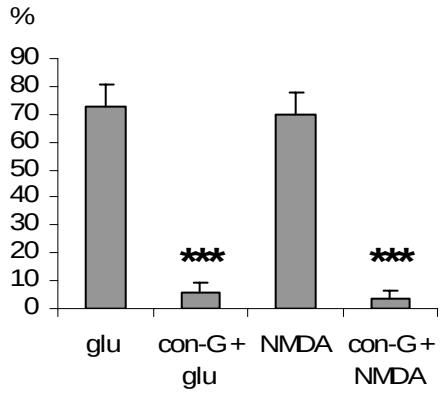

Figure 53. *The effect of conG (1 µM) was compared in bath application of NMDA (50 µM) and glutamate (50 µM). In both cases blockade of the NR2B subunit lead to reduction of necrotic cell death from 70 % to 10 %. Statistical significant differences (two-tailed unpaired T-Test) are indicated with asterisks (*** $p < 0{,}001$). Error bars: SEM.*

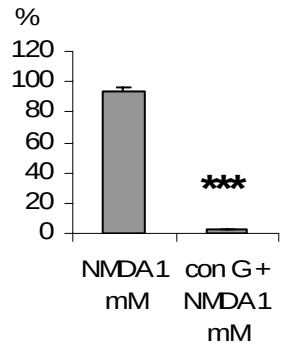

Figure 54. *A reduction in the potency of conG could not be observed at high concentrations of NMDA (1 mM). Statistical significant differences (two-tailed unpaired T-Test) are indicated with asterisks (*** p < 0,001). Error bars: SEM.*

ConG is also capable of preventing mitochondrial depolarization upon NMDA application (Figure 55), with the slow increase in fluorescence most likely being a unspecific depolarization due to suboptimal pH conditions during the measurement in living cells.

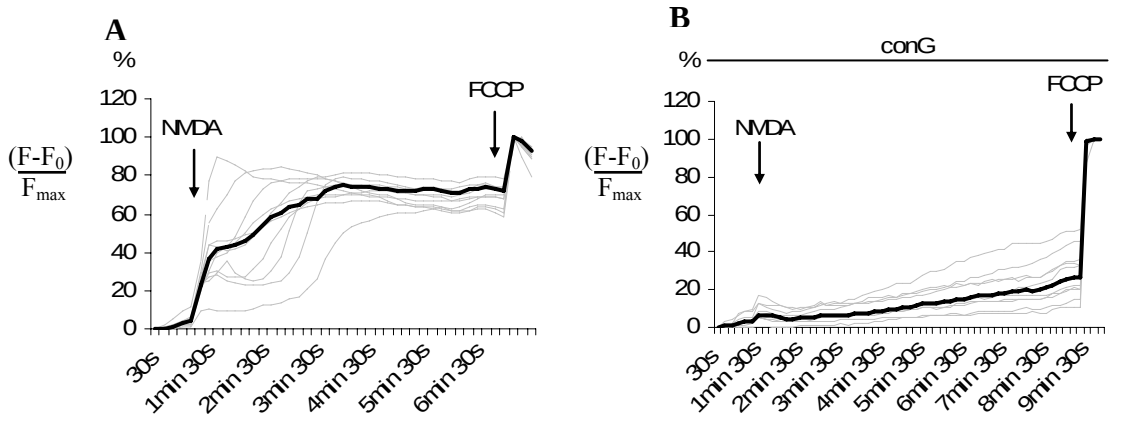

Figure 55. ***A)*** *NMDA bath application (50 µM) leads to an almost complete loss of the mitochondrial membrane potential within 4 min.. B) In presence of 1 µM conG this loss was significantly inhibited.*

Specific blockade of synaptic NMDA receptors has previously been achieved by activating synaptic NMDA receptors with bicuculline and subsequent blockade with the NMDA receptor open channel blocker MK-801. The only NMDA receptors remaining unblocked thereafter are the extrasynaptic NMDA receptors (Hardingham et al., 2002). To verify the blockade of extrasynaptic NMDA receptors by conG, synaptic NMDA receptors were blocked like described above. In addition to MK-801 the AMPA receptor blocker CNQX was added to prevent any calcium influx via non-NMDA receptors during the measurement (Figure 56). Application of 50 µM NMDA thereafter induced a calcium plateau that resulted from opening of previously unblocked extrasynaptic NMDA receptors. In a parallel experiment in the presence of 1 µM conG

the NMDA response was completely absent, indicating a complete blockade of extrasynaptic NMDA receptors by conG, as observed during a combined application of NMDA and the NMDA receptor blocker APV.

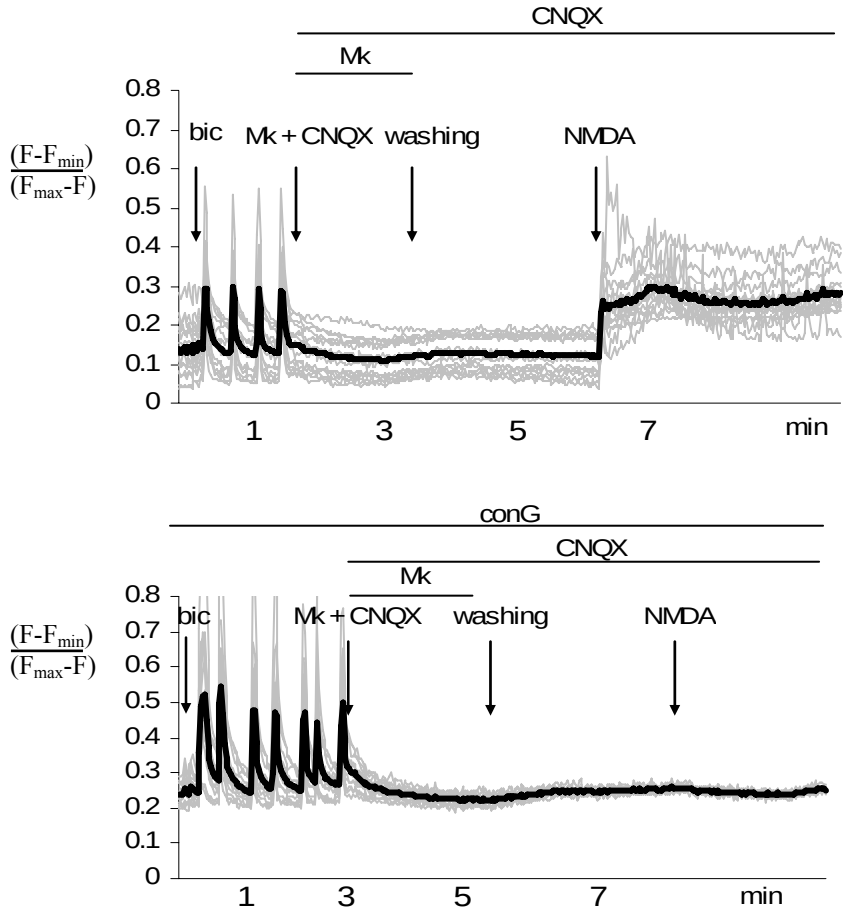

Figure 56. *Calcium imaging of differential activation of NMDA receptors. Synaptic NMDA receptors were activated by bicuculline (bic, 50 µM) and subsequently blocked by Mk-801 (Mk, 20µM) and CNQX (50µM). After washout of MK-801 all remaining unopened NMDA receptors were opened by 50 µM NMDA bath application in the presence of CNQX. This lead to opening of the previously unopened extrasynaptic NMDA receptors. The same stimulation protocol in the presence of 1 µM conG completely blocked calcium influx through extrasynaptic NMDA receptors as did the presence of APV (500 µM).*

Addition of 4-AP after induction of synaptic activity by bicuculline resulted in an increase in the intracellular calcium baseline mediated by synaptic NMDA receptors. Addition of 50 µM NMDA on top of this baseline resulted in a further rise in calcium to an elevated calcium plateau. The presence of conG does not attenuate the synaptically mediated baseline, but completely prevents the NMDA-mediated rise in calcium (Figure 57). Surprisingly, in the presence of conG there seems to be a transient depolarization

after addition of 4-AP, which drops to a calcium baseline comparable to control experiments within 1 min.

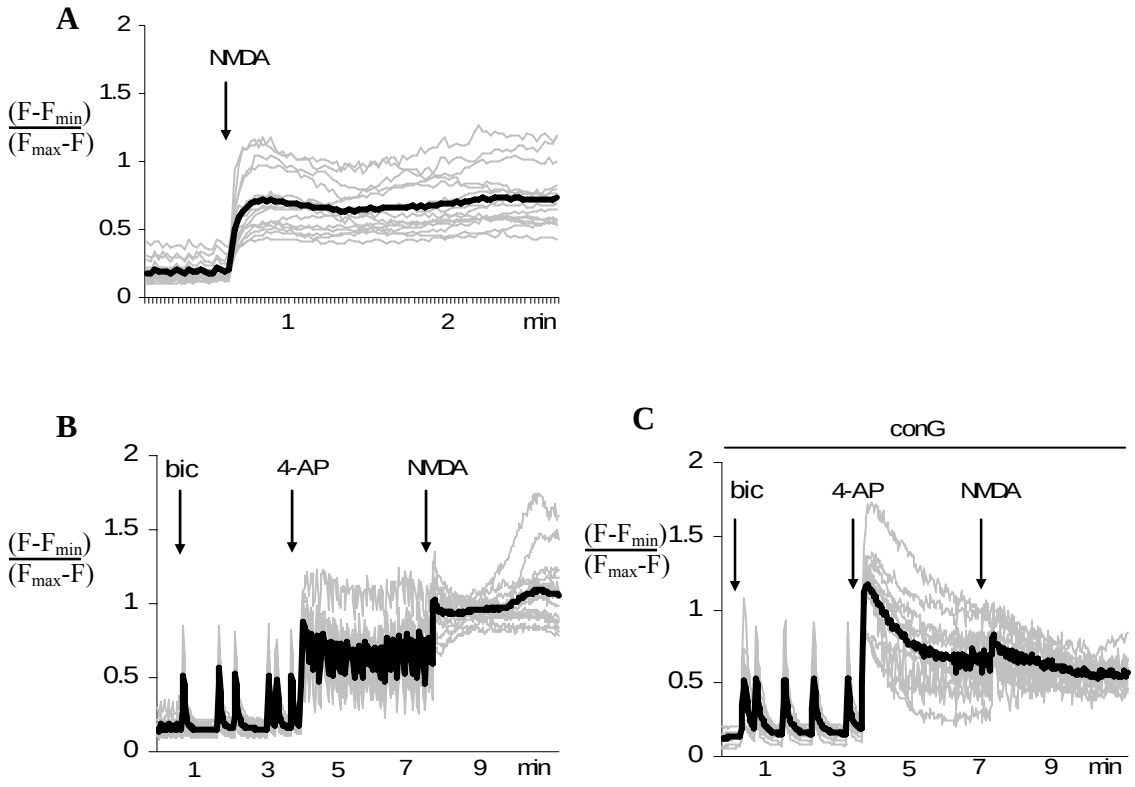

Figure 57. *Effect of conG on glutamate bath application. A) Control experiment: Induction of a calcium plateau with NMDA (50 µM). B) A calcium plateau mediated by calcium influx through synaptic NMDA receptors was evoked with bicuculline (50 µM) and 4AP (2,5 mM). NMDA bath application resulted in a further rise of calcium levels to a plateau. C) This was abolished in the presence of conG (1 µM).*

4.2.6. Patch clamp analysis of conG effects

The potency of conG was tested on a single cell level by patch clamp recordings by Peter Bengtson (IZN). Figure 58 shows examples of EPSC (A) and puff responses (B) in the absence of 1 µM conG. The Conantokin blocked a large fraction of the synaptic EPSC as well as the majority of the puff response. This indicates that both synaptic and extrasynaptic NMDA receptors contain NR2B subunits, which are all inhibited by conG.

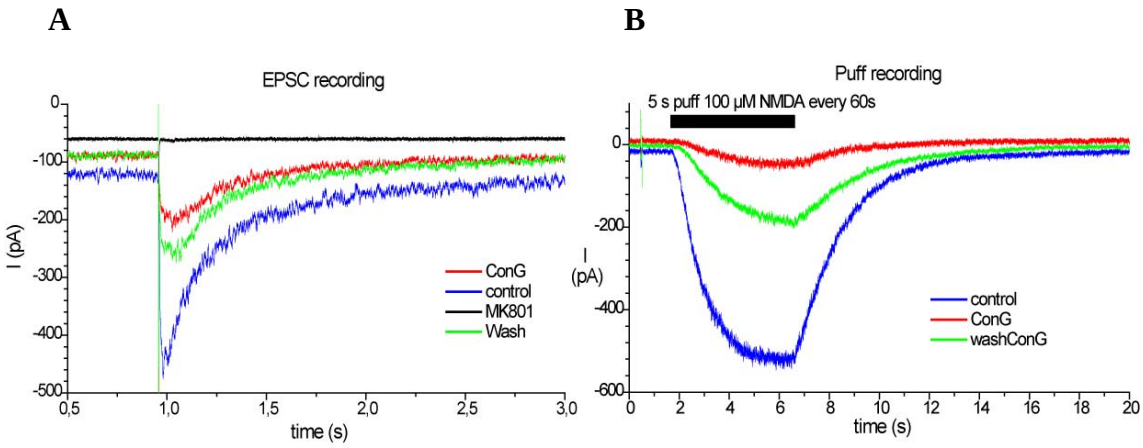

Figure 58. *EPSCs (A) and puff responses (B) were recorded in the presence of conG (1 µM) with a holding potential of -60 mV.*

4.2.7. Development of a NR2B antagonist specific for extrasynaptic NMDA receptors

4.2.7.1. Modification of conG

Antagonists against the NR2B subunit will not be sufficient to solely block extrasynaptic NMDA receptors as the NR2B subunit is also a component of NMDA receptors residing within the synapse. As a method to prevent conG from entering the synapse and therefore to specifically block NMDA receptors outside the synapse I attempted to bind conG peptides to commercially available beads. These beads should have a mean diameter greater than the synaptic cleft (20-40 nm), which would prevent any conG molecules attached to it from interacting with receptors within the synapse (Figure 59). Subsequent application of NMDA would then only lead to opening of NMDA receptors within the synapse, activating pro-survival and LTP-inducing events, while death-inducing stimuli from extrasynaptic NMDA receptors would be blocked.

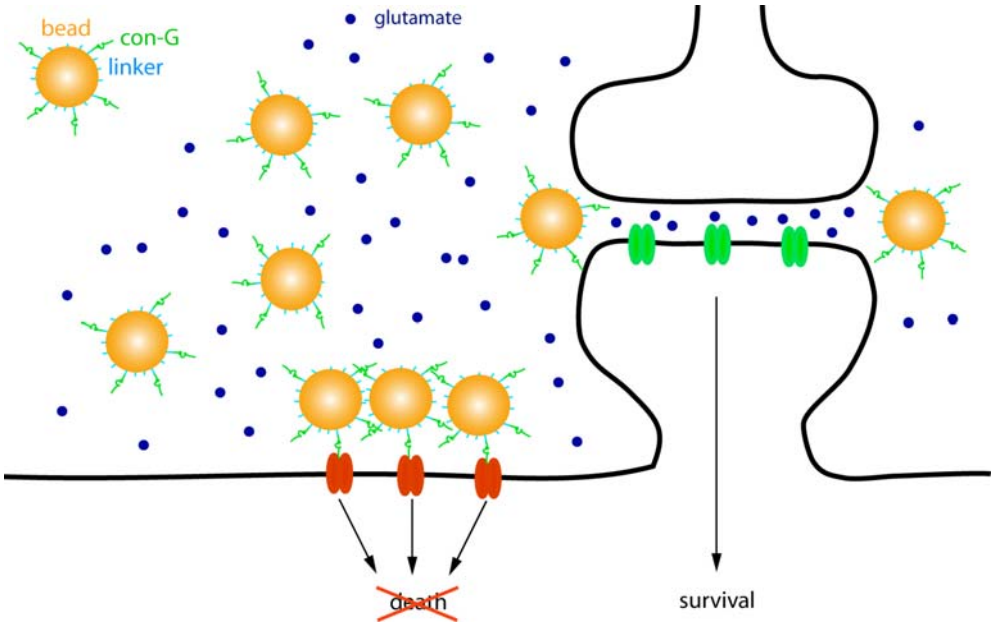

Figure 59. *Specific blockade of extrasynaptic NMDA receptors should be achieved by coupling Conantokin-G to beads. Thereby death-inducing pathways of extrasynaptic NMDA receptors (red) would not be activated by NMDA or glutamate bath application while survival-promoting mechanisms mediated by activation of synaptic NMDA receptors (green) would not be impaired.*

As the potency of conG to block NMDA receptors was shown to be impaired after exchanging amino acids at the N-terminus, while the amino acids at the C-terminus were not important for its activity (Castellino and Prorok, 2000), it was assumed that conG would bind to the NMDA receptor with its N-terminus. Therefore addition of amino acids to the C-terminus should not impair its function but allow binding to diverse substrates.

ConG was synthesized with an additional cys residue at the C-terminus (conG-cys) and chemically bound to BSA (Peptide speciality laboratories, Heidelberg), with one BSA molecule containing approximately 17 molecules of conG-cys (personal communication with H.R. Rackwitz, Peptide Speciality Laboratories, Heidelberg). The thiol groups of BSA would allow ether reactions with the cys groups of conG-cys. These complexes should then be coupled to gold beads. The gold beads used had a mean diameter of 90 nm, and would, in combination with several conG-BSA complexes bound to each bead, give a complex greater than the diameter of a synaptic cleft.

conG-cys sequence:

H-Gly-Glu-Gla-Gla-Leu-Gln-Gla-Asn-Gln-Gla-Leu-Ile-Arg-Gla-Lys-Ser-Asn-Cys-Amid

Gla: Gamma-carboxyglutamate

Several experiments were carried out to ensure preservation of the binding properties of conG after linking it to BSA and to test if not the creation of BSA complexes with several conG molecules bound to it would already be big enough to restrict conG from entering the synaptic cleft:

The optimal concentration of conG-BSA was determined by a 1 h incubation on neurons and subsequent addition of 50 µM NMDA for 5 min (Figure 60). Assessment of pyknotic nuclei after 4 h reveals that 3 µg conG-BSA reduces the amount of cell death from 55 % to 35 %, while 15 µg and 30 µg are equally protective with a reduction to 20 % and 25 % respectively. Therefore a concentration of 15 µg was used in all following experiments. All concentrations of the BSA-conG complexes will be given as micrograms, as the exact molecular weight of the BSA-conG complex might differ slightly between molecules.

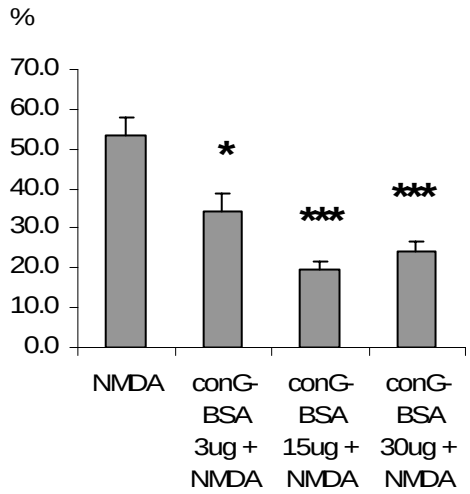

Figure 60. *ConG-BSA blocks necrotic cell death induced by NMDA (50 µM) most efficiently at amounts of 15 µg or higher. Statistical significant differences (two-tailed unpaired T-Test) are indicated with asterisks (* $p < 0,05$; *** $p < 0,001$). Error bars: SEM.*

4.2.7.2. Conantokin-G protects against oxygen-glucose deprivation

To assess the protective properties of conG in a context that is more related to pathophysiological events like ischemia, neuronal cell death was induced by oxygen glucose deprivation (OGD). Therefore, the transfection medium was replaced with glucose-free transfection medium and neurons were kept at 5 % CO_2 and 95 % N_2 in a humidified atmosphere for 4 h. Quantifications of pyknotic nuclei of cells pre-incubated with native conG and BSA-conG show an almost complete protection from cell death compared to control cells (Figure 61).

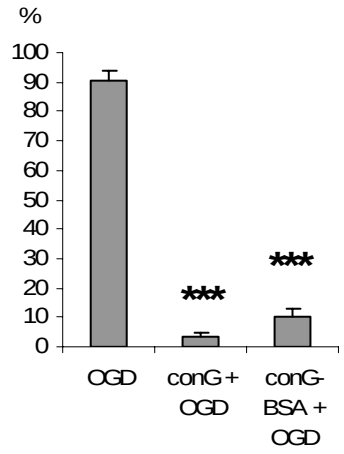

Figure 61. *ConG and conG-BSA equally protect against cell death under hypoxic conditions. Cells were treated with ConG (1 µM) and conG-BSA (15 µg) for 20 min and cell death quantified by immunofluorescence 4 h after oxygen-glucose deprivation (OGD). Statistical significant differences (two-tailed unpaired T-Test) are indicated with asterisks (*** $p < 0{,}001$). Error bars: SEM.*

A potential protection by blockers of certain intracellular pathways that have been shown to be involved in cell death was tested in a similar fashion. Neither of the reagents used showed any protection against OGD, apart from ifenprodil, a blocker of the NR2B subunit of NMDA receptors (Figure 62). However, the blockade of NMDA receptors by ifenprodil is expected to be much weaker than with conG, as the potency of ifenprodil has been shown to be highly dependent on the subunit composition of the NMDA receptor (Tovar and Westbrook, 1999). The effects of native conG and conG-BSA were less pronounced than in previous experiments with a remaining death rate of 30 % to 35 %, which could be due to technical variations. The medium in different experiments could have had traces of O_2 or the density of the culture used could have been different which would effect the severity of the induction of cell death.

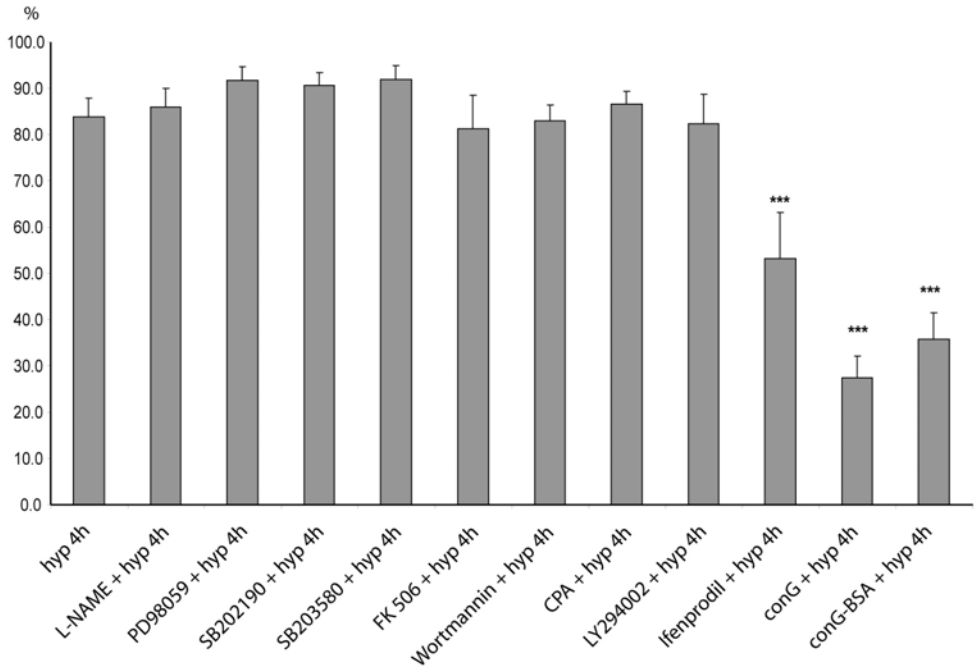

Figure 62. *Analysis of hypoxic cell death (hyp) after OGD. Neurons were treated for 1 h with various pharmacological inhibitors: (L-NAME 0,5 µM; PD98059 50 µM, SB202190 10 µM; SB203580 10 µM; FK506 1 µM; Wortmannin 100 nM; CPA 10 µM; Ly294002 10 µM; Ifenprodil 10 µM; conG 1 µM; conG-BSA 15 µg). Statistical significant differences (two-tailed unpaired T-Test) are indicated with asterisks (*** $p < 0{,}001$). Error bars: SEM.*

4.2.7.3. Colocalization of conG-BSA and synaptic markers

To examine the localization of the conG-BSA complexes, it was synthesized with a different ratio with each BSA molecule containing approximately 10 conG peptides and 7 FITC molecules (Peptide Speciality Laboratories, Heidelberg). These fluorescently labeled conG-BSA complexes were then colocalized by confocal microscopy with the synaptic markers synaptophysin and synapsin I (Figure 63). There was only little colocalization of conG-BSA with the synaptic markers used, with Synapsin I colocalizing slightly more frequently than synaptophysin. Therefore it can be concluded that although conG-BSA is still capable of entering the synaptic cleft, this happens only occasionally and that a majority of the complexes is restricted to the extrasynaptic space.

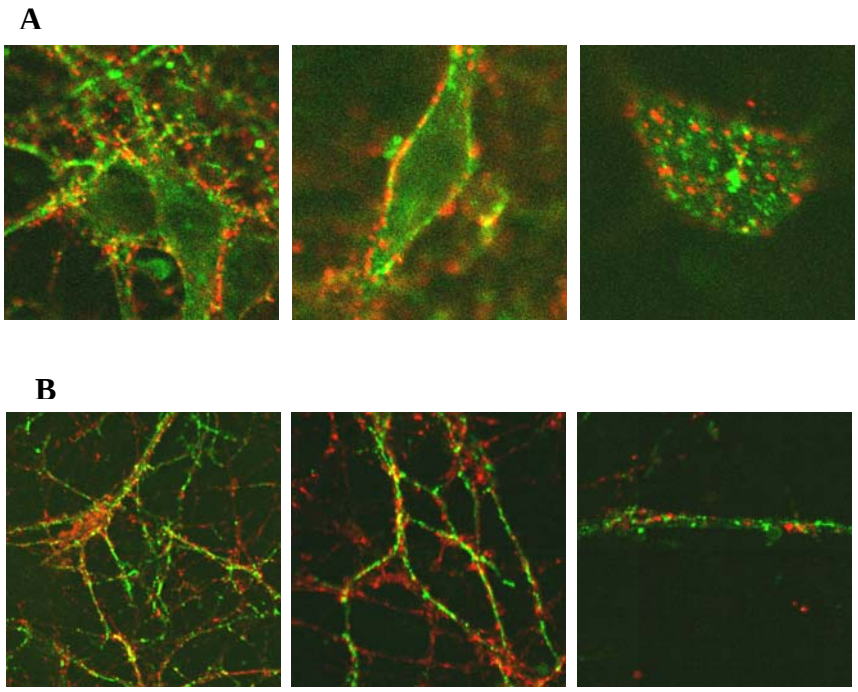

Figure 63. *Colocalization of conG-BSA containing FITC and synaptic markers by confocal microscopy. The conG-BSA complexes (green) only rarely colocalized (yellow) with synaptophysin (A, red) or synapsin I (B, red), indicating that the conG-BSA complexes mainly block extrasynaptic NMDA receptors.*

4.2.7.4. Multi Electrode Array (MEA) recordings

To explore the binding capacities to synaptic NMDA receptors of both native conG and conG-BSA, electrical recordings of entire neuronal networks were performed by MEA recordings. Therefore cultures were plated onto MEAs like usual and pre-treated with conG or one of its derivatives 1 h prior to addition of bicuculline (Figure 64). The peptides were present during the entire experiment. Figure 65 shows that under control conditions stimulation of synaptic NMDA receptors by bicuculline induces an almost maximal response, measured as the percentage of spikes that reside within a burst. After an application of bicuculline for 15 min, bicuculline was removed by a complete medium exchange and the bursting frequency was measured at distinct time points. After washout of bicuculline the neurons on MEAs continued to burst up to 48 h, which has been implicated to induce long term potentiation (LTP) in neurons (Arnold et al., 2004).

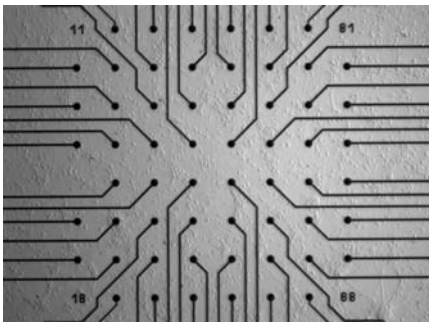

Figure 64. *DIC image of a typical hippocampal cell culture on a Multi Electrode Array (MEA).*

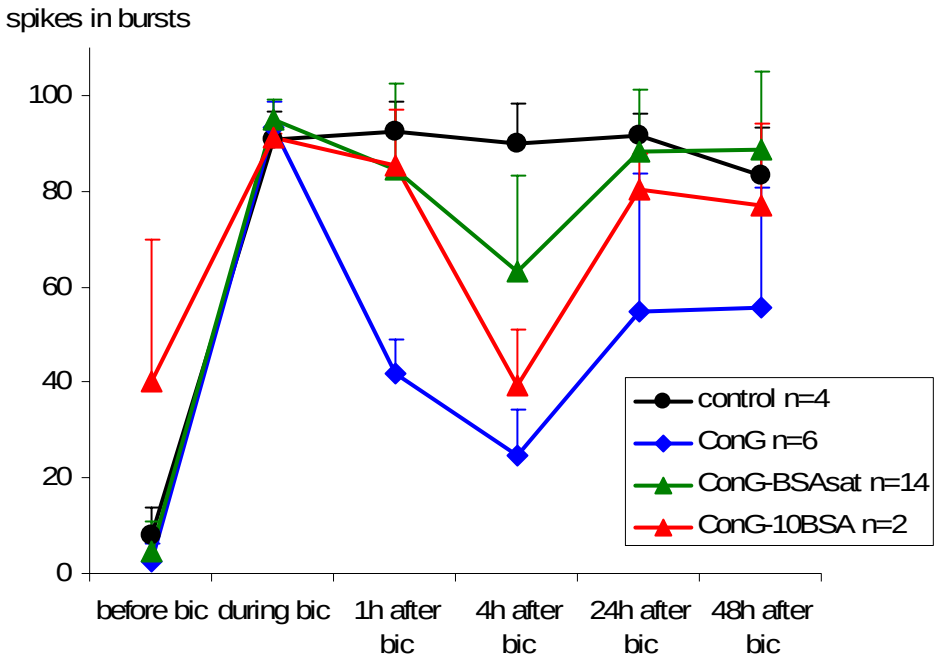

Figure 65. *Comparison of the effects of different variants of conG on the bicuculline-induced burst frequency on MEAs. Control: normal stimulation with bicuculline (50 µM) and MEA recordings at the indicated time points; conG: native conG present during application of bicuculline; conG-BSAsat: BSA with saturating amounts of conG; conG-10BSA: BSA with 10 conG peptides and about 7 FITC molecules. The native conG (blue) has a maximal blocking effect, while the blockade with conG-10BSA (red) is slightly weaker. Synaptic NMDA receptors are only marginally blocked by conG-BSAsat (green).*

In the presence of native conG this burst frequency is also induced to levels comparable to that of control experiments, but after washout of bicuculline it rapidly decays to about 40 % of spikes in bursts after 1 h and to 20 % after 4 h. Surprisingly, a recovery to 50 % can be observed 24 h after washout which is most likely due to recruitment of new and therefore unblocked NMDA receptors into the synaptic cleft. The conG-BSA complex containing 10 conG peptides and additional FITC molecules (conG-10BSA) shows little

impairment of synaptic activity after 1 h, but a blockade that is comparable to native conG after 4 h. The BSA containing saturating amounts (approximately 17) of conG peptides (conG-BSAsat) shows a decrease of spikes in bursts that is significantly lower, decreasing from about 90 % after induction to only 60 % after 4 h. In this case a complete recovery is visible after 24 h, comparable to control conditions.

Therefore it can be concluded that the conG-BSA complexes containing saturating amounts of conG peptides have a much lower ability to block synaptic NMDA receptors than the native conG peptide and even lower than that of conG-BSA complexes containing half-maximal amounts of conG (conG-10BSA). A higher number of conG molecules might increase the size of the complex and thereby decrease its ability to enter the synapse. Another possibility is the high negative charge due to the 5 gamma-carboxyglutamates contained in each conG, which leads to an increase of the overall negative charge of a conG-BSA complex with a growing number of conG molecules attached to it. Therefore it cannot be excluded that the reduced synaptic blockade of conG-BSAsat is not due to electrostatic interactions between the complex and proteins of the plasma membrane and the synaptic cleft.

To determine the ability of conG-BSA to block calcium influx via NMDA receptors the NMDA-induced calcium influx was measured after blockade by conG-BSA (Figure 66).

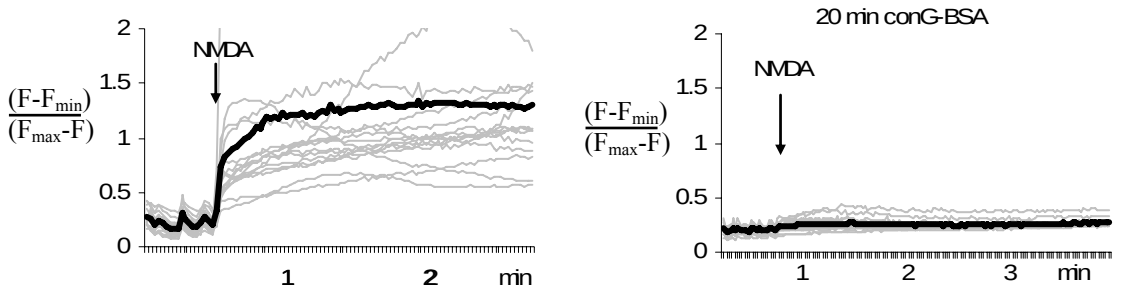

Figure 66. *Calcium imaging of NMDA bath application (50 µM) after different incubation times with conG-BSA.*

In addition to a blockade of calcium influx, the ability to prevent depolarization of the mitochondrial membrane potential was assessed (Figure 67). ConG-BSA almost completely prevents the breakdown of $\Delta\Psi_m$ after a toxic stimulus of 50 µM NMDA.

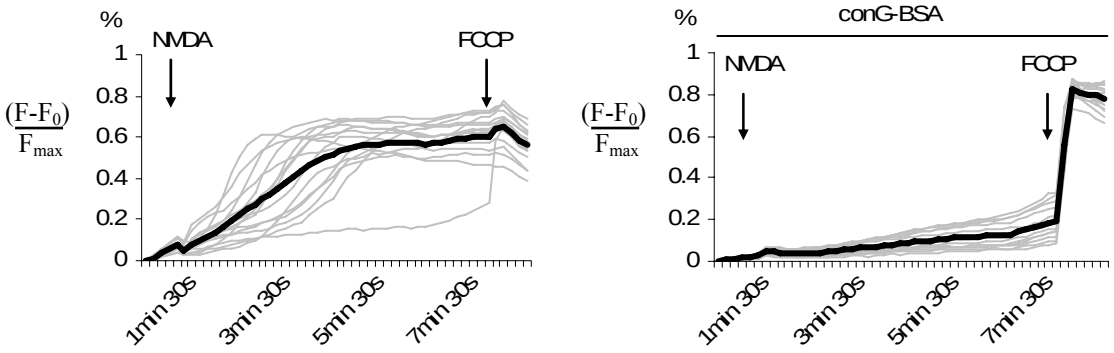

Figure 67. *Measurements of the mitochondrial membrane potential during NMDA bath application after blockade with conG-BSA.*

The neuroprotective effect of conG-BSA is comparable to that of the native form of the peptide, as both reduce necrotic cell death induced by NMDA from 90% to about 15% (Figure 68).

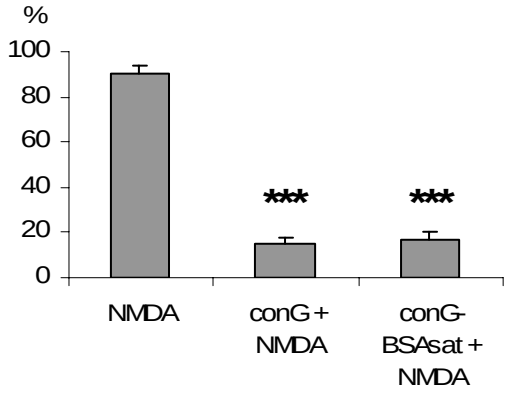

Figure 68. *comparison of the neuroprotective effects of native conG and conG-BSA. Statistical significant differences (two-tailed unpaired T-Test) are indicated with asterisks (*** $p < 0{,}001$). Error bars: SEM.*

To explore the effects of conG-BSA in older cultures which should have a different composition of NMDA receptors (Li et al., 1998), neurons were cultivated to 18 day in vitro (DIV) and synaptic calcium influx induced by bicuculline. Subsequent activation of extrasynaptic NMDA receptors by NMDA gave a calcium plateau of 1,9 x kd compared to about 1,5 x kd in younger cultures (Figure 69). The presence of conG-BSA

severly attenuated this rise, leaving only a minor calcium plateau of about 0,6 x kd, which corresponded to the height of the bicuculline calcium peak.

The protective effects of native conG and conG-BSA were equally efficient at 20 DIV with a reduction of cell death from 100 % to about 40 % (Figure 70), although this protective effect was significantly lower than the one observed between 10-13 DIV.

It is therefore assumed that neurons either suffer from general degeneration after three weeks in culture or that not all of the extrasynaptic NMDA receptors at this age contain the NR2B subunit.

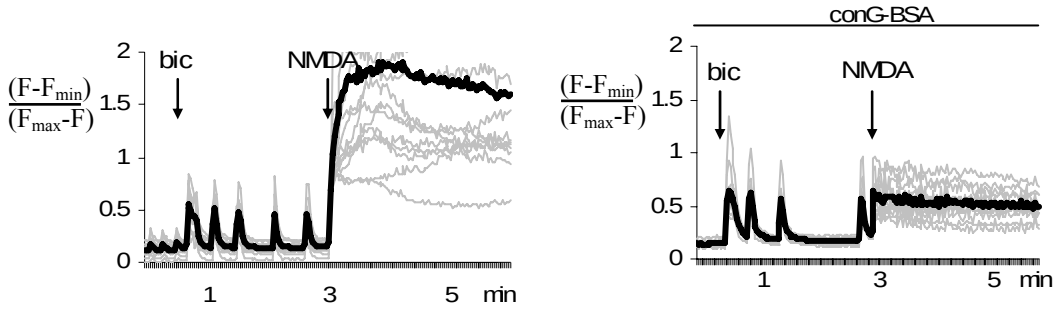

Figure 69. *Calcium imaging in neurons at 18 days in vitro (DIV). ConG-BSA largely prevents calcium influx during NMDA bath application (50 µM), although a minor calcium plateau still appeared.*

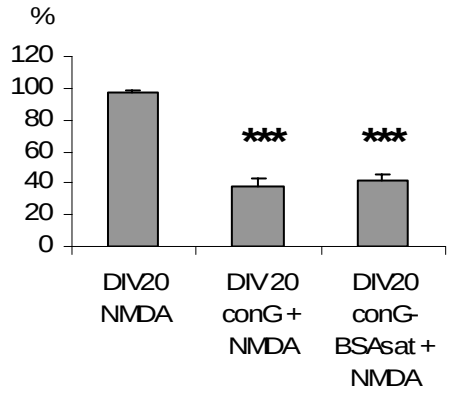

Figure 70. *The neuroprotective effects of conG (1 µM) and conG-BSA (15 µg) were comparable in cultures of 20 days in vitro (DIV). Statistical significant differences (two-tailed unpaired T-Test) are indicated with asterisks (*** $p < 0,001$). Error bars: SEM.*

4.2.7.5. Coupling of conG-BSA to gold beads

As the experiments above have shown that conG can be modified and even bound to other proteins like BSA without severe impairment of its function, the next step was to attach it to beads that would prevent it from entering the synaptic cleft.

For this purpose a coupling protocol was set up to irreversibly attach conG-BSA to the surface of gold beads.

To test for aggregation of beads, a simple gold aggregation test was performed (Cordes et al., 1997):
The gold-peptide mixture was added to a cuvette with an equal volume of 10 % NaCl (0,5 M) and the absorbance measured after 5 min at 580 nm. As long as the absorbance would still decrease (visible as a color change from red to blue) there are insufficient amounts of protein in the mixture as the gold beads still aggregate in the presence of high NaCl.

The amounts of conG-BSA needed to coat most, if not all, of the gold beads were determined experimentally and lead to the following protocol:
Gold beads were washed by slow centrifugation and titurated to pH 9,0 with K_2CO_3. The washed beads were incubated with 30 µl conG-BSA [3,3 µg/µl] for 3 h at RT, slowly shaking. Unbound peptides were removed by slow centrifugation. The loose pellet was resuspended in borax buffer [2 mM], washed once more and finally resuspended in 500 µl CO_2-independent SGG medium containing 1 % BSA.

Unfortunately the gold beads aggregated under all conditions tested, although conG-BSA-beads aggregated slower than those coupled with a control peptide attached to BSA (RFLKTNLKGSKITRC).
Borax buffer was replaced by different wash buffers, including different PO_4 buffers, buffer A and finally CO_2-independent SGG medium containing BSA at 1 %. Although the presence of BSA in the medium prevented aggregation of the gold beads, it most likely also competed with conG-BSA for available gold surface. Higher centrifugation speeds rapidly lead to formation of undissolvable bead pellets.

A final protocol for coupling to gold beads included the incubation of 1 ml of washed beads with 100 µg of conG-BSA [3,3 µg/µl] for 3 h, slowly shaking. The beads were centrifuged twice and resuspended each time in 1 ml buffer A. After a final centrifugation step the loose pellet was resuspended in 500 µl CO_2-independent SGG medium containing 1 % BSA. The aggregation test showed no sign of the formation of gold aggregates.
The resuspended pellet as well as the supernatant from the last purification step were tested in a cell death assay after preincubation for 1 h (Figure 71). Although the

resuspended pellet containing the conG-BSA-gold beads significantly protected neurons from excitotoxicity, the supernatant was even more protective. This indicates that a major fraction of conG-BSA did not bind to the gold beads.

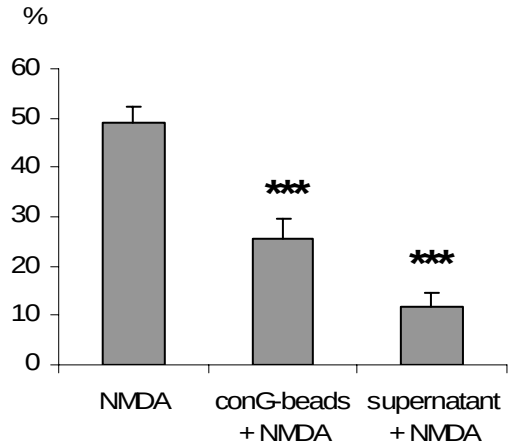

Figure 71. *effect of conG-BSA-coated gold beads on excitotoxicity. Supernatant and pellet of the conG-BSA and gold bead coupling reaction were both protective, indicating an incomplete binding of the peptide to beads. Statistical significant differences (two-tailed unpaired T-Test) are indicated with asterisks (*** $p < 0{,}001$). Error bars: SEM.*

To reliably purify conG-BSA-coated beads the resuspended pellet was purified in a glycerol gradient ranging from 30 % to 90 %, with a 100 % cushion at the bottom of the tube. After 1 h centrifugation of 4000 rpm at 4°C, three fraction were taken from the gradient and measured for the presence of proteins:

fraction	**OD595**
upper	2,295
middle	0,027
lower	0,536

Although the majority of protein seemed to be present in the upper fraction, it was clearly visible by eye that the majority of gold beads, identified by a red band, was at the edge to the 100 % cushion at the bottom of the tube. Protein estimations from that fraction showed that there was obviously some conG-BSA still bound to beads, but the majority seemed to fall off at the beginning of the gradient purification or was never stably attached to the beads. A possible explanation for this would be that the carboxy groups in of the gamma-carboxyglutamates interfere with electrostatic interactions between BSA and gold, thereby preventing the formation of a stable coupling reaction.

4.2.7.6. Patch-clamp analysis of the effects of conG-gold beads

The potency of conG-BSA coupled to gold beads was tested on a single cell level by patch clamp recordings by Peter Bengtson (IZN). Figure 72 shows example of EPSCs and puff responses in the presence of 30 µg/ml conG-BSA. The Conantokin blocked a large fraction of the synaptic EPSC, while the puff response was blocked less efficiently than by the native peptide. This indicates that conG-BSA complexes might be less effective due to steric hindrance on the gold beads.

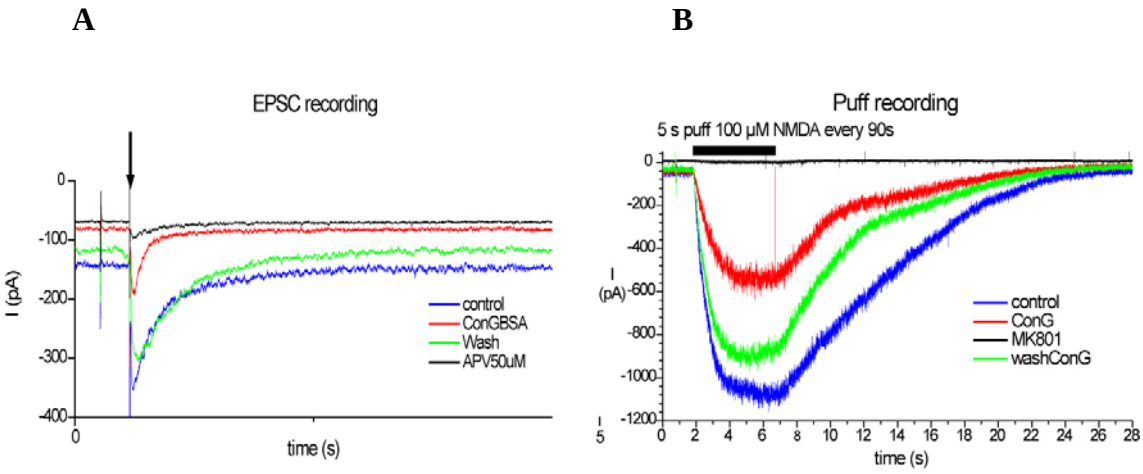

Figure 72. *EPSCs (A) and puff responses (B) were recorded in the presence of conG-BSA (30 µg/ml) with a holding potential of -60 mV.*

4.2.7.7. Coupling of conG to latex beads

As coupling of conG to gold beads was not successful, the next approach was to change the type of beads used. The choice fell on aliphatic/amine latex beads (IDC) which should be chemically coupled to a conG containing a cysteine residue at the C-terminus (conGcys) by a crosslinker called sulfo-SMCC. This crosslinker contains an NHS ester which coupled to primary amines at the bead surface and a maleimide group binding to the sulfhydryl groups of cysteine of conG.

The amount of protein for a complete labelling of the surface of these beads was indicated by the supplier as the ratio of the amount for saturating 1 µM particles and the size of the beads, which were 80 nm. Therefore 62,5 µg conGcys would be needed for a complete saturation. The coupling reactions were carried out with much lower concentrations of conG-cys to prevent electrostatic interactions of the negatively charged peptides.

The amount of beads used for labelling was 250 µl latex beads, corresponding to a weight of 6 mg and 6,25 µg conGcys, being 10 % of the amount needed for complete labelling of the bead surface.

The beads were washed in MES buffer and the chemical crosslinker sulfo-SMCC added for the first reaction for 1 h at RT. After various washing steps in MES buffer conGcys was added for 3 h at RT. The solution was afterwards washed in MES buffer several times and resuspended in transfection medium.

After adding these potential conG-latex beads to neurons, large aggregates were observed by light microscopy. A further coupling attempt with subsequent sonication of the final bead suspension for 15 min at 55°C lead to dissolvation of the aggregates. Preincubation of neurons with these aggregates for 1 h and subsequent addition of 50 µM NMDA, however, did not show any protective effect of the labelled latex beads (Figure 73).

This might be due to remaining aggregates after sonication that are too small to be observed by light microscopy.

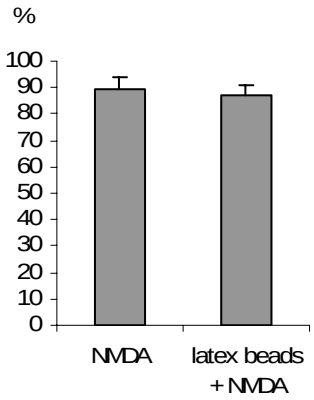

Figure 73. *ConG coupled to latex beads did not show any protective effect during NMDA bath application (50 µM). Error bars: SEM.*

4.2.7.8. Coupling of conG to beads via a myc tag

A further attempt for attachment to beads was taken with a conG peptide containing a myc tag at the C-terminus, connect via a gly linker (MW 3847,7):

H - Gly-Glu-O-O-Leu-Gln-O-Asn-Gln-O-Leu-Ile-Arg-O-Lys-Ser-Asn-Gly-Gly-Gly-Gly-Gly-Glu-Gln-Lys-Leu-Ile-Ser-Glu-Glu-Asp-Leu-Asn - $CONH_2$ (Amide)

An additional Asn residue was added to the C-terminus of the myc tag recognition sequence to facilitate the recognition by the antibody.

To examine if conG containing a myc tag at the C-terminus was still capable of inhibiting the NMDA receptor, a cell death assay was performed by incubating conGmyc for 30 min at different concentrations. A concentration of 1 µM only marginally lowered the amount of cell death, while 5 µM and 10 µM were equally potent and reduced cell death from 100 % to about 10-15 % (Figure 74).

The NMDA-induced calcium plateau was significantly decreased with conGmyc at 1 µM, while cell death was completely prevented at 5 µM and 10µM (Figure 75).

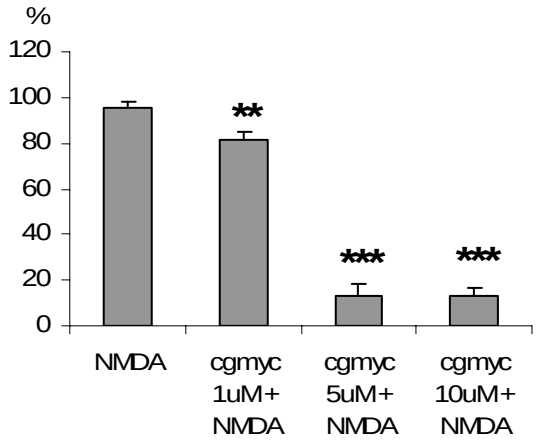

Figure 74. *Comparison of the protective effects of different concentrations of conG-myc. Statistical significant differences (two-tailed unpaired T-Test) are indicated with asterisks (** p < 0,005; *** p < 0,001). Error bars: SEM.*

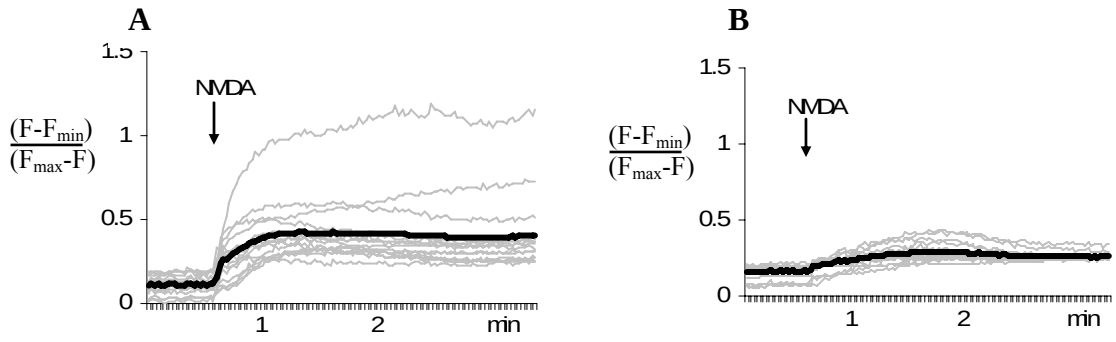

Figure 75. *Effect of conG-myc on NMDA-induced (50 µM) calcium influx. A) calcium imaging in the presence of 1 µM conGmyc B) calcium imaging in the presence of 5 µM conG-myc*

A comparison of native conG, conGcys and conGmyc showed that the potency of the antagonist slightly decreased with increasing length of the c-terminal tag. However, even with a tag as long as myc a decrease of cell death from 100 % to 10 % could be achieved (Figure 76).

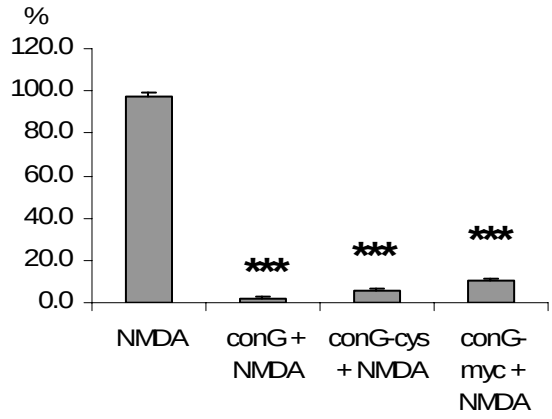

Figure 76. *Comparison of the neuroprotective effects of native conG (1 µM), conG-cys (1 µM) and conG-myc (5 µM) during 50 µM NMDA bath application. Statistical significant differences (two-tailed unpaired T-Test) are indicated with asterisks (*** p < 0,001). Error bars: SEM.*

To attach conGmyc to gold beads, 20 µl [1mM stock] were incubated for 2 h with 1 ml of a monoclonal α-myc tag antibody (clone 9E10, 0,3 mg/ml). To get rid of unbound conGmyc the complexes were dialysed overnight at 4°C against PBS and another 1 h against CO_2-independend SGG to obtain the complexes in an appropriate buffer for incubation on cells.

However, efforts to remove the unbound peptides by dialysis were not successful, as a negative control containing only native conG was still protective in a cell death assay after dialysis. This could be due to the extreme negative charge of the peptide. Usage of other dialysis tubings gave equal results.

To confirm that at least in principle a binding of the antibody to conGmyc can take place, conGmyc was analysed by Western Blot analysis in comparison to a control protein containing a myc tag (Figure 79). Even after high overdevelopment of the blot there was no signal visible in low molecular range where conGmyc was expected to appear. Detection with commercial or a home-made α-myc antibody from hybridoma cells gave equal negative results as did detection of conGmyc by immunofluorescence.

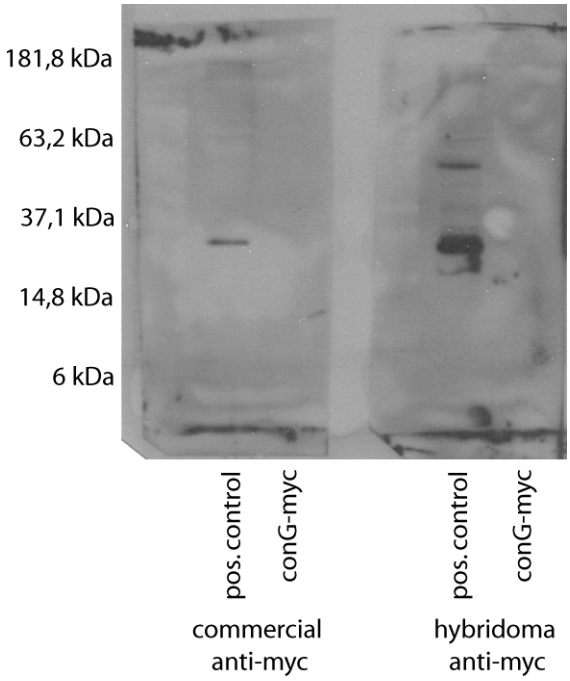

Figure 79. *Unsuccessful detection of conG-myc by Western Blotting. The commercial (Left) as well as home-made (Right) 9E10 antibody against myc tag did detect a positive control protein containing a myc tag, but not the conG-myc peptide (expected at ~4 kDa).*

For unknown reasons the myc-tag added to conG was not detectable by α-myc antibodies, which again could be due to the negative charge of the peptide and the corresponding conformation. This might lead to masking of the epitope and thereby prevent binding of the antibody.

4.2.7.9. Coupling of conG-biotin to streptavidin beads

As the chemical coupling reaction to latex beads turned out to be critical regarding the many washing steps needed, which most likely lead to loss of material, a next approach was the direct coupling of biotinylated conG to streptavidin-coated beads.

The approximate binding capacity of streptavidin-beads was given by the manufacturer as being 3 µg/mg for BSA (65 kDa) and 2,5 µg/mg for BlgG (150 kDa). Interpolation of these data lead to an approximate capacity of 3,375 µg/mg for conG-biotin.
The amount of beads used for 1 coupling reaction was 30 µl with a total weight of 28,29 mg. The amount of conG-biotin needed to completely saturate the binding sites of these beads is 95,48 µg, corresponding to 34,6 µl of the 1 mM stock of conG-biotin.
To prevent a saturation of these beads which would lead to an excess of unbound peptides in the solution, the amount of conG-biotin was kept well below the calculated capacity. Several attempts were carried out ranging from 1 µl to 10 µl of conG-biotin (2,76 µg to 27,6 µg conG-biotin).

To prevent electrostatic hindrance of the heavily charged peptides on the bead surface, biocytin (lysine-biotin) was added in during the coupling reaction. This has a slightly positive charge and should therefore compensate for the negative charges of conG-biotin.

A rough estimation resulted in a capacity of the beads of 4,6 µg biocytin. In a coupling reaction with 30 µl beads this would lead to saturation at 130,1 µg of biocytin, corresponding to 130 µl of a 1 mM stock.

Several coupling reactions and combinations of different concentrations of conG-biotin peptides, biocytin molecules and beads were used. The reactions were carried out in transfection medium, biocytin (if any) and conG-biotin were pre-mixed in the medium. Subsequently the beads were added dropwise while stirring the solution with a magnet. The reaction mixture was incubated for 30 to 45 min and filled to 500 µl with transfection medium. This final solution was then incubated on neurons for 1 h before addition of NMDA. The purpose of this simplified coupling protocol was to remove any purification steps and unsuitable buffers from the reaction mixture and to prevent the loss of beads.

The assessment of cell death was in most cases done by simple light microscopy in cell culture, as necrotic neurons can be simply identified without the need to perform immunofluorescent stainings.

The biotinylated conG (conG-biotin) was tested for its potency to protect against excitotoxicity in a cell death assay (Figure 80). Concentrations of 1 µM, 5 µM or 10 µM were equally potent in protection. The concentrations used for coupling to streptavidin beads were therefore 1 µM and 5 µM.

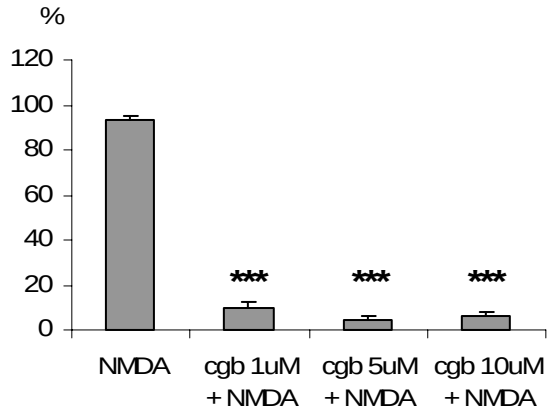

Figure 80. *Biotinylation of conG does not affect its potency. Concentrations of 1 µM, 5 µM and 10 µM are equally potent in preventing excitotoxicity by NMDA (50 µM). Statistical significant differences (two-tailed unpaired T-Test) are indicated with asterisks (*** $p < 0,001$). Error bars: SEM.*

The results with all ratios of peptides to beads were negative and showed no impact on cell death. A possible explanation for this was the density of the neuronal network: as the exact amount of extrasynaptic NMDA receptors is unknown, it might be possible that many of the receptors within the neuronal network are not accessible by the relatively large beads to which conG-biotin was attached. Therefore the cell culture was modified to get a network consisting of much less neurons than usual, reducing the likelyhood that the majority of extrasynaptic NMDA receptors are inaccessible to the beads.

In short, cortical cells were plated onto dishes. At DIV 1 and DIV 2 these were washed with PBS at 4°C to remove any neurons, generating a pure glial cell culture. At DIV 7 hippocampal neurons were dissected and plated onto the glial cell layer at a very low density (Figure 81). These neurons formed a neuronal network in which synaptic activity could be induced by bicuculline (Figure 82) and which was therefore regarded as a fully functional "low density" neuronal network.

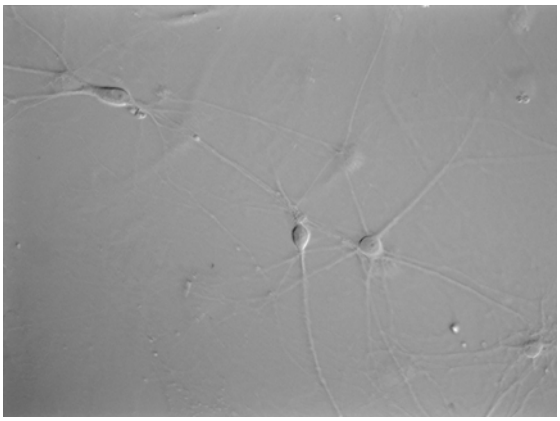

Figure 81. *Low density culture of hippocampal neurons at DIV 11.*

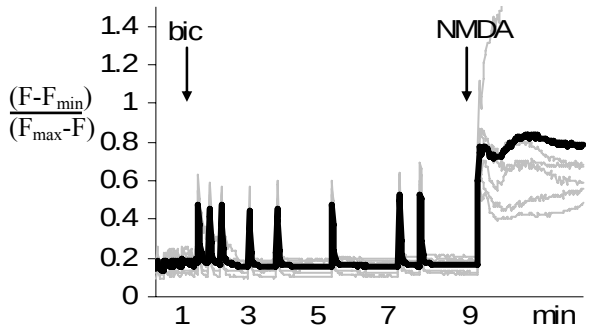

Figure 82. *Calcium imaging in low density cultures. Bicuculline evoked normal synaptic bursting and NMDA bath application (50 µM) lead to the expected calcium plateau.*

To assess the sensitivity of the low density network to death-inducing stimuli a NMDA dose response experiment was performed and pyknotic nuclei were quantified (Figure 83). The variation in these dilute neurons was higher than in a normal cell culture network and these neurons seemed to be more resistant to cell death, giving only 25 %

death with 35 µM NMDA. This indicates that these neurons have undergone a certain selection process due to their low density and the limited amount of secreted growth factors and synaptic input. Nevertheless they served as a useful assay to evaluate the functionality of conG-beads.

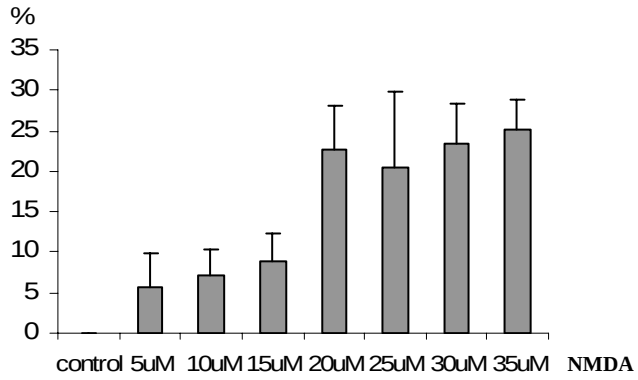

Figure 83. *Quantification of cell death in low density cultures after application of different concentrations of NMDA, ranging from 5 to 35 µM. Error bars: SEM.*

Figure 84 shows the quantification of an immunofluorescence staining of NMDA-treated low density cultures after incubation with various ratios of conG-biotin to beads. Surprisingly, a conG-biotin complex consisting of 1 µM or 5 µM conG-biotin and 30 µl beads did not show any protective effect, while the same ratio in the presence of 2 µl (740 µM) biocytin or 7,4 µl (2,7 mM) biocytin always lead to a complete protection. The amount of 740 µM was just below saturation, while 2,7 mM was totally saturated. The idea behind those concentrations was to control the amount of conG-biotin on the beads, with only few active peptides and a total saturation of the remaining binding sites by biocytin. This should result in a better compensation of the negative charges of conG by the positively charged biocytin.

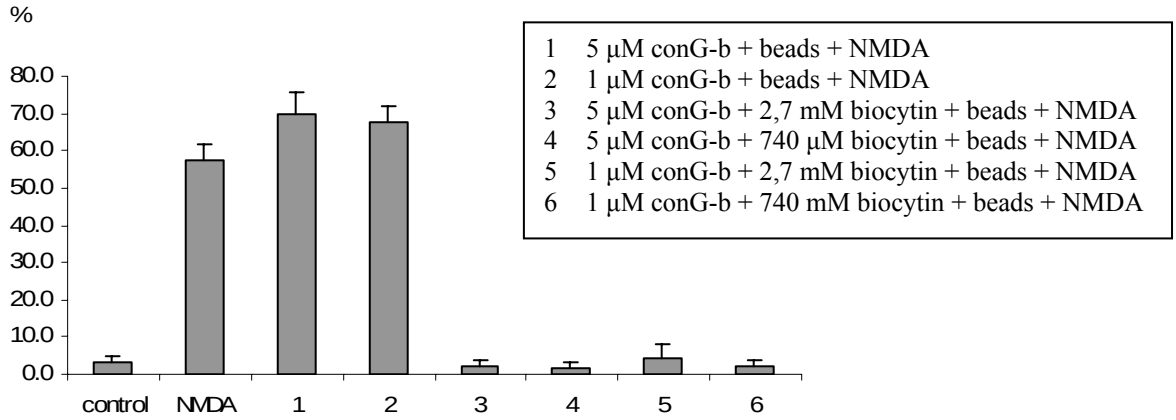

Figure 84. *Quantification of NMDA-induced (50 µM) cell death after incubation with various ratios of conG-biotin to streptavidin beads (30 µl). Concentrations of 1 µM or 5 µM conG-biotin bound to beads did not result in any protection, but completely protected neurons if the coupling was performed in the presence of biocytin. Error bars: SEM.*

A repetition of the experiment with a lower amount of biocytin showed that increasing concentrations of conG-biotin were only protective in the presence of biocytin. It can be concluded that biocytin interferes with the binding of conG-biotin and that not the beads themselves were protective but that the supernatant containing unbound peptide confered protection. To examine if conG-biotin would bind to these beads in the absence of biocytin, a simple spin-down assay was used. Therefore the peptide-bead mixture was spun down at high speed to collect all beads in a undissolvable pellet. The supernatant containing any potential unbound peptides was tested in a cell death assay. In a parallel protocol the peptide-bead mixture was added to cells without pelleting. Figure 85 shows that conG-biotin at 5 µM was protective in all ratios of beads and biocytin tested but that this protection was mediated by unbound peptide as shown by the protection of the supernatants. It can be concluded that a stable conG-bead coupling cannot be achieved with the method applied here, as there is always a fraction of active peptide that does not stably bind to beads and therefore will disturb the experiment.

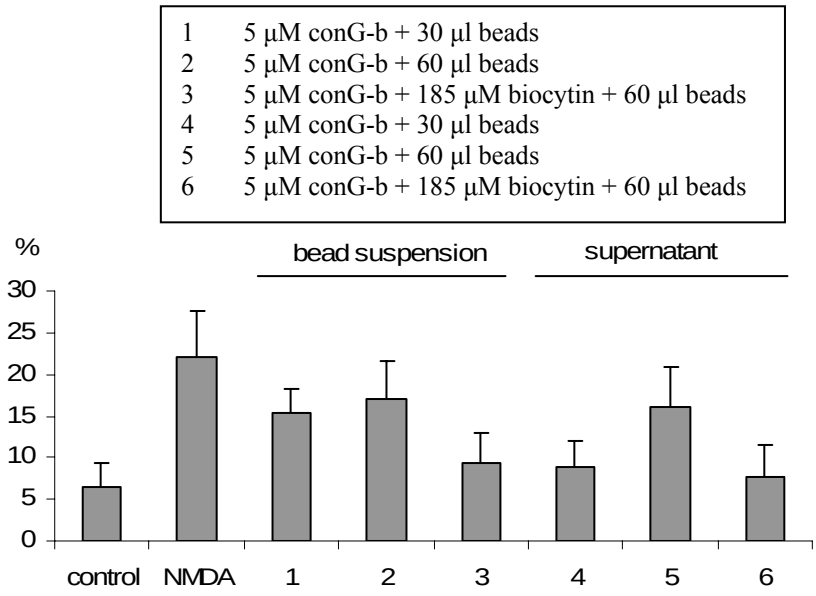

Figure 85. *Effects of conG-biotin-beads in suspension and supernatants on cell death in low density cultures. The neuroprotection mediated by bead suspensions was also present in the supernatant fraction after pelleting, indicating that large amounts of conG-biotin are not bound to beads.*

4.2.7.10. Patch-clamping of conG-biotin coupled to beads

The potency of conG-Biotin coupled to gold beads was tested on a single cell level by patch clamp recordings by Peter Bengtson (IZN). Figure 86 shows an example of EPSCs and puff responses in the presence of 0,5 µM and 5 µM conG-biotin and the same amounts of conG-biotin coupled to beads. Although conG-biotin beads at the higher concentration of 5 µM did not significantly attenuate synaptic responses, there was also complete lack of inhibition of puff responses. This indicates that coupling of conG to beads dramatically reduces its potency. A specific blockade of extrasynaptic NMDA receptors therefore is currently regarded as impossible using the attempts shown here due to technical reasons.

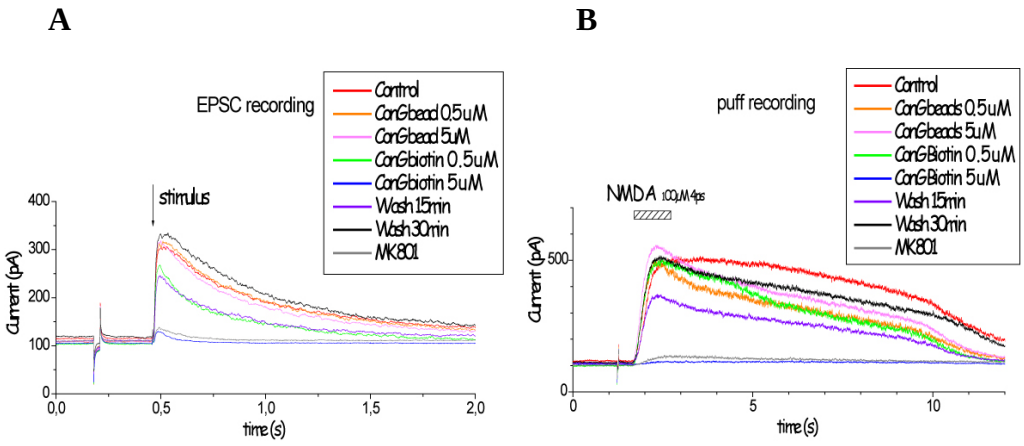

Figure 86. *EPSCs (A) and puff responses (B) were recorded at a holding potential of +40 mV in the presence of conG-biotin at 0,5 µM or 5 µM with and without prior coupling to beads.*

5. Discussion

5.1. Nuclear shape

5.1.1. Nuclear infoldings

Synaptic activity leads to calcium influx through NMDA receptors and a nuclear calcium signal that triggers CREB phosphorylation (Hardingham et al., 2001a). Calcium diffuses into the nucleus passively through nuclear pores although certain calcium pumps exist in the cell that might also be present within the nuclear membrane and facilitate the flow of calcium. An increase in nuclear calcium kinetics would have a major impact on enzymatic reactions within the nucleus, including gene transcription.

I attempted to localize SERCA pumps in the nuclear membrane with fluorescently labelled thapsigargin in live cells. This led to the surprising observation that not only the nuclear membrane is positive for SERCA pumps but that the pump is localised to fine structures traversing the nucleus. They were also positive for ER-Tracker indicating the presence of Endoplasmic Reticulum. Fine structures traversing the nucleus composed of both inner and outer nuclear membrane were identified by electron microscopy in neuronal cell culture as well as in cryo sections, ruling out any cell culture artefact mediated by adherence of cells. The morphology of such structures was not immediately evident as there had been reports from various cell lines describing tubular channels within the cell nucleus (Fricker et al., 1997). It has also been shown that a direct link exists in certain cell lines between a nucleoplasmic reticulum and the localized influx of calcium into the nucleoplasm (Echevarria et al., 2003).

As the morphology of those structures might play a role in nuclear calcium-regulated processes and as there might be differences in nuclear architecture between cell lines and primary cells, we attempted to make 3D reconstructions from primary hippocampal neurons in culture. Immunofluorescent stainings for lamin B served as a reliable marker for these structures, as it allows scanning of multiple confocal stacks without bleaching and is known to be primarily localized to the nuclear lamina adjacent to the inner nuclear membrane (Fawcett, 1966).

Unfortunately the antibody against lamin B gave only very weak signals and a suboptimal signal to noise ratio in brain slices, therefore all reconstructions were done from cultured neurons. The 3D models obtained from these reconstructions revealed

that the observed structures are not of a tubular nature but are instead infoldings of both nuclear membranes that sometimes project deeply into the nucleus. In certain cases nuclei were almost divided into two parts by the deep membrane infoldings.

Deep nuclear infoldings can certainly not be regarded as a nucleoplasmic reticulum that serves as a specific nuclear calcium store as previously suggested (Echevarria et al., 2003) because both nuclear membranes are present and thus the infoldings although being continuous with the ER, represent extensions of the cytoplasm into the nucleus. This offers a greater surface area for potential connectivity and diffusional continuity between the nucleoplasm and the cytoplasm. Infoldings that project into the nucleus and that include cytoplasm will most likely have effects on all calcium-regulated processes within the nucleus. The diffusion distances from the nuclear membrane to any location within the nucleus will become shorter in infolded nuclei, possibly giving rise to faster calcium exchange. It should be noted that the infoldings visualized in these 3D models are still an underestimation of the membrane that is being infolded. Very fine structures that are visible by eye in immunofluorescent confocal images often cannot be reconstructed due to limitations of the algorithm used which has to set a threshhold for distinguishing between signal and background.

The question remained how the nucleus can accomplish an infolding of this size. The two possible mechanisms are either loss of volume, perhaps by eflux of water from the nucleoplasm, or incorporation of additional membranes. Calculation of the surface area and volume from confocal stacks was performed by Gillian Queisser (IWR) using a mathematical algorithm. It turned out that infolded nuclei on average have significantly increased surface areas of nuclear membrane compared to non-infolded nuclei. As there is basically no difference in volume, the first hypothesis that a loss of volume causes infoldings can be ruled out. It is currently unknown how exactly the membranes are inserted and from where they originate. A potential pool could be recruitment of membranes from the endoplasmic reticulum, another possibility would be de-novo generation of membranes by enzymes at the nuclear membrane. Indeed, a translocation of CTP:phosphocholine cytidylyl-transferase-α (CTTα) to nuclear tubules and insertion into the inner nuclear membrane has been reported in CHO cells (Lagace and Ridgway, 2005). CTTα is also present in neurons of the central nervous system (Vance et al., 1994) and catalyzes the rate-limiting reaction for biosynthesis of phosphatidylcholine, the most abundant phospholipid in membranes. It is therefore possible that this enzyme is also involved in the generation of new membranes in primary neurons.

5.1.2. Destabilization of nuclear infoldings

The nuclear infoldings observed in hippocampal neurons did not undergo visible morphological changes as described previously for tubular channels (Fricker et al., 1997), indicating that the structures might not be related to each other. Surprisingly there was a dramatic change after NMDA bath application, which activates extrasynaptic NMDA receptors. The activation of extrasynaptic NMDA receptors has been shown to counteract the pro-survival action of synaptic NMDA receptors and to lead to cell death (Hardingham et al., 2002). NMDA treatment resulted in complete loss of the infoldings within 15 minutes. The loss of infoldings seemed to be due to a swelling of the nucleus, whereby the infoldings are pushed to the outside due to an expansion of nuclear volume. This correlated with a small increase in the diameter of the nucleus, suggesting that water influx from the cytoplasm might be the reason for this nuclear swelling.

When neurons were transfected with lamin B-GFP, two phenotypes could be observed: one with moderate levels of the protein that resembled the normal morphology of infoldings observed in immunofluorescence, and one that resulted from a dramatic overexpression of lamin B. In the latter phenotype, the infoldings were drastically enhanced, resulting in curly-looking circular structures that filled the entire nucleus. Addition of toxic concentrations of NMDA to these neurons did not result in the nuclear swelling observed in moderately expressing cells. Although the nuclear structure of these nuclei seemed to be resistant to swelling, no statement can be made about the viability of these cells. It seems likely that a dramatic overexpression of this structural component will sooner or later result in death of the neuron, most probably through disturbance of lamin's function in chromatin organization (Luderus et al., 1992; Taniura et al., 1995; Zhao et al., 1996) and gene transcription (Moir et al., 1995; Nili et al., 2001; Spann et al., 2002).

5.1.3. Synaptic NMDA receptors induce infoldings in nuclear membranes

Administration of bicuculline induces synchronous bursting in the neuronal network and results in calcium influx through synaptic NMDA receptors and voltage gated calcium channels (Hardingham et al., 2001a). Calcium influx through synaptic NMDA

receptors triggers phosphorylation of CREB and participates in the induction of pro-survival mechanisms (Hardingham et al., 2002). The induction of synchronous bursting did not change the morphology of existing nuclear infoldings, but led to induction of new infoldings in previously non-infolded nuclei. The average number of neurons showing infoldings increased from about 30 % to 70 % after addition of bicuculline for one hour. The induction of infoldings was primarily mediated by NMDA receptors, as NMDA receptor antagonists prevented the induction. Neither calcium influx through L-type channels nor elevation of cAMP levels could increase the number of infoldings.
Live imaging of the induction of infoldings shows a progressive appearance of new infoldings within one hour after addition of bicuculline.

5.1.4. Signaling cascades regulating infolding of nuclear membranes

Opening of synaptic NMDA receptors leads to calcium influx, activation of MAP kinase cascades and propagation of a transcription-enhancing signal into the nucleus. It therefore seemed possible that these pathways downstream of synaptic NMDA receptors are also involved in the generation of infoldings. Indeed, blockade of the ERK-MAP kinase pathway by inhibitors of an upstream target, MEK1, prevented the bicuculline-induced infolding of the nucleus, as did calmidazolium, an inhibitor of calmodulin. In contrast, inhibitors of the calmodulin-dependent protein kinase II had no effects on the induction. This shows that the mechanism is calcium dependent and effectors of the mechanism that drives the nuclear membrane to infold are located downstream of the ERK signaling cascade. An inhibitor of nitric oxide occasionally reduced the induction of infoldings, but as these effects were relatively weak and unreliable this could be due to some indirect mechanisms.
The effects of calmidazolium were not due to non-specific effects onto bicuculline-induced NMDA receptor-mediated calcium influx, as this was unchanged in the presence of calmidazolium. Western Blots confirmed that calmidazolium did not have unspecific effects on ERK. This shows that at least two parallel mechanisms lead to the induction of nuclear infoldings: the binding of calcium by calmodulin and phosphorylation of ERK.
To examine in which cellular compartment the calcium signal exhibits its crucial function, a calmodulin-binding peptide (CamBP4) was introduced by transient transfection. Although the average number of cells containing infoldings was slightly higher after transfection, an induction of nuclear infoldings by bicuculline could not be

observed in the presence of the peptide. In contrast, transfection of a calmodulin-kinase IV dominant negative mutant, which localises exclusively to the nucleus, did not impair the induction of nuclear infoldings by bicuculline. An involvement of calmodulin-dependent kinases is therefore unlikely, a finding that is supported by a lack of effect of pharmacological inhibitors of calmodulin-dependent kinase II on the induction of nuclear infoldings. These results indicate that nuclear but not cytoplasmic calmodulin is involved in mediating the induction of nuclear infoldings. This indicates that the calcium wave activated by synaptic NMDA receptors leads to a nuclear calcium signal that then locally activates a calmodulin-dependent mechanism leading to growth of the nuclear membrane.

Members of the Rho family were not involved in the mechanism described, as transfections of different dominant negative Rho mutants and Rho-inactivating plasmids did not lower numbers of infolded nuclei and did not prevent their induction by bicuculline.

5.1.5. Stability of nuclear infoldings

In all experiments carried out the basal number of neurons with nuclear infoldings was never below 25 – 30 %. As the induction happened through activation of synaptic NMDA receptors and as the cultures always displayed a certain degree of spontaneous activity, it was likely that these were also responsible for the constant basal level. Nevertheless, silencing of synaptic activity over night with tetrodotoxin or a general inhibitor of NMDA receptors did not decrease the basal level. Addition of the NMDA receptor antagonist kynurenic in the presence of high magnesium during the maturation phase of the neuronal culture could significantly decrease the basal number of neurons with nuclear infoldings. This shows that NMDA receptor dependent mechanisms induce a robust modification of nuclear membranes during maturation in a certain subset of neurons. It remains to be determined if these neurons are in general more active and therefore require nuclear infoldings, and what role these infoldings play in the context of neuronal activity. As the nucleoplasmic reticulum in epithelial cells has been shown to be involved in localized calcium release within the nucleus (Echevarria et al., 2003) this led to speculations about an analogous role of the nuclear infoldings observed in primary neurons. Calcium influx in the vicinity of the infolded membrane could be involved in the regulation of localized processes within the nucleus, as has been shown for the local activation and translocation of PKC by nuclear calcium (Echevarria et al.,

2003). An enhancement of nuclear calcium influx might have effects onto gene transcription as gene transcription mediated by the cAMP response element (CRE), CRE-binding protein (CREB) or CREB-binding protein (CBP) depend specifically on increases in nuclear calcium (Hardingham et al., 1997; Chawla et al., 1998).

The question remained whether only the basal level of infoldings would be stable after synaptic silencing or if newly induced infoldings would be comparable in stability. Neurons were therefore silenced with tetrodotoxin for specific time points between 30 minutes and 7 hours either directly after stimulation with bicuculline for one hour or two days after bicuculline stimulation. A comparison of the decay kinetics clearly shows that freshly induced infoldings disappear within one hour after synaptic silencing while those that had been induced two days before showed a significantly slower decay. This points to an additional mechanism that is used to stabilize nuclear infoldings after prolonged synaptic activity. The kinetics of this stabilization raise the possibility that gene transcription might be involved and lead to enhanced membrane turnover or stabilization of the nuclear lamina.

5.1.6. Differences in synaptic activity in infolded nuclei

In a nucleus that has deep infoldings invaginating into the nucleoplasm all diffusion distances for calcium from the cytoplasm to penetrate the nucleoplasm are shorter. Therefore it seemed likely that the calcium signals measured in infolded nuclei would show different kinetics than those of non-infolded nuclei. Indeed, in measurements of bicuculline-induced calcium transients the amplitudes of spikes seemed to be higher in infolded nuclei, raising the possibility that more NMDA receptors or L-type channels are expressed leading to higher calcium levels in general. Unfortunately the differences between individual cultures were too variable and the average number of all experiments did not reach statistical significance. This could be due to the variability of the culture system or due to technical limitations of the imaging system that might be too slow. The absolute peaks of each spike might be missed during the imaging experiments, especially if the calcium signals in infolded and non-infolded neurons would be shifted in time.

Therefore patch clamp recordings were carried out in a collaborative event by Simon Wiegert (IZN) to look at the basal activity of individual neurons. Grouping activity profiles into three groups of silent neurons, neurons exhibiting random activity and those showing recurrent bursting did not lead to a clear correlation with the presence of

infoldings. Although more of the randomly active neurons lacked infoldings while more infolded neurons were bursting, the differences between infolded and non-infolded nuclei were not convincing. A possible reason could be a technical problem during preparation of the measurement, as the coverslips had to be transferred to a recording chamber with new medium, which could change the activity pattern of some neurons due to mechanical stress. Therefore no conclusion can be made at this point as to what extent the presence of nuclear infoldings impacts on neuronal calcium signals or electrical activity.

5.1.7. Enhanced upregulation of immediate early genes

The potential for nuclear infoldings to affect enzyme kinetics in the nucleus could facilitate rapid activation of gene transcription in neurons. This possibility was analysed by quantifications of the immediate early gene cfos that is upregulated by bicuculline in parallel with the induction of infoldings.
Surprisingly the cfos levels were significantly higher in infolded nuclei two hours after bicuculline stimulation, but again matched the levels of non-infolded nuclei after three hours. This raises the possibility that neurons that contain infoldings or in which infoldings are induced, can upregulate protein levels of cfos more quickly. It remains to be determined why this is only the case in such a short time window. It can only be speculated that neurons with newly induced infoldings might require enhanced gene transcription compared to non-infolded neurons for a certain time to synthesize proteins required for the stabilization and maintenance of infoldings.

5.1.8. The density of nuclear pore complexes stays constant

As previous experiments have demonstrated an increased nuclear membrane surface area in cells containing nuclear infoldings, this raised the question to what extent protein transport across the nuclear membrane would be altered. To examine if the number of nuclear pores would be different after the induction of nuclear infoldings and subsequent generation of new membranes, the average density of nuclear pores was measured. It turned out that the average number of pore complexes in infolded neurons was about 15 % higher than in non-infolded ones before stimulation by bicuculline. This corresponds well to the enlargement of nuclear membranes in infolded nuclei, showing that the pore density per membrane area stays constant.

After stimulation with bicuculline for one hour the average number of pores in the cell population with infolded nuclei decreased and almost exactly matched the number of pores in non-infolded neurons. This directly shows that nuclei that created new infoldings after stimulation had not yet upregulated their number of pores during growth of the membrane and therefore had a lower pore density on average than nuclei that were already infolded before the stimulation. As no differentiation could be made between previously infolded and newly infolded nuclei after bicuculline stimulation, the lower pore density of newly infolded nuclei led to a dilution effect of the overall pore density in the pool of infolded nuclei. This resulted in a decrease in the average number of pores in this pool of nuclei.

This experiment verifies that nuclear infoldings are generated by synthesis or recruitment of additional nuclear membranes, as a loss of nuclear volume would not lead to a change in nuclear pore density. New membranes are thereby likely to be inserted at multiple sites at the nuclear envelope as infoldings were readily decorated with nuclear pore complexes one hour after induction. Therefore there probably is no local synthesis of membranes giving rise to an infolding but rather a general membrane growth along the entire nuclear membrane. Alternatively a quick redistribution of nuclear pores cannot be ruled out after a local synthesis, leading to a constant pore density along the nuclear membrane. How exactly the membrane is made to infold remains to be determined.

In summary it can be concluded that the neuronal nucleus is a dynamic structure that can undergo morphological changes in response to very specific stimuli. The deep nuclear infoldings observed in primary hippocampal neurons can be induced by activation of the synaptic NMDA receptor and destabilized after activation of extrasynaptic NMDA receptors. Synaptic NMDA receptors are involved in hippocampal synaptic potentiation, a model for memory, while extrasynaptic NMDA receptor activation is central to the pathophysiology of stroke.

The induction of infoldings requires activation of the ERK-MAP kinase cascade and a nuclear calcium signal binding nuclear calmodulin.

The infoldings are generated by an increase in the surface area of the nuclear membrane and are followed subsequently by a recruitment of new nuclear pore complexes into newly induced infoldings, resulting in a constant density of nuclear pores per membrane area.

Nuclear infoldings are stabilized after several days of synaptic activity, resulting in a slower loss of infoldings after synaptic silencing compared to newly induced infoldings. This indicates the possibility of an involvement of gene transcription in the stabilization process. Indeed, the immediate early gene cfos showed a higher induction by synaptic activation at distinct time points. The biological significance of this remains to be determined. Attempts to identify enhancements on calcium kinetics or electrical activity in neurons containing infolded nuclei have not yet been successful, possibly due to a low sensitivity of available assays and technical limitations.

5.2. Cell fate

5.2.1. Extrasynaptic NMDA receptors mediate excitotoxicity

NMDA receptors can have profound effects on numerous cellular processes, ranging from cell survival induced by synaptic NMDA receptors to neuronal cell death after stimulation of extrasynaptic NMDA receptors (Hardingham et al., 2002). Although a number of both pharmacological and peptide antagonists for NMDA receptors exist, it is not possible to specifically target these to the extrasynaptic NMDA receptors. To develop such a blocker a fluorescence-based cell death assay based on the quantification of pyknotic nuclei was set up (Fujikawa et al., 2000). It turned out that NMDA concentrations of 30 μM to 50 μM are equally potent in inducing nearly complete excitotoxic cell death in hippocampal neuronal cultures. Slight variations do exist though, which are most likely due to differences in the density of the neuronal network in different cultures. At a higher density neurons are more likely to develop spontaneous activity and to manifest a synchronous bursting pattern. A direct consequence of this will be calcium influx via synaptic NMDA receptors, resembling the synchronous activity induced by application of bicuculline which has been shown to confer neuroprotection (Hardingham et al., 2002).

Long lasting opening of extrasynaptic NMDA receptors by NMDA bath application is not necessary to induce excitotoxicity in a large fraction of the culture, as an application as short as ten seconds already had detrimental effects. A potent blocker of extrasynaptic NMDA receptors, regardless of its subunit selectivity should protect

against excitotoxic cell death. Ifenprodil, a chemical antagonist against the NR2B subunit, has been shown to confer different affinities to NMDA receptors depending on the subunit composition. While having a high affinity for diheteromeric NMDA receptors containing two copies of NR2B, the presence of other NR2 subunits led to reduced sensitivity of the antagonist (Hatton and Paoletti, 2005).

The kind of cell death induced by NMDA bath application was necrotic, as shown by lack of cleavage of pro-caspase-3 even 22 h after activation of extrasynaptic NMDA receptors. This also correlates with observations done by light microscopy, where neuronal swelling was clearly visible one hour after induction of excitotoxicity which is too fast for apoptosis and known to be a typical phenomenon of necrotic cell death.

The calcium signal observed after toxic concentrations of NMDA quickly increased to a plateau and is paralleled by the breakdown of the mitochondrial membrane potential, as shown previously (Hardingham et al., 2002).

While opening of extrasynaptic NMDA receptors led to induction of excitotoxic cell death, this could be partially prevented by preincubation with bicuculline, leading to opening of synaptic NMDA receptors and the induction of bursting. It has been shown before that bicuculline confers protection from staurosporine-induced apoptotic death (Hardingham et al., 2002). As stimulation of synaptic NMDA receptors protects from both apoptotic and excitotoxic cell death, the downstream effects are likely to have a general effect on cell viability rather than a blockade of a specific pro-death pathway.

The minimal incubation time with bicuculline needed for a significant protection from excitotoxicity was ten hours, an enhancement of protection was achieved after enhancing calcium influx by addition of 4-AP. This indicates that the protection is mediated by calcium-regulated processes and most likely involves gene transcription.

5.2.2. Extrasynaptic NMDA receptors mediate shut-off pathways

Extrasynaptic NMDA receptors are dominant over synaptic NMDA receptors with respect to the induction of cell death, as combined activation of both types will always be deadly for the cell. Surprisingly a short incubation of one minute with NMDA leads to transient phosphorylation of MAP kinases like ERK1/2 and p38, but prolonged incubation triggers a dephosphorylation as soon as five minutes after opening of the receptor.

Calcium influx through L-type channels is a potent activator of CREB, while glutamate bath application activates CREB only transiently and leads to a CREB shut-off

mechanisms within 15 minutes. Extrasynaptic NMDA receptors therefore counteract the survival-promoting activity of CREB (Hardingham et al., 2002). The molecular mechanism that initiates dephosphorylation of CREB are unknown, but as activation of extrasynaptic NMDA receptors leads to depolarization of mitochondria it was speculated that the generation of reactive oxygen species might be involved in this process. Scavengers of reactive oxygen species have previously been shown to mediate neuroprotective effects in neurons (Vergun et al., 2001) and this effect might involve prevention of the CREB shut-off pathway. Phosphorylation of CREB was initiated by calcium influx through L-type channels using its agonist FPL 64176. Several scavengers of radicals, peroxynitrites and nitric oxide were therefore tested for a potential effect on the dephosphorylation of CREB by NMDA bath application, but none of these could reduce the shut-off mechanism. A possible explanation could be insufficient concentrations or incubation times as there were no positive controls or indicators for the proper function of these compounds, therefore the concentrations used were based on the literature. It could also be that the inhibitor for the crucial molecule was not included in the assay or that several intracellular shut-off mechanisms can compensate for each other, which would make a direct analysis of the mechanism rather complicated.

5.2.3. Potency of Conantokin-G

To be able to differentiate between intracellular pathways downstream of synaptic versus extrasynaptic NMDA receptors a specific blockade of each type would be necessary. Although synaptic NMDA receptors can be blocked by combined application of bicuculline and MK-801 (Hardingham et al., 2002) a specific blockade of extrasynaptic NMDA receptors has not been reported. Therefore a potent blocker had to be found that could be modified to enhance its specificity for extrasynaptic NMDA receptors.

The choice fell on Conantokin-G (conG), a selective antagonist for the NR2B subunit (Donevan and McCabe, 2000; Klein et al., 2001). Native conG efficiently inhibited the induction of a calcium plateau by NMDA bath application as well as depolarization of the mitochondrial membrane potential. It was also extremely potent in protecting hippocampal neurons from excitotoxic cell death, even after addition of excessive NMDA concentrations of up to 1 mM. ConG did not show a major impact on synaptic NMDA receptors but completely blocks extrasynaptic ones in calcium imaging

experiments. A combined activation of synaptic NMDA receptors with bicuculline and 4-aminopyridine led to a rise of the calcium baseline. Bath application of NMDA resulted in a further increase that could largely be prevented by the presence of conG, although a minor and transient rise was still visible. Patch clamping experiments performed by C Peter Bengtson (IZN) finally revealed that although puff responses are almost completely blocked by conG, enhanced post synaptic currents (EPSCs) also are greatly reduced.

This indicates that there are NR2B-containing NMDA receptors present in the synapse and that native conG alone will not be suitable to dissect the different molecular pathways as it blocks synaptic NMDA receptors to a certain extend. The fact that the blockade of synaptic NMDA receptors was not visible during calcium imaging is most likely due to the fact that L-type calcium channels highly contribute to the bicuculline-induced calcium influx. A blockade of a certain amount of synaptic NMDA receptors does not necessarily lead to a visible decrease in calcium influx as this is masked by calcium influx through L-type channels.

5.2.4. Modifications of Conantokin-G

To develop such a blocker for extrasynaptic NMDA receptors I attempted to couple conG to beads of a specific size to prevent it from binding NMDA receptors within the synaptic cleft, while extrasynaptic NMDA receptors would be blocked by conG.

ConG was synthesized with a cysteine residue at the c-terminus and then coupled to BSA as a carrier protein. Immunofluorescence studies with a FITC-tagged conG-BSA complex revealed that the complexes showed little colocalisation with the synaptic markers synaptophysin and synapsin I. This is regarded as a first indicator that the concept of a specific blockade of extrasynaptic NMDA receptors might prove true as the conG-BSA complexes already are big enough to impede diffusion into the synaptic cleft.

The conG-BSA complexes significantly protected from excitotoxicity, although at a lower efficiency than the native form of conG. This indicates that either not all peptides were bound to BSA in an orientation compatible with blockade of NMDA receptors, or that the concentration of ConG-BSA molecules was not sufficient for blockade of all receptors in the plasma membrane. However, both native and BSA-coupled conG were highly protective in an assay of oxygen-glucose deprivation (OGD).

Evaluation of any protective effects of inhibitors of intracellular signaling cascades which have previously been implicated in neuronal cell death showed no effect on the OGD model of cell death. This might be due to the concentrations used for these inhibitors. Positive controls for these compounds were not feasible and concentrations were chosen according to published estimates of their potency. Both native and BSA-coupled conG were more protective than the NR2B blocker Ifenprodil at supramaximal concentrations, suggesting that heterotrimeric NMDA receptors contributed to the hypoxic cell death.

A comparison of the effects of native conG and different versions of BSA-coupled conG on Multi Electrode Arrays revealed that the BSA complex containing saturating amounts of conG had little impact on burst induction. This effect was much lower than with native conG and even slightly less than using a BSA complex containing only 10 conG peptides. This indicates that either the saturation of BSA with conG gives rise to a larger complex that is less likely to enter the synaptic cleft for sterical reasons, or that possibly eletrical charges of the molecule might play a role. ConG is an extremely charged molecule with five gamma-carboxyglutamates and the combined negative charges of 17 peptides within one complex might lead to a repelling of the complex by negatively charged proteins within the synaptic cleft and the negatively charged neuron membrane.

ConG-BSA-sat and native conG were equally capable of inhibiting excitotoxicity in older cultures of 18-20 days *in vitro*. Surprisingly this protection was weaker in older than in younger cultures for both peptides. During maturation the cultures are expected to change the composition of subunits within the synapse from a mixture of NR2A and NR2B to a mainly NR2A-containing population of NMDA receptors (Li et al., 1998; Tovar and Westbrook, 1999). This should lead to an even better blockade of excitotoxic cell death, as extrasynaptic NMDA receptors are more accessible. A possible explanation the higher amount of cell death could be the general health of neurons in culture after 20 days, which could make them more vulnerable to other forms of cell death and general degeneration that would not be blocked by the antagonists used here. Alternatively, the presence of some NMDA receptors composed of only the NR2A subunit in the extrasynaptic membrane cannot be excluded.

5.2.5. Coupling of conG to beads

Attempts to couple conG to any kind of bead have all failed in the end. In all cases the stability of the reaction carried out was less than expected from the literature. This is most likely the cause of the high negative charge of the conG peptide, having five gamma-carboxyglutamate residues. High numbers of peptides on the bead surface require tight packing which might lead to electrostatic repulsions due to their close proximity.

In the case of coupling conG-BSA to gold beads the binding of BSA might actually be interfered with due to the high negative charge of the BSA complex, which is saturated with conG peptides. Any reaction taking place finally has turned out to be unstable, resulting in a major fraction of conG-BSA complexes that did not migrate together with the bead fraction in the glycerol gradient. Patch clamp recordings revealed that a large fraction of the synaptic EPSCs was blocked, while the puff response was only impaired by about 50 %. This is most likely due to dissociation of the conG-BSA complexes from the beads during the experiment, which then were able to diffuse into the synaptic cleft. The weaker blockade of extrasynaptic NMDA receptors compared to native conG indicates a lower potency of the BSA complex and results most likely from a high density of extrasynaptic NMDA receptors. If these are tightly packed, for example as receptor clusters on lipid rafts (Besshoh et al., 2005) the large conG-BSA complex would not block all receptors due to the limited number of peptides on its surface and steric hindrance of large conG-BSA complexes competing for tightly packed receptors.

Coupling to latex beads via chemical cross-linkers was also not successful. Again the high negative charge of conG is believed to be responsible for this as it might interfere with the chemistry of the coupling reaction.

A further attempt was to couple conG to antibodies over a C-terminal myc-tag. The presence of the tag did not interfere with the protective function of the peptide although higher concentrations were needed for a complete blockade of excitotoxicity. It also potently blocked most of the calcium influx induced by NMDA bath application, showing that attachment of comparatively large tags to the C-terminus of conG does not inhibit its antagonizing function at the NMDA receptor. However, conG-myc could not reliably be coupled to antibodies, as removement of unbound peptides by dialysis failed. This was not the cause of the presence of the myc tag, as native conG could also not be dialysed. A possible explanation would be repelling of the highly negatively charged peptides by the dialysis membrane. In addition, detection of conG-myc failed after

Western Blotting with both a home-made anti-myc (9E10) as well as a commercial antibody. This could be due to the generation of secondary or tertiary structures which could mask the epitope and prevent binding of the antibody.
Coupling of a biotinylated conG to Streptavidin-beads was also not successful, even though the negative charge of conG was compensated for by addition of positively charged biocytin. This seemed to have greater binding capacity than conG-Biotin and competed for binding sites on the surface of the beads. Lowering the amount of biocytin still did not improve the binding. A possibility that had not been previously examined was the accessibility of extrasynaptic NMDA receptors to the dense network of dendrites that usually forms in neuronal cultures. Beads coated with conG might not be small enough to get access to NMDA receptors at the junctions of dendrites, while these would still be activated by NMDA. Lowering the density of the neuronal culture by first plating a glial feeder layer onto which only few neurons were plated seemed to be the solution to this problem. These neurons did in fact form networks in which bursting and therefore activation of synaptic NMDA receptors could be induced and they could be killed by NMDA bath application, although higher doses were necessary. This is probably due to a selection process during formation of the network, where only the most resistant neurons survive. Nevertheless, different concentrations and ratios of conG to beads were tested but a major fraction of the peptide always seemed to detach from the beads, as shown by the protection mediated by supernatants of conG-bead suspensions after pelleting the beads. Surprisingly, in patch clamp recordings the EPSCs were not significantly inhibited, but the puff recordings also lacked inhibition by conG-bead suspensions. This could be explained by a differential response of individual neurons, as especially in low density cultures not all neurons responded equally to high concentrations of NMDA.

In summary it can be concluded that attachment of a C-terminal tag to conG does not significantly interfere with its blocking ability. ConG is extremely potent in inhibiting NMDA receptor-induced excitotoxic death as well as neuronal death induced by oxygen glucose deprivation. Any attachment to beads failed in all attempts most likely due to negative charges of the peptide that interfered with the coupling reaction.
Previous reports of peptides and proteins bound to beads did not encounter the problems faced here as they did not require a complete binding of all peptides in solution to beads (Cordes et al., 1997; Yasuda et al., 2001). The purpose of these experiments were to

visualize beads bound to the protein of choice, while unbound protein did not interfere with the observations. The application in this thesis differed in that not only the beads had to contain sufficient amounts of a functional peptide but also any unbound peptides had to be removed from the bead solution. This has turned out the be extremely difficult as purification of beads as small as required here is not feasible without substantial loss. Other reliable methods to prevent uncoupling of bound peptides are not known. Therefore a specific blocker for extrasynaptic NMDA receptors could not be designed using the methods described here for technical reasons.

6. Material and Methods

6.1. Materials

Commonly used laboratory chemicals were supplied by the following companies:

Calbiochem, USA
Molecular Probes, Netherlands
Bio-Rad, München
Clontech, Heidelberg
Gibco BRL / Life Technologies, Eggenstein
Invitrogen, Netherlands
MBI Fermentas, Lithuania
Merck, Darmstadt
New England Biolabs, USA
Qiagen, Hilden
Roche, Mannheim
Sigma, USA
Chemicon, USA

6.1.1. Special Equipment

KL 1500 LCD Binocular	Schott
Ludin chamber 12mm	Live imaging series
Centrifuge 5417C	Eppendorf
Megafuge 1.0R	Kendro
Biofuge pico	Kendro
Omnifuge 2.0RS	Heraeus Sepatech
Thermal cycler PTC-200	MJ Research
bacterial incubator	Heraeus
Gel Jet imager	Intas
Leica confocal laser scanning microscope SP2	Leica
Hyperfilm ECL	Amersham Biosciences
Beckmann J2-MC	Beckman
Spectrophotometer Ultrospec 3000	Pharmacia Biotech
Blockthermostat BBT 100	Kleinfeld
Cell culture incubator	Heraeus Instruments
Zeiss Axiophot	Zeiss
Thermomixer 5436	Eppendorf
Wet Blot Apparatus	IDEA Scientific Company
Cryostat Jung Frigocut 2800N	Leica
Gradient mixer	Sigma
Digital Oxymeter GMH 3690	Greisinger electronic

6.1.2. General reagents

β-mercaptoethanol	Merck
1,4-Dithiothreitol (DTT)	Applichem
4-(2-hydroxyethyl-)piperazin-1-ethansulfonic acid (HEPES)	Roth
Bovine Serum Albumin	Applichem
Bromophenol blue	Serva
Cytosine Arabinoside	Sigma
D-(+)-glucose	Sigma
DiD (DilC18(5))	Molecular Imaging Products
Dimethylsulfoxide (DMSO)	Merck
ECL, Detection Reagents 1 and 2	Amersham Biosciences
EGTA	Sigma
Ethylendiaminetetraacetic acid (EDTA)	Roth
Foetal calf serum (FCS)	Gibco
Glycerol, 99%	Zentrallager
Glycine	Riedel-de Haen
Isopropanol	Applichem
Laminin	BD Biosciences
L-Glutamine	Sigma
Lipofectamine 2000	Invitrogen
Magnesium acetate	J.T. Baker
Magnesium chloride hexahydrate	Fluka / Sigma
Minimum Essential Medium (MEM)	Gibco
Mowiol	Calbiochem
N,N,N´,N´-Tetramethyl-ethylendiamine (TEMED)	Serva
OptiMEM	Gibco
Penicillin/Streptomycin solution	Sigma
Phenol red	Sigma
Poly-D-Lysine	BD Biosciences
Potassium acetate	Sigma
potassium carbonate	Sigma
Potassium chloride	Sigma
Potassium hydroxyte	Riedel-de Haen
Potassium sulfate	Sigma
Protein marker (Page Ruler Protein Ladder)	Fermentas
Putrescine	Sigma
Sodium acetate	Neolab
Sodium chloride	Sigma
Sodium dihydrogene phosphate (Na_2HPO_4)	Applichem
Sodium hydroxyte	Merck
Sodium sulfate	Sigma
Sodiumdodecylsulfate (SDS)	Serva
Tris-(hydroxymethyl)-aminomethane (Tris)	Roth
Triton X-100	Sigma
Trypsin/EDTA-solution HBSS w/o ca&mg	Gibco
Tween 20	Sigma

6.1.3. Plasmids

CamBP4-NLS	laboratory of Hilmar Bading, University of Heidelberg
CamKIV-DN	laboratory of Hilmar Bading, University of Heidelberg
hrGFP	laboratory of Hilmar Bading, University of Heidelberg
laminB-GFP	laboratory of Jan Ellenberg, EMBL
p190	laboratory of Rohini Kuner, University of Heidelberg
Rac-L61	laboratory of Rohini Kuner, University of Heidelberg
Rho-N19	laboratory of Rohini Kuner, University of Heidelberg
Rho-V14	laboratory of Rohini Kuner, University of Heidelberg

6.1.4. Beads

Gold beads 80 nm	BBI International
White Aliphatic Amin-Latex beads 78 nm	Interfacial Dynamics Corp.
Streptavidin Coated Microspheres 120 nm	Bangs Lab Inc.

6.1.5. Peptide toxins and pharmacological substances

4-Aminopyridin (4-AP)	Calbiochem
APV	Sigma
BDNF	Calbiochem
Bicuculline	Sigma
Calmidazolium Chloride	Calbiochem
Catalase from murine liver	Sigma
Conantokin-G	Peptide Speciality Laboratories, Heidelberg
Conantokin-G coupled to BSA (saturated)	Peptide Speciality Laboratories, Heidelberg
Conantokin-G coupled to BSA (with FITC)	Peptide Speciality Laboratories, Heidelberg
Conantokin-G with c-terminal Biotin	Peptide Speciality Laboratories, Heidelberg
Conantokin-G with c-terminal cysteine	Peptide Speciality Laboratories, Heidelberg
Cyclopiazonic Acid	Calbiochem
Cyclosporin A	Fluka
FCCP	Sigma
FK506	Calbiochem
Ifenprodil tartrate salt	N-Methyl-D-Aspartic acid
Ionomycin calcium salt	MP Biomedicals
L-Ascorbic Acid	Sigma
LY 294002	Calbiochem
MK-801 Maleate	Calbiochem
MnTBAP	Calbiochem
Nifedipine	Sigma
N-Methyl-D-Aspartic acid	Sigma
N_w-Nitro-L-arginine methyl ester	Sigma

hydrochloride (L-NAME)	
SB 216763	Tocris
Staurosporine	Calbiochem
Tautomycin	Calbiochem
Tempo	Sigma
Trolox	Calbiochem
W-7, Hydrochloride	Calbiochem

6.1.6. Conantokin variants

conG (native)

H - Gly-Glu-O-O-Leu-Gln-O-Asn-Gln-O-Leu-Ile-Arg-O-Lys-Ser-Asn- $CONH_2$ (Amide)

conG-myc

the amino acid sequences of conG and the myc-tag were connected by a spacer composed of 5 glycine residues.

H - Gly-Glu-O-O-Leu-Gln-O-Asn-Gln-O-Leu-Ile-Arg-O-Lys-Ser-Asn-Gly-Gly-Gly-Gly-Gly-Glu-Gln-Lys-Leu-Ile-Ser-Glu-Glu-Asp-Leu-Asn - $CONH_2$ (Amide)

conG-cys

H - Gly-Glu-O-O-Leu-Gln-O-Asn-Gln-O-Leu-Ile-Arg-O-Lys-Ser-Asn-Cys-$CONH_2$ (Amide)

6.1.7. Fluorescent dyes

DiD (DilC18(5))	BioTrend
Er Tracker Blue-White DPX	Molecular Probes
Fluo-3	Molecular Probes
Hoechst/ bisBENZIMIDE 33258 Trihydrochloride	Sigma
Mito Tracker Deep Red 633	Molecular Probes
Rhodamine 123	Molecular Probes
Streptavidin-FITC	Sigma

6.1.8. Primary cells

primary neurons were prepared from the following outbread rat strains:

Long Evans	Charles River
Sprague Dawley	Charles River

6.1.8.1. Media for primary hippocampal neurons

Dissociation medium (DM)

Na_2SO_4 (1 M)	20,45 ml
K_2SO_4 (0,25 M)	30 ml
$MgCl_2$ (1,9 M)	0,77 ml
$CaCl_2$ (1 M)	0,063 ml
Hepes (1 M)	0,25 ml
Phenol Red	0,5 ml
Glucose (2,5 M)	2 ml
H_2O	to 250 ml

filter sterile through 0,22µm millipore filter

Ky/Mg solution

1) 158,56 mg Kynurenic acid
2) add 10ml H_2O
3) add 0,4ml Phenol Red
4) add 5x 200µl of 1N NaOH
5) vortex extremely!
6) After Kynurenic acid is in solution, add 0,4ml 1M Hepes
7) vortex
8) add 4ml $MgCl_2$ (2M)
9) add H_2O to 80ml final
10) filter sterile
11) store 5ml aliquots at -80°C

Salt Glucose Glycine solution (SGG)

NaCl (5 M)	11,4 ml
NaHCO3 (7,5 % solution)	14,6 ml
KCl (3 M)	0,882 ml
$MgCl_2$ (1,9 M)	0,264 ml
$CaCl_2$ (1 M)	1 ml
Hepes (1 M)	5 ml
Glycine (1 M)	0,5 ml
Glucose (2,5 M)	6 ml
Na pyruvate (0,1 M)	2,5 ml
Phenol Red	1 ml
H_2O	to 500 ml

filter sterile through 0,22µm millipore filter

Salt glucose Glycine solution (SGG) CO_2-independent

NaCl (5 M)	14,01 ml
KCl (3 M)	0,882 ml
$MgCl_2$ (1,9 M)	0,264 ml
$CaCl_2$ (1 M)	1 ml
Hepes (1 M)	5 ml
Glycine (1 M)	0,5 ml
Glucose (2,5 M)	6 ml
Na pyruvate (0,1 M)	2,5 ml
Phenol Red	1 ml
H_2O	to 500 ml

filter sterile through 0,22µm millipore filter

Transfection Medium (TM)

SGG	88 ml
MEM (without glutamine)	10 ml
Insulin-Transferrin-Sodium (ITS)	1,5 ml
Pen/Strep	0,5 ml

filter sterile through 0,22µm millipore filter

L17 medium

add to a bottle of L15 medium:
1) 86 ml H_2O
2) 17,45 ml $NaHCO_3$ (7,5 % solution)

Transferrin

100 mg dissolved in 20 ml PBS
sterile filtered and aliquoted, stored at -20°C

Putrescine

40 ml dissolved in 25 ml PBS
sterile filtered and aliquoted, stored at -20°C

ITS

dissolve one bottle in 50 ml H_2O
sterile filtered and aliquoted, stored at -20°C

112

Glucose (2,5 M)	58,8 ml
L-glutamine	21 ml
Pen/Strep	21 ml

sterile filtered and aliquoted, stored at -20°C

Growth medium

L17 medium	91,5 ml
SVM	0,45 ml
Progesterone (1 mM)	12 µl
112	2,4 ml
ITS	0,5 ml
Putrescine (1,6 mg/ml)	0,5 ml
Transferrrin (5 mg/ml)	0,5 ml
Rat serum	3 ml
B27	2 ml

Enzymes solution

1) add 5 ml Ky (1mM) /Mg (10mM) solution to 45 ml of dissociation medium
2) add 50 ml of Ky/Mg + dissociation medium to a bottle containing 22,5 mg of L-cysteine
3) add NaOH (0,2 M) until pH is OK (between 300 µl and 800 µl needed)
4) add 500 units of papain latex
5) Once papain latex is in solution (takes 10-15 min), sterile filter
6) aliquot and store at -20°C

Inhibitor solution

1) add 10 ml Ky/Mg to 90 ml of dissociation medium
2) add 96 ml of dissociation medium + Ky/Mg solution to a 250 ml bottle containing 1g of trypsin inhibitor (corresponding to one bottle)
3) add NaOH (0,2 M) until pH is OK
4) make sure trypsin inhibitor is in solution, then sterile filter
5) aliquot and store at -20°C

6.1.9. Buffers and solutions

6.1.9.1. Buffers for working with proteins

Antibody dilution buffer

PBS
2% BSA 99%
0,1% TX100
0,04% azide

Mowiol 4-88 mounting medium

glycerol
Mowiol 4-88 (Merck #4094)
0,2 M Tris pH 8.5

Resolving gel (8 %)

46 % H_2O
30 % acrylamide mix
1,5 M Tris (pH 8,8)
10 % SDS
10 % ammonium persulfate
0,06 % TEMED

Stacking gel (5 %)

69 % H_2O
30 % acrylamide mix
1,5 M Tris (pH 8,8)
10 % SDS
10 % ammonium persulfate
0,1 % TEMED

SDS-PAGE sample buffer

10 % glycerol
3 % SDS
10 mM Tris-HCl pH 6,8
5 % 2-mercaptoethanol
Very small amount of bromphenolblue

Tris-glycine reservoir buffer

25 mM Tris base
200 mM glycine
0,1 % SDS

Membrane washing buffer PBST

0,01 % Tween 20
PBS

6.1.10. Antibodies

6.1.10.1. Primary antibodies

Monoclonal anti Tubulin α	Sigma
Monoclonal anti NeuN	Chemicon
Polyclonal anti phospho-ERK1/2 (phospho-p44/42)	Cell Signaling
Monoclonal anti phospho-p38	Cell Signaling
Monoclonal anti LaminB	Laboratory of Harald Herrmann, DKFZ Heidelberg
Monoclonal anti SERCA2 ATPase clone IID8	Sigma
Monoclonal anti synaptophysin	Chemicon
Polyclonal anti cleaved Caspase3	Cell Signaling
Monoclonal anti Synapsin I	BD Biosciences
Polyclonal anti c-Fos SC-52	Santa Cruz
Monoclonal anti Nuclear Pore Complex Proteins	Biozol

6.1.10.2. Secondary antibodies

Cy3 - Goat anti-mouse - Goat anti-rabbit	Dianova GmbH
Alexa 488 - Goat anti-mouse - Goat anti-rabbit	Dianova GmbH
Peroxidase Hrp - goat anti-rabbit - anti-mouse	Dianova GmbH

6.1.11. Software

LCS Lite Version 2.5 Build 1227	Leica Microsystems Heidelberg
BLAST	NCBI
ClustalX	Thompson, J.D., Higgins, D.G. and Gibson, T.J. (1994)
Vector NTI Advance 9.1	Invitrogen
BioEdit 5.0.9	Hall, T.A. 1999. BioEdit: a user-friendly biological sequence alignment editor and analysis program for Windows 95/98/NT. Nucl. Acids. Symp. Ser. 41:95-98.
ImageJ 1.32J	NIH
Illustrator CS	Adobe
Microsoft Excel 2002	Microsoft
Microsoft Word 2002	Microsoft
Photoshop 7.0	Adobe
Endnote 7.0	ISI Research Soft

6.2. Methods

6.2.1. Cell Biology Methods

6.2.1.1. General procedures

For the experiments described, primary hippocampal neurons were prepared on a weekly basis from P0 rats. After 3 days in vitro (DIV) Ara C (10 µM) was added to prevent further growth of the glial cell layer underlying the neuronal network. As most experiments carried out were highly dependent on NMDA receptors, whose subtype composition is developmentally regulated, all experiments were carried out between 10 to 14 DIV.

16 h before cell plating all dishes and coverslips were coated with Poly-D-lysine/laminin over night and washed twice with ddH_2O directly before the dissection.

6.2.1.2. Coating of cell culture dishes with Poly-D-lysine and laminin

Cell culture dishes were coated for plating of primary neurons with Poly-D-Lysine (106,6 µM) and laminin (7,4 nM) over night in a cell culture incubator. Before the dissection of rat brains the dishes were washed two times with ddH2O and dried at RT.

6.2.1.3. Dissection of Hippocampi from neonatal rats

Kynurenic / Mg^{2+} solution was thawed at 37°C and diluted 1:10 in dissociation medium. The pH was adjusted to slight pink with 100 µl NaOH (0,2 N).

Animals were killed for 10 to 15 min in a CO_2 chamber and fixed on a silicon plate with injection capillaries. The skull was opened from top with microdissection scissors and -forceps and both hemispheres removed with three precise cuts: between cortex and olfactory bulb, between both hemispheres and between each cortex and the cerebellum. The hemispheres were put to a 10,5 mM Kynurenic / Mg^{2+} solution in dissociation medium to inhibit any electrical activity of the neurons.

Hippocampi were extracted from hemispheres under a KL1500 LCD binocular (Schott) with micro-dissection scissors and forceps.

All hippocampi were kept in dissociation medium containing Kynurenic / Mg^{2+} until dissociation.

6.2.1.4. Dissociation of neurons

During dissection the enzyme and inhibitor solutions were warmed to 37°C. Hippocampi were transferred to a sterile round bottom tube containing a stirrer. The medium was aspirated and hippocampi were incubated in 3 ml enzyme solution for 20 min at 37°C in a waterbath, stirring slowly at ~15 rpm. The solution was aspirated and hippocampi were incubated another 20 min in enzyme solution like before. The solution was aspirated and hippocampi were washed three times with 1,5 ml dissociation medium with Ky (1mM) / Mg (10mM). Thereafter hippocampi were incubated three times for 5 min in 2 ml inhibitor solution, following three washes with ~1,5 ml growth medium. For tituration, cells were suspended 50 times in 2 ml growth medium with a 2 ml pipette. 2 ml were added and hippocampal fragments left to settle to the tube bottom for 5 min. The supernatant was removed to a new tube and tituration procedure was repeated twice. During the second repetition the plastic pipette was pressed against the bottom of the tube to assure complete dissociation. The single cell suspension was transferred to the collection tube and these 10 ml were diluted with OPTIMEM including 4 ml glucose (2,5 M) to obtain a cell suspension of 0,25 to 0,3 hippocampi per 2 ml.

2 ml of this suspension were plated onto 35 mm dishes either containing coverslips for micoscopy of empty dishes for Western Blots.

After 3 days in vitro the division of glial cells was stopped by addition of cytosine arabinoside (10 μM). The medium was changed to serum-free transfection medium at 8 DIV and renewed at 10 DIV.

6.2.1.5. Oxygen glucose deprivation (OGD)

The normal transfection medium of neurons was replaced immediately before the experiment (DIV 10-13) with glucose and O_2-free hypoxia medium. Therefore, SGG medium was prepared without glucose while the amounts of ITS and MEM were similar to normal transfection medium. O_2 was removed from the medium by application of vacuum in an excicator for about 15 min. Immediately afterwards the medium was aliquoted for storage into 15 ml falcon tubes leaving no space for oxygen within the tubes.

In the experiments described here this incubator consisted of a former bacterial incubator (Heraeus B6) connected to a gas supply of 5 % CO_2 and 95 % N_2. A humid atmosphere was created by adding tubs of H_2O. To prevent O_2 leakage into the

incubator a low but continous influx of gas was applied during the course of the experiment.

For induction of hypoxia, transfection medium of neurons was replaced with pre-warmed hypoxic medium and cells were immediately transfered to the running hypoxic incubator for 4 h. O_2 levels were measured during the experiment using a digital oxymeter (Greisinger electronic). After the experiment neurons were fixed in PFA.

6.2.1.6. Cell fixation with Paraformaldeyde

The coverslips on which the cells were growing were fixed in fixation solution of 2 % paraformaldehyde and 2 % sucrose in PBS for 10 min at RT. Afterwards the fixed cells were washed with PBS and the aldehyde groups quenched by immersing the coverslip for 10 minutes in 10 mM glycine. Afterwards the coverslips were either directly stained with antibodies or stored in PBS at 4 °C.

6.2.1.7. Rat brain perfusion

Perfusion of rat brains was carried out by Matthias Klugmann (IZN).

Rat brains were perfused using standard procedures (Klugmann et al., 2005). In short, rats were killed by transcardiac perfusion under deep anesthesia (pentobarbital). After perfusion with 0.9 % NaCl, brains were fixed in situ with 10 % buffered neutral formalin, pH 7.4 (Sigma), removed, and postfixed overnight before cryoprotection in 30 % sucrose/PBS. Sagital sections (40 µm) were cut using a cryostat (Jung Frigocut 2800 N, Leica).

6.2.1.8. Immunostaining of free-floating brain sections

Sections were washed four times for 10 min in PBS and blocked for 2 h in PBS with 0,2 % TX-100 and 5 % BSA. After a further washing step in PBS for 10 min the sections were incubated over night with a monoclonal antibody against lamin B (kind gift from laboratory of Herrmann, DKFZ) at 4°C. After washing four times in PBS for 10 min, sections were stained with a secondary alexa 488 α-mouse antibody for 2 h at RT. After washing three times for 10 min in PBS they were mounted onto glass slides with Mowiol mounting medium.

6.2.1.9. Immunostaining

Each 12 mm coverslip was put onto parafilm with cells on the upper side and covered with 70 µl of the primary antibody diluted in antibody dilution buffer for 15 to 60 min at

RT (depending on the primary antibody). The coverslips were washed twice by removing the antibody solution with a vacuum pump and covering the coverslip with PBS for 5 min. Afterwards the coverslips were incubated with the secondary antibody for 15 min at RT and washed three times with PBS. Hoechst DNA dye was added for 5 min during these washing steps. The coverslips were mounted upside down onto glass slides using 6 µl of Mowiol mounting medium and stored at 4°C.

6.2.1.10. Transfection with Lipofectamine

The coverslips were put to 4-well dishes prior to transfection and overlaid with 500 µl transfection medium lacking antibiotics. 1,5 µg plasmid DNA were mixed with 100 µl transfection medium and 5 µl lipofectamine with 100 µl transfection medium. Both solutions were combined and incubated for 30 min at RT. 800 µl transfection medium were then added and 500 µl used for transfection of one coverslip. After 2 ½ to 3 h the medium was changed to fresh transfection medium and cells were used for experiments after 16 to 48 h.

6.2.2. Microscopy

6.2.2.1. Quantifications of immunostained cells

Neurons immunostained with anti-NeuN or anti-laminB and costained with Hoechst were quantified in a DMIRE2 fluorescence microsope (Leica) by counting all cells in 10 fields of view with a 40x or 63x oil objective, according to cell density. All values were then analysed in Excel 2002.

6.2.2.2. Colocalizations

Immunostained fixed cells were scanned with the confocal laser scanning microscope SP2 (Leica) using either a 40x/1,4 oil objective or a a 63x/1,4 oil objective. Images of different fluorophores were scanned separately with the Leica imaging software and projected into an overlay in Photoshop 7.0.

6.2.2.3. Live calcium imaging

Primary neurons on coverslips were loaded with 3,4 µM of the calcium-sensitive fluorescent dye fluo-3 in CO_2-independent SGG for 20 min at RT to prevent incorporation of the dye into organelles. The coverslips were then mounted into a Ludin chamber (Live imaging services) for live imaging and overlaid with 1 ml of CO_2-

independent SGG medium. Excitation of the dye was carried out at 488 nm and emitted light was detected between 500 nm and 600 nm. Time lapse recordings were carried out at a maximal frame rate of 1 image per 1,7 sec at dimensions of 512 x 512 pixels, and the objective used was a 40x oil objective (Leica). The pinhole during recordings was opened to a width of 3 airy, corresponding to a thickness of the slice of 4 µM.
Fluorescence values of neurons or intraneuronal regions were obtained using the LCS Lite Version and calibrated in Excel 2002.

6.2.2.4. Live imaging of the mitochondrial membrane potential

To visualize integrity or breakdown of the mitochondrial membrane potential during a stimulus, the fluorescent dye Rhodamine 123 (Rh123, Molecular Probes) was used. Rh123 incorporates into mitochondria along their membrane potential where its fluorescence is quenched due to differences in pH. When the mitochondrial membrane potential collapses, Rh123 diffuses into the cytosol and can be excited at a wavelength of 488 nm. The emission was detected in a spectrum of 500 to 600 nm.
Neurons on coverslips were loaded with Rh123 at 25 µM in CO2-independent SGG at RT for 20 min and then mounted into a Ludin chamber. Time lapse recordings were carried out maximal frame rate of 1 image per 1,7 sec at dimensions of 512 x 512 pixels with a 40x oil objective (Leica). The pinhole during recordings was opened to a width of 3 airy, corresponding to a thickness of the slice of 5 µM. Fluorescence values of neurons or intraneuronal regions were obtained using the LCS Lite Version and calibrated in Excel 2002.

6.2.2.5. Live imaging of nuclear infoldings

To visualize the formation of nuclear infoldings after a stimulus, the fluorescent membrane dye DiD (Molecular Imaging Products) was loaded into cells at 0,5 µM for 20 min at RT. Alternatively neurons were transfected with lamin B-GFP (kind gift of the laboratory of Jan Ellenberg, EMBL Heidelberg) and analysed after 24 h. Neurons on coverslips were then mounted into a Ludin chamber. XYZT time lapse recordings were carried out in an 40x objective at a zoom factor of approximately 2x. To prevent bleaching of the signal the number of confocal slices in z dimension in case of DiD imaging was limited to 6 and recordings were done at 1 stack per 90 sec. Lamin B-GFP recordings were typically carried out by scanning 30 confocal stacks per time point, at intervals of 5 min. The excitation of DiD was set to a wavelength of 633 nm and detected at an emission of 640-710 nm.

Afterwards the images of each stack were projected into one plane using ImageJ (NIH) and the corresponding projections converted into a time lapse, thereby showing projections of the recorded cells over time.

6.2.2.6. Quantification of cfos levels by immunofluorescence

Fixed coverslips were stained with a primary antibody against cfos (sc-52, Santa Cruz) over night at 4°C and subsequently with an antibody against laminB (X223, Herrmann DKFZ) for 1 h at RT. LaminB was visualized with a secondary alexa-488 goat α-mouse antibody and cfos was detected with a secondary cy3-labelled goat α-rabbit antibody. Confocal stacks were recorded spanning the entire height of all nuclei using a 63x objective. The confocal stacks were then projected (summed) into a single plane with ImageJ (NIH). Infolded and non-infolded nuclei were identified by laminB staining, mean fluoresence values of cfos staining were measured densitometrically in ImageJ and averages compared using Excel (Microsoft).

6.2.2.7. Quantification of Nuclear Pore Complexes by immunofluorescence

Fixed coverslips were stained with a primary antibody against Nuclear Pore Complex Proteins (Mab414, Biozol) for 1 h at RT. Secondary antibodies were either Cy3 goat anti mouse or Alexa488 goat anti mouse. Confocal stacks were recorded spanning the entire height of all nuclei using a 63x objective. The confocal stacks were then projected (summed) into a single plane with ImageJ (NIH). Infolded and non-infolded nuclei were densitometrically analysed using ImageJ and Excel (Microsoft).

6.2.2.8. Transmission Electron Microscopy

EM sample preparation and imaging were done by Andrea Helwig (IZN).

Samples for electron microscopy were prepared following standard procedures (Reynolds, 1963; Rustom et al., 2004). In short, samples were fixed with 2 % glutaraldehyde in 0,1 M sodium cacodylate (pH 7,4), postfixed with 1 % OsO_4/1,5 % $K_4Fe(CN)_6$ in the same buffer and contrasted en bloc with 1 % uranyl acetate in 0,05 M maleate buffer (pH 5,2). Coverslips were contrasted by immersion in the same substances. After dehydration with a graded series of ethanol and the intermedium propylene oxide they were embedded into an epoxy resin. After polymerization at 60°C ultrathin sections were cut with a Reichert Ultracut S ultramicrotome. They were

contrasted with uranyl acetate and lead citrate and examined in a ZEISS EM 10 CR at an acceleration voltage of 80 kV.

6.2.2.9. 3D reconstructions

Three-dimensional reconstructions of confocal images were preformed by Gillian Queisser (IWR) (Broser et al., 2004).

In short, the confocal images of cultured neurons were reconstructed using anisotropic filtering, image segmentation by Otsu and calculation of the surface using a Dijkstra graph search algorithm. Membane surface area and nuclear volume were calculated using a mathematical algorithm called “Marching-Front-operation”.

6.2.3. Biochemistry methods

6.2.3.1. SDS-PAGE

Proteins were usually analyzed on 0.75 mm thick minigel (Laemmli, 1970). The separating gel contained 6-15 % acrylamide (Bio Rad, 30 % acrylamide stock containing 0,8 % bisacrylamide), 390 mM Tris-HCl pH 8.8, 0.1 % SDS and 0.1 % ammonium persulfate. The polymerisation was started by the addition of 1 µl N,N,N’,N’-tetramethylenediamine per ml gel solution. The stacking gel contained 5 % acrylamide, 130 mM Tris-HCl pH 6.8, 0.1 % SDS and 0.1 % ammonium persulfate. The polymerization was started as above. The gels were run in Tris-glycine reservoir buffer at a current of 35 mA per gel.

6.2.3.2. Western blot

The sandwich blot consisted of a membrane and a protein gel packed between several sheets of Whatman paper soaked in reservoir buffer. Wet blots were done using an Wet blot apparatus (IDEA scientific company) in Tris-glycine reservoir buffer lacking SDS but containing 20 % methanol for 100 min at a constant voltage of 20 V. Usually Protran nitrocellulose transfer membranes (Schleicher & Schuell) were used. The membrane was stained after blotting in 0.2 % ponceau S solution (Serva).

6.2.3.3. Immunostaining of Western blots

Specific bands on the blot were visualized by staining with enzyme-conjugated antibodies and detection on scientific imaging films.

The blots were washed in ddH_2O and excess adsorption sites were blocked by incubation in 5 % non-fat milk powder in PBS for 30 min to prevent unspecific binding of antibodies. Afterwards the primary antibody was diluted in adequate concentration into 5 % non-fat milk in PBS and the incubation was carried out for approximately 2 h. In case of anti-phospho antigens both blocking and incubation with the primary antibody were done in 5 % BSA in PBS instead of milk, to prevent loss of signal due to phosphatases in the milk powder.
The blots were then washed two times shortly and three times 5 min in washing buffer PBST 0,1 %. The secondary antibody conjugated to peroxidase was diluted in 5 % non-fat milk in PBS; working dilutions were 1:5000 for anti-mouse and anti-rabbit. After an incubation of 45 to 60 min the blots were washed as above in PBST 0,1 % and incubated for 1 min in a 1:1 mixture of the ECL detection reagents (amersham). The chemiluminescent signal was detected on scientific imaging film (Kodak). Molecular masses were estimated by comparison with the bands of the prestained protein marker.

6.2.3.4. Bead coupling of conantokins

coupling to gold beads

1 ml Gold beads with a diameter of 80 nm (BBI International) were washed by slow centrifugation at 3500 rpm for 1 min in an eppendorf tube and resuspended in buffer A. The beads were then incubated with 30 µl conG-BSA [3,3µg/µl] for 3 h at RT, slowly shaking. Unbound peptides were removed by slow centrifugation at 3500 rpm for 1 min. The loose pellet was resuspended in buffer A, washed once more and finally resuspended in 500 µl CO_2-independent SGG medium containing 1 % BSA.

The same protocol was applied to beads after tituration to pH 9,0 with K_2CO_3.
Other buffers used for washing and resuspension were Borax [2mM], PO_4 buffers at different pH ranging from 5 to 9 and CO_2-independent medium containing 1 % BSA.

buffer A

NaCl	137mM
KCl	2,68mM
Tris/HCl	1M
BSA	0,1%
pH to 8,2	

Gold beads coupled to conG-BSA were separated from unound conG-BSA on a glycerol gradient and protein content analysed using a Bradford assay.

Coupling to amine-latex beads

250 µl amine-latex beads with a mean diameter of 80 nm ((IDC) in an 1,5 ml Eppendorf tube were washed twice in 1 ml MES buffer pH 6,0 (Sigma) and spun at 13000 rpm for 10 min. After resuspension in 500 µl MES buffer (pH 7,3), 3 mg sulfo-SMCC (Pierce) were added and the solution incubated for 1 h at RT slowly mixing. Afterwards the pH was titurated to pH 6,0 with 1 M HCl and and the bead suspension washed twice in 1 ml MES buffer pH 6,0 by centrifugation at 13000 rpm. The pellet was resuspended in 500 µl MES buffer pH 7,3 and conGcys was added to a final concetration of 40 µM. The solution was incubated for 3 h at RT and titurated to pH 6,0 with 1 M HCl. Unbound peptide was removed by washing twice with 1 ml MES buffer pH 6,0 and centrifugation at 13000 rpm. The beads were finally resuspended in 1 ml CO_2-independent SGG medium and 100 µl were sonicated for 15 min in a sonicator water bath at 55°C, using a self-made glass tube. Finally 100 µl were added to a coverslip with neurons in a 4-well dish (Nunclon) for 30 min before NMDA bath application..

ConG-myc

Dialysis was performed against 1 L PBS at 4°C over night using an appropriate dialysis membrane Spectro/ Por, MWCO 50000, 12 mm (Roth).

Coupling to streptavidin-beads

Streptavidin-beads (Dynabeads M-270 Streptavidin, Dynal Biotech) at different amounts were incubated with conG-Biotin at different concentrations, ranging from 30 µl to 120 µl for beads and from 1 µM to 10 µM for the peptide. Typically 30 µl beads were mixed with 100 µl transfection medium in an Eppendorf tube containing a small magnet. 2 µM (1 µl of a 1 mM stock) of conG-Biotin were slowly added while stirring and incubated for 30 min at RT, gently shaking every 5 min. The tube was then filled to 500 µl with transfection medium and entirely added to neurons on a coverslip in a 4-well dish (Nunclon) for 30 min before NMDA bath application.

In certain experiments Biocytin was added to the reaction before addition of conG-Biotin at different concentrations of either 740 µM or 2,7 mM.

6.2.3.5. Glycerol gradients

Gradients for the separation of conG-BSA-beads were prepared using a gradient mixer (Sigma). 100 % Glycerol were filled into a centrifuge tube (Beckman) as cushion. The gradient mixer containing a small magnet in one of its two connected chambers was placed onto a magnetic stirrer and connected to the centrifuge tube by a tubing running through a peristaltic pump (BioRad). The chambers contained glycerol / H_2O mixtures of 10 % and 80 % respectively, with the higher concentrated solution being in the chamber connected to the pump. The pump was set to a speed of 0,5 ml/min and the tubing was slowly pulled upwards during generation of the gradient. After carefully adding conG-BSA-beads the gradient was centrifuged at 4000 rpm for 1 h in a ultracentifuge (Beckman) and fractions taken for analysis of protein content.

6.2.3.6. Protein detection

Protein concentrations during conG-BSA coupling reactions were measured using a quick Bradford assay. Therefore, 780 µl H_2O and 20 µl of the fraction to be analysed were mixed with 200 µl Bradford reagent (BioRad) in a plastic cuvette and the absorption measured after 5 min at 595 nm in a photometer (Pharmacia Biotech).

6.2.4. Electrophysiology

6.2.4.1. Multi Electrode Array (MEA) recordings

MEA recordings were carried out by Frank Hofmann (IZN):

Hippocampal neurons from new-born Long-Evans or Sprague Dawley rats were prepared as described (Bading & Greenberg, 1991) except that growth media was supplemented with B27 (Gibco/BRL). Neurons were plated onto microelectrode array (MEA) dishes containing a grid of 60 planar electrodes (Multi Channel Systems, Reutlingen, Germany) at a density of about 400 cells (neurons and glia) per mm^2. The distance between the electrodes on the MEA dishes was 200 µm and the electrode diameter was 30 µm. Recordings were acquired with an MEA-60 amplifier board (10Hz-35kHz, gain 1200, sampling frequency 20 kHz, Multi Channel Systems, Reutlingen, Germany). Stimulations and recordings were done after a culturing period of 10 to 14 days. Before stimulation, network activity was recorded for three minutes; cultures with spontaneous bursting activity were excluded. Recurrent synchronous

network bursting was induced by treatment of the neurons with 50 µM bicuculline dissolved in DMSO. The final concentration of DMSO did not exceed 0.05 % which caused no independent effects for the incubation periods used (maximum 15 min.). After another three minutes of recording, bicuculline was washed away by changing the medium three times. Cultures were put back into the incubator and three minutes recordings were repeatedly performed at different time points from 1 h up to 48 h following the washout of bicuculline. Native conG and the various conjugates were pre-incubated for 1 hour. These compounds were also co-applied during bicuculline treatment and washout. Spikes were detected with the integrated spike detector of the MC Rack software (Multi Channel Systems, Reutlingen, Germany). Burst analysis was done with Neuroexplorer (NEX Technologies). All results are given as mean ± SEM. Statistical tests were done by comparing data sets from treated cultures to controls for each time point separately by an independent samples t-test.

6.2.4.2. Puff and eEPSC analysis

The following protocol was applied in a collaboration by C. Peter Bengtson (IZN):

Whole-cell patch clamp recordings were made from 10-14 DIV cultured hippocampal neurons plated on coverslips placed in a recording chamber (PM-1, Warner Instruments, Hamden, CT, USA) mounted on a fixed-stage upright microscope (BX51WI, Olympus, Hamburg, Germany). Differential interference contrast optics, infrared illumination and a CCD camera (Photometrics Coolsnap HQ, Visitron Systems, Puchheim, Germany) were used to view neurons on a computer monitor using a software interface (Metamorph, Universal Imaging Systems, Downington PA, USA). Patch electrodes (3-4 MΩ) were made from borosilicate glass (1.5 mm, WPI, Sarasota, FL, USA) and filled with a cesium methane sulphonate based solution (containing in mM: $CsMeSO_3$ 135, CsCl 20, spermine 0.6, EGTA 0.6, HEPES 10, Na_2-phosphocreatine 10, QX-314 3 (Alomone), Mg_2-ATP 2, Na_3-GTP 0.3; pH 7.35 with CsOH). The extracellular solution was a salt-glucose-glycine solution containing (in mM) NaCl 140, KCl 5.3, $MgCl_2$ 1, $CaCl_2$ 2, HEPES 10, glycine 0.01, glucose 30, Na-pyruvate 0.5. Recordings were made with a Multiclamp 700A amplifier, digitized through a Digidata 1322A A/D converter, acquired and analysed using pClamp 9 software (Axon Instruments, Union City, CA, USA). NMDA receptor mediated currents were recorded either at a holding potential of +40 mV in the presence of 1 mM extracellular Mg^{2+} (all recordings of conG-Biotin) or

at a holding potential of –60 mV in extracellular solutions with no added Mg^{2+}, termed Mg^{2+}-free solutions (all recordings of native conG and conG-BSA). Evoked excitatory post-synaptic currents (eEPSCs) were recorded in response to single 100 µs long constant current pulse stimuli (80 to 200 µA) from an A365 stimulus isolator using a bipolar tungsten stereotrode (WPI, Sarasota, FL, USA). These stimulators were epoxy and silicone coated except for the tips which were separated by around 100 µm and positioned in contact with the tissue matrix on the surface of the coverslip on either side of the recorded cell. All recordings were performed in the presence of picrotoxin (100 µM, Tocris), -(-)bicuculline (50 µM, Sigma), 6-cyano-7-nitroquinoxaline-2, 3-dione (CNQX, 20 µM, Tocris), strychnine (1 µM, Sigma). Whole cell responses (ie. mediated by synaptic and extrasynaptic NMDA receptors) to exogenous NMDA were evoked using local pressure application (5 psi for 3 s) of NMDA (100 µM, Tocris) using a picospritzer (PV800, WPI) from an electrode (1-2 µM tip diameter) positioned around 50 µM from the cell. After establishing the baseline eEPSC and NMDA puff response amplitudes, conG coupled to beads was bath applied through the perfusion system in ascending concentrations (typically 0.1 µM, 1 µM, 10 µM) allowing 5 to 10 min incubation time (without perfusion) at each concentration before remeasuring eEPSCs and NMDA puff responses. NMDA puff responses were always measured under perfusion as this was found to strongly affect their amplitude and kinetics. EEPSCs were recorded with or without perfusion which did not affect them. At the completion of each experiment, any residual NR2B mediated current was identified by applying 10µM Conantokin-G-biotin and re-recording responses. Any residual eEPSC was confirmed as NMDA receptor mediated by their total blockade by +(-)MK-801 (10 µM, Tocris). Access (range: 10 – 28 MΩ) and membrane resistance (range: 150 – 650 MΩ) were monitored regularly during voltage clamp recordings and data was rejected if changes greater than 20% occurred. Data is expressed as mean ± standard error of the mean. Statistical comparisons were made using independent t tests, the results of which are expressed as t (degrees of freedom) = *t value*, p = *p value*.

6.2.4.3. Analysis of spontaneous activity for correlation with infolded nuclei

The following protocol was applied in a collaboration by Simon Wiegert (IZN):
To test neuronal activity in respect of nuclear infoldings electrophysiological recordings were performed as described above with the following exceptions: Patch electrodes (~6 MΩ) were made from borosilicate glass (1.5 mm, WPI, Sarasota, FL, USA) and filled

with a potassium gluconate based solution (containing in mM: K-gluconate 155, $MgCl_2$ 2, HEPES 10, K_2-phosphocreatine 5, Mg^{2+}-ATP 2, Na3-GTP 0.3; pH 7.35 with KOH) which contained neurobiotin (VECTOR) at a concentration of 0,3%. Neurons were patched at the apical dendrite in order to avoid disturbance of the nuclear envelope by the recording pipette. Cell-attached recordings were done to assess activity of the cells. EPSCs were recorded in voltage-clamp mode at potential of -70 mV. Spikes were recorded in current-clamp mode. Recordings were discarded when the resting membrane potential was less than -50 mV.

Cells were split into three groups in respect to their electrical activity, which were (1) non-spiking cells, (2) randomly spiking cells and (3) rhythmic bursting cells.

After recording, the whole coverslip was immediately fixed with a para-formaldehyde/sucrose (2%/2%) solution.

Cells were incubated with a monoclonal anti-lamin B antibody (laboratory of Herrmann, DKFZ) 1:5 for 1 h at RT in antibody dilution buffer. After washing twice in PBS for 5 min neurons were stained for 1 h at RT using a Cy3 goat anti-mouse antibody (1:300) and Streptavidin-FITC (Sigma). Subsequently coverslips were washed 3 times in PBS for 5 min. Hoechst DNA dye was added for 5 min during these washing steps. The coverslips were mounted upside down onto glass slides using 6 µl of Mowiol mounting medium and stored at 4°C.

7. Bibliography

Adachi M, Fukuda M, Nishida E (2000) Nuclear export of MAP kinase (ERK) involves a MAP kinase kinase (MEK)-dependent active transport mechanism. J Cell Biol 148:849-856.

Alessandrini A, Namura S, Moskowitz MA, Bonventre JV (1999) MEK1 protein kinase inhibition protects against damage resulting from focal cerebral ischemia. Proc Natl Acad Sci U S A 96:12866-12869.

Aoki C, Venkatesan C, Go CG, Mong JA, Dawson TM (1994) Cellular and subcellular localization of NMDA-R1 subunit immunoreactivity in the visual cortex of adult and neonatal rats. J Neurosci 14:5202-5222.

Arnold F, Hofmann F, Bengtson P, Wittmann M, Vanhoutte P, Bading H (2004) Microelectrode array recordings of cultured hippocampal networks reveal a simple model for transcription and protein synthesis-dependent plasticity. J Physiol.

Bading H (2000) Transcription-dependent neuronal plasticity the nuclear calcium hypothesis. Eur J Biochem 267:5280-5283.

Bading H, Greenberg ME (1991) Stimulation of protein tyrosine phosphorylation by NMDA receptor activation. Science 253:912-914.

Bading H, Ginty DD, Greenberg ME (1993) Regulation of gene expression in hippocampal neurons by distinct calcium signaling pathways. Science 260:181-186.

Barco A, Alarcon JM, Kandel ER (2002) Expression of constitutively active CREB protein facilitates the late phase of long-term potentiation by enhancing synaptic capture. Cell 108:689-703.

Barone FC, Irving EA, Ray AM, Lee JC, Kassis S, Kumar S, Badger AM, Legos JJ, Erhardt JA, Ohlstein EH, Hunter AJ, Harrison DC, Philpott K, Smith BR, Adams JL, Parsons AA (2001) Inhibition of p38 mitogen-activated protein kinase provides neuroprotection in cerebral focal ischemia. Med Res Rev 21:129-145.

Bear MF, Malenka RC (1994) Synaptic plasticity: LTP and LTD. Curr Opin Neurobiol 4:389-399.

Benavente R, Krohne G, Franke WW (1985) Cell type-specific expression of nuclear lamina proteins during development of Xenopus laevis. Cell 41:177-190.

Benveniste H, Drejer J, Schousboe A, Diemer NH (1984) Elevation of the extracellular concentrations of glutamate and aspartate in rat hippocampus during transient

cerebral ischemia monitored by intracerebral microdialysis. J Neurochem 43:1369-1374.

Besshoh S, Bawa D, Teves L, Wallace MC, Gurd JW (2005) Increased phosphorylation and redistribution of NMDA receptors between synaptic lipid rafts and post-synaptic densities following transient global ischemia in the rat brain. J Neurochem 93:186-194.

Bito H, Deisseroth K, Tsien RW (1996) CREB phosphorylation and dephosphorylation: a Ca(2+)- and stimulus duration-dependent switch for hippocampal gene expression. Cell 87:1203-1214.

Bonni A, Brunet A, West AE, Datta SR, Takasu MA, Greenberg ME (1999) Cell survival promoted by the Ras-MAPK signaling pathway by transcription-dependent and -independent mechanisms. Science 286:1358-1362.

Bossy-Wetzel E, Talantova MV, Lee WD, Scholzke MN, Harrop A, Mathews E, Gotz T, Han J, Ellisman MH, Perkins GA, Lipton SA (2004) Crosstalk between nitric oxide and zinc pathways to neuronal cell death involving mitochondrial dysfunction and p38-activated K+ channels. Neuron 41:351-365.

Bourgeois CA, Hemon D, Bouteille M (1979) Structural relationship between the nucleolus and the nuclear envelope. J Ultrastruct Res 68:328-340.

Bramlett HM, Dietrich WD (2004) Pathophysiology of cerebral ischemia and brain trauma: similarities and differences. J Cereb Blood Flow Metab 24:133-150.

Brenman JE, Christopherson KS, Craven SE, McGee AW, Bredt DS (1996) Cloning and characterization of postsynaptic density 93, a nitric oxide synthase interacting protein. J Neurosci 16:7407-7415.

Brenneman DE, Forsythe ID, Nicol T, Nelson PG (1990) N-methyl-D-aspartate receptors influence neuronal survival in developing spinal cord cultures. Brain Res Dev Brain Res 51:63-68.

Brickley SG, Misra C, Mok MH, Mishina M, Cull-Candy SG (2003) NR2B and NR2D subunits coassemble in cerebellar Golgi cells to form a distinct NMDA receptor subtype restricted to extrasynaptic sites. J Neurosci 23:4958-4966.

Broser PJ, Schulte R, Lang S, Roth A, Helmchen F, Waters J, Sakmann B, Wittum G (2004) Nonlinear anisotropic diffusion filtering of three-dimensional image data from two-photon microscopy. J Biomed Opt 9:1253-1264.

Cammarota M, Bevilaqua LR, Ardenghi P, Paratcha G, Levi de Stein M, Izquierdo I, Medina JH (2000) Learning-associated activation of nuclear MAPK, CREB and Elk-1, along with Fos production, in the rat hippocampus after a one-trial avoidance learning: abolition by NMDA receptor blockade. Brain Res Mol Brain Res 76:36-46.

Canettieri G, Morantte I, Guzman E, Asahara H, Herzig S, Anderson SD, Yates JR, 3rd, Montminy M (2003) Attenuation of a phosphorylation-dependent activator by an HDAC-PP1 complex. Nat Struct Biol 10:175-181.

Cao J, Semenova MM, Solovyan VT, Han J, Coffey ET, Courtney MJ (2004) Distinct requirements for p38alpha and c-Jun N-terminal kinase stress-activated protein kinases in different forms of apoptotic neuronal death. J Biol Chem 279:35903-35913.

Carmignoto G, Vicini S (1992) Activity-dependent decrease in NMDA receptor responses during development of the visual cortex. Science 258:1007-1011.

Castellino FJ, Prorok M (2000) Conantokins: inhibitors of ion flow through the N-methyl-D-aspartate receptor channels. Curr Drug Targets 1:219-235.

Chan-Palay V, Palay SL, Billings-Gagliardi SM (1974) Meynert cells in the primate visual cortex. J Neurocytol 3:631-658.

Charton JP, Herkert M, Becker CM, Schroder H (1999) Cellular and subcellular localization of the 2B-subunit of the NMDA receptor in the adult rat telencephalon. Brain Res 816:609-617.

Chawla S, Hardingham GE, Quinn DR, Bading H (1998) CBP: a signal-regulated transcriptional coactivator controlled by nuclear calcium and CaM kinase IV. Science 281:1505-1509.

Chazot PL (2004) The NMDA receptor NR2B subunit: a valid therapeutic target for multiple CNS pathologies. Curr Med Chem 11:389-396.

Chen Y, Swanson RA (2003) Astrocytes and brain injury. J Cereb Blood Flow Metab 23:137-149.

Cheng A, Chan SL, Milhavet O, Wang S, Mattson MP (2001) p38 MAP kinase mediates nitric oxide-induced apoptosis of neural progenitor cells. J Biol Chem 276:43320-43327.

Cho YH, Giese KP, Tanila H, Silva AJ, Eichenbaum H (1998) Abnormal hippocampal spatial representations in alphaCaMKIIT286A and CREBalphaDelta- mice. Science 279:867-869.

Chu CT, Levinthal DJ, Kulich SM, Chalovich EM, DeFranco DB (2004) Oxidative neuronal injury. The dark side of ERK1/2. Eur J Biochem 271:2060-2066.

Ciani E, Rizzi S, Paulsen RE, Contestabile A (1997) Chronic pre-explant blockade of the NMDA receptor affects survival of cerebellar granule cells explanted in vitro. Brain Res Dev Brain Res 99:112-117.

Clark BA, Farrant M, Cull-Candy SG (1997) A direct comparison of the single-channel properties of synaptic and extrasynaptic NMDA receptors. J Neurosci 17:107-116.

Cole AJ, Saffen DW, Baraban JM, Worley PF (1989) Rapid increase of an immediate early gene messenger RNA in hippocampal neurons by synaptic NMDA receptor activation. Nature 340:474-476.

Cordes VC, Rackwitz HR, Reidenbach S (1997) Mediators of nuclear protein import target karyophilic proteins to pore complexes of cytoplasmic annulate lamellae. Exp Cell Res 237:419-433.

Cull-Candy S, Brickley S, Farrant M (2001) NMDA receptor subunits: diversity, development and disease. Curr Opin Neurobiol 11:327-335.

Cull-Candy SG, Brickley SG, Misra C, Feldmeyer D, Momiyama A, Farrant M (1998) NMDA receptor diversity in the cerebellum: identification of subunits contributing to functional receptors. Neuropharmacology 37:1369-1380.

Daigle N, Beaudouin J, Hartnell L, Imreh G, Hallberg E, Lippincott-Schwartz J, Ellenberg J (2001) Nuclear pore complexes form immobile networks and have a very low turnover in live mammalian cells. J Cell Biol 154:71-84.

Danial NN, Gramm CF, Scorrano L, Zhang CY, Krauss S, Ranger AM, Datta SR, Greenberg ME, Licklider LJ, Lowell BB, Gygi SP, Korsmeyer SJ (2003) BAD and glucokinase reside in a mitochondrial complex that integrates glycolysis and apoptosis. Nature 424:952-956.

Davis M, Perry RH, Mendelow AD (1997) The effect of non-competitive N-methyl-D-aspartate receptor antagonism on cerebral oedema and cerebral infarct size in the aging ischaemic brain. Acta Neurochir Suppl 70:30-33.

Dawson VL, Dawson TM, London ED, Bredt DS, Snyder SH (1991) Nitric oxide mediates glutamate neurotoxicity in primary cortical cultures. Proc Natl Acad Sci U S A 88:6368-6371.

de Noronha CM, Sherman MP, Lin HW, Cavrois MV, Moir RD, Goldman RD, Greene WC (2001) Dynamic disruptions in nuclear envelope architecture and integrity induced by HIV-1 Vpr. Science 294:1105-1108.

Deng X, Xiao L, Lang W, Gao F, Ruvolo P, May WS, Jr. (2001) Novel role for JNK as a stress-activated Bcl2 kinase. J Biol Chem 276:23681-23688.

Dickinson HG, Bell PR (1972) Structures resembling nuclear pores at the orifice of nuclear invaginations in developing microspores of Pinus banksiana. Dev Biol 27:425-429.

Dingledine R, Borges K, Bowie D, Traynelis SF (1999) The glutamate receptor ion channels. Pharmacol Rev 51:7-61.

Dirnagl U, Iadecola C, Moskowitz MA (1999) Pathobiology of ischaemic stroke: an integrated view. Trends Neurosci 22:391-397.

Donevan SD, McCabe RT (2000) Conantokin G is an NR2B-selective competitive antagonist of N-methyl-D-aspartate receptors. Mol Pharmacol 58:614-623.

Dougherty CJ, Kubasiak LA, Prentice H, Andreka P, Bishopric NH, Webster KA (2002) Activation of c-Jun N-terminal kinase promotes survival of cardiac myocytes after oxidative stress. Biochem J 362:561-571.

Echevarria W, Leite MF, Guerra MT, Zipfel WR, Nathanson MH (2003) Regulation of calcium signals in the nucleus by a nucleoplasmic reticulum. Nat Cell Biol 5:440-446.

Eimerl S, Schramm M (1994) The quantity of calcium that appears to induce neuronal death. J Neurochem 62:1223-1226.

Farlow MR (2004) NMDA receptor antagonists. A new therapeutic approach for Alzheimer's disease. Geriatrics 59:22-27.

Fawcett DW (1966) On the occurrence of a fibrous lamina on the inner aspect of the nuclear envelope in certain cells of vertebrates. Am J Anat 119:129-145.

Fink CC, Meyer T (2002) Molecular mechanisms of CaMKII activation in neuronal plasticity. Curr Opin Neurobiol 12:293-299.

Finkbeiner S (2000) CREB couples neurotrophin signals to survival messages. Neuron 25:11-14.

Finkbeiner S, Greenberg ME (1996) Ca(2+)-dependent routes to Ras: mechanisms for neuronal survival, differentiation, and plasticity? Neuron 16:233-236.

Flint AC, Maisch US, Weishaupt JH, Kriegstein AR, Monyer H (1997) NR2A subunit expression shortens NMDA receptor synaptic currents in developing neocortex. J Neurosci 17:2469-2476.

Fricker M, Hollinshead M, White N, Vaux D (1997) Interphase nuclei of many mammalian cell types contain deep, dynamic, tubular membrane-bound invaginations of the nuclear envelope. J Cell Biol 136:531-544.

Fujikawa DG, Shinmei SS, Cai B (2000) Kainic acid-induced seizures produce necrotic, not apoptotic, neurons with internucleosomal DNA cleavage: implications for programmed cell death mechanisms. Neuroscience 98:41-53.

Furthauer M, Lin W, Ang SL, Thisse B, Thisse C (2002) Sef is a feedback-induced antagonist of Ras/MAPK-mediated FGF signalling. Nat Cell Biol 4:170-174.

Ghosh A, Carnahan J, Greenberg ME (1994) Requirement for BDNF in activity-dependent survival of cortical neurons. Science 263:1618-1623.

Ginty DD, Kornhauser JM, Thompson MA, Bading H, Mayo KE, Takahashi JS, Greenberg ME (1993) Regulation of CREB phosphorylation in the suprachiasmatic nucleus by light and a circadian clock. Science 260:238-241.

Goldman RD, Gruenbaum Y, Moir RD, Shumaker DK, Spann TP (2002) Nuclear lamins: building blocks of nuclear architecture. Genes Dev 16:533-547.

Goldman RD, Shumaker DK, Erdos MR, Eriksson M, Goldman AE, Gordon LB, Gruenbaum Y, Khuon S, Mendez M, Varga R, Collins FS (2004) Accumulation of mutant lamin A causes progressive changes in nuclear architecture in Hutchinson-Gilford progeria syndrome. Proc Natl Acad Sci U S A 101:8963-8968.

Hardingham GE, Bading H (2002) Coupling of extrasynaptic NMDA receptors to a CREB shut-off pathway is developmentally regulated. Biochim Biophys Acta 1600:148-153.

Hardingham GE, Bading H (2003) The Yin and Yang of NMDA receptor signalling. Trends Neurosci 26:81-89.

Hardingham GE, Arnold FJ, Bading H (2001a) Nuclear calcium signaling controls CREB-mediated gene expression triggered by synaptic activity. Nat Neurosci 4:261-267.

Hardingham GE, Arnold FJ, Bading H (2001b) A calcium microdomain near NMDA receptors: on switch for ERK-dependent synapse-to-nucleus communication. Nat Neurosci 4:565-566.

Hardingham GE, Fukunaga Y, Bading H (2002) Extrasynaptic NMDARs oppose synaptic NMDARs by triggering CREB shut-off and cell death pathways. Nat Neurosci 5:405-414.

Hardingham GE, Chawla S, Johnson CM, Bading H (1997) Distinct functions of nuclear and cytoplasmic calcium in the control of gene expression. Nature 385:260-265.

Hardingham GE, Chawla S, Cruzalegui FH, Bading H (1999) Control of recruitment and transcription-activating function of CBP determines gene regulation by NMDA receptors and L-type calcium channels. Neuron 22:789-798.

Hartley DM, Kurth MC, Bjerkness L, Weiss JH, Choi DW (1993) Glutamate receptor-induced 45Ca2+ accumulation in cortical cell culture correlates with subsequent neuronal degeneration. J Neurosci 13:1993-2000.

Hatton CJ, Paoletti P (2005) Modulation of triheteromeric NMDA receptors by N-terminal domain ligands. Neuron 46:261-274.

Hetman M, Gozdz A (2004) Role of extracellular signal regulated kinases 1 and 2 in neuronal survival. Eur J Biochem 271:2050-2055.

Hochstrasser M, Sedat JW (1987) Three-dimensional organization of Drosophila melanogaster interphase nuclei. II. Chromosome spatial organization and gene regulation. J Cell Biol 104:1471-1483.

Hou ST, Xie X, Baggley A, Park DS, Chen G, Walker T (2002) Activation of the Rb/E2F1 pathway by the non-proliferative p38 MAP kinase during Fas (APO1/CD95)-mediated neuronal apoptosis. J Biol Chem.

Hou ST, Cowan E, Dostanic S, Rasquinha I, Comas T, Morley P, MacManus JP (2001) Increased expression of the transcription factor E2F1 during dopamine-evoked, caspase-3-mediated apoptosis in rat cortical neurons. Neurosci Lett 306:153-156.

Hou ST, Callaghan D, Fournier MC, Hill I, Kang L, Massie B, Morley P, Murray C, Rasquinha I, Slack R, MacManus JP (2000) The transcription factor E2F1 modulates apoptosis of neurons. J Neurochem 75:91-100.

Hozak P, Sasseville AM, Raymond Y, Cook PR (1995) Lamin proteins form an internal nucleoskeleton as well as a peripheral lamina in human cells. J Cell Sci 108 (Pt 2):635-644.

Husi H, Ward MA, Choudhary JS, Blackstock WP, Grant SG (2000) Proteomic analysis of NMDA receptor-adhesion protein signaling complexes. Nat Neurosci 3:661-669.

Ikonomidou C, Turski L (2002) Why did NMDA receptor antagonists fail clinical trials for stroke and traumatic brain injury? Lancet Neurol 1:383-386.

Ikonomidou C, Stefovska V, Turski L (2000) Neuronal death enhanced by N-methyl-D-aspartate antagonists. Proc Natl Acad Sci U S A 97:12885-12890.

Ikonomidou C, Bosch F, Miksa M, Bittigau P, Vockler J, Dikranian K, Tenkova TI, Stefovska V, Turski L, Olney JW (1999) Blockade of NMDA receptors and apoptotic neurodegeneration in the developing brain. Science 283:70-74.

Impey S, Goodman RH (2001) CREB signaling--timing is everything. Sci STKE 2001:PE1.

Impey S, Fong AL, Wang Y, Cardinaux JR, Fass DM, Obrietan K, Wayman GA, Storm DR, Soderling TR, Goodman RH (2002) Phosphorylation of CBP mediates transcriptional activation by neural activity and CaM kinase IV. Neuron 34:235-244.

Jiang Q, Gu Z, Zhang G, Jing G (2000) N-methyl-D-aspartate receptor activation results in regulation of extracellular signal-regulated kinases by protein kinases and phosphatases in glutamate-induced neuronal apototic-like death. Brain Res 887:285-292.

Jin K, Mao XO, Zhu Y, Greenberg DA (2002) MEK and ERK protect hypoxic cortical neurons via phosphorylation of Bad. J Neurochem 80:119-125.

Kaul M, Garden GA, Lipton SA (2001) Pathways to neuronal injury and apoptosis in HIV-associated dementia. Nature 410:988-994.

Kawasaki H, Morooka T, Shimohama S, Kimura J, Hirano T, Gotoh Y, Nishida E (1997) Activation and involvement of p38 mitogen-activated protein kinase in glutamate-induced apoptosis in rat cerebellar granule cells. J Biol Chem 272:18518-18521.

Keelan J, Vergun O, Duchen MR (1999) Excitotoxic mitochondrial depolarisation requires both calcium and nitric oxide in rat hippocampal neurons. J Physiol 520 Pt 3:797-813.

Klein RC, Galdzicki Z, Castellino FJ (1999) Inhibition of NMDA-induced currents by conantokin-G and conantokin-T in cultured embryonic murine hippocampal neurons. Neuropharmacology 38:1819-1829.

Klein RC, Prorok M, Galdzicki Z, Castellino FJ (2001) The amino acid residue at sequence position 5 in the conantokin peptides partially governs subunit-selective antagonism of recombinant N-methyl-D-aspartate receptors. J Biol Chem 276:26860-26867.

Klugmann M, Wymond Symes C, Leichtlein CB, Klaussner BK, Dunning J, Fong D, Young D, During MJ (2005) AAV-mediated hippocampal expression of short and long Homer 1 proteins differentially affect cognition and seizure activity in adult rats. Mol Cell Neurosci 28:347-360.

Kohr G, Jensen V, Koester HJ, Mihaljevic AL, Utvik JK, Kvello A, Ottersen OP, Seeburg PH, Sprengel R, Hvalby O (2003) Intracellular domains of NMDA receptor subtypes are determinants for long-term potentiation induction. J Neurosci 23:10791-10799.

Kovalenko D, Yang X, Nadeau RJ, Harkins LK, Friesel R (2003) Sef inhibits fibroblast growth factor signaling by inhibiting FGFR1 tyrosine phosphorylation and subsequent ERK activation. J Biol Chem 278:14087-14091.

Krupp JJ, Vissel B, Heinemann SF, Westbrook GL (1996) Calcium-dependent inactivation of recombinant N-methyl-D-aspartate receptors is NR2 subunit specific. Mol Pharmacol 50:1680-1688.

Kundrotiene J, Cebers G, Wagner A, Liljequist S (2004) The NMDA NR2B subunit-selective receptor antagonist, CP-101,606, enhances the functional recovery the NMDA NR2B subunit-selective receptor and reduces brain damage after cortical compression-induced brain ischemia. J Neurotrauma 21:83-93.

Laemmli UK (1970) Cleavage of structural proteins during the assembly of the head of bacteriophage T4. Nature 227:680-685.

Lagace TA, Ridgway ND (2005) The rate-limiting enzyme in phosphatidylcholine synthesis regulates proliferation of the nucleoplasmic reticulum. Mol Biol Cell 16:1120-1130.

Lagace TA, Miller JR, Ridgway ND (2002) Caspase processing and nuclear export of CTP:phosphocholine cytidylyltransferase alpha during farnesol-induced apoptosis. Mol Cell Biol 22:4851-4862.

Lancelot E, Revaud ML, Boulu RG, Plotkine M, Callebert J (1998) A microdialysis study investigating the mechanisms of hydroxyl radical formation in rat striatum exposed to glutamate. Brain Res 809:294-296.

Lazebnik YA, Takahashi A, Moir RD, Goldman RD, Poirier GG, Kaufmann SH, Earnshaw WC (1995) Studies of the lamin proteinase reveal multiple parallel biochemical pathways during apoptotic execution. Proc Natl Acad Sci U S A 92:9042-9046.

Lees GJ (2000) Pharmacology of AMPA/kainate receptor ligands and their therapeutic potential in neurological and psychiatric disorders. Drugs 59:33-78.

Li F, Omori N, Jin G, Wang SJ, Sato K, Nagano I, Shoji M, Abe K (2003) Cooperative expression of survival p-ERK and p-Akt signals in rat brain neurons after transient MCAO. Brain Res 962:21-26.

Li FL, Dickinson HG (1987) The structure and function of nuclear invaginations characteristic of microsporogenesis in Pinus banksiana. Annals of Botany 60:321-330.

Li JH, Wang YH, Wolfe BB, Krueger KE, Corsi L, Stocca G, Vicini S (1998) Developmental changes in localization of NMDA receptor subunits in primary cultures of cortical neurons. Eur J Neurosci 10:1704-1715.

Liao D, Zhang X, O'Brien R, Ehlers MD, Huganir RL (1999) Regulation of morphological postsynaptic silent synapses in developing hippocampal neurons. Nat Neurosci 2:37-43.

Lipton P (1999a) Ischemic cell death in brain neurons. Physiol Rev 79:1431-1568.

Lipton SA (1999b) Neuronal protection and destruction by NO. Cell Death Differ 6:943-951.

Lipton SA, Rosenberg PA (1994) Excitatory amino acids as a final common pathway for neurologic disorders. N Engl J Med 330:613-622.

Liu J, Rolef Ben-Shahar T, Riemer D, Treinin M, Spann P, Weber K, Fire A, Gruenbaum Y (2000) Essential roles for Caenorhabditis elegans lamin gene in nuclear organization, cell cycle progression, and spatial organization of nuclear pore complexes. Mol Biol Cell 11:3937-3947.

Lonze BE, Riccio A, Cohen S, Ginty DD (2002) Apoptosis, axonal growth defects, and degeneration of peripheral neurons in mice lacking CREB. Neuron 34:371-385.

Lopez de Armentia M, Sah P (2003) Development and subunit composition of synaptic NMDA receptors in the amygdala: NR2B synapses in the adult central amygdala. J Neurosci 23:6876-6883.

Low SJ, Roland CL (2004) Review of NMDA antagonist-induced neurotoxicity and implications for clinical development. Int J Clin Pharmacol Ther 42:1-14.

Lu YM, Yin HZ, Chiang J, Weiss JH (1996) Ca(2+)-permeable AMPA/kainate and NMDA channels: high rate of Ca2+ influx underlies potent induction of injury. J Neurosci 16:5457-5465.

Luderus ME, de Graaf A, Mattia E, den Blaauwen JL, Grande MA, de Jong L, van Driel R (1992) Binding of matrix attachment regions to lamin B1. Cell 70:949-959.

Luetjens CM, Bui NT, Sengpiel B, Munstermann G, Poppe M, Krohn AJ, Bauerbach E, Krieglstein J, Prehn JH (2000) Delayed mitochondrial dysfunction in excitotoxic neuron death: cytochrome c release and a secondary increase in superoxide production. J Neurosci 20:5715-5723.

Malenka RC, Nicoll RA (1999) Long-term potentiation--a decade of progress? Science 285:1870-1874.

Mandl M, Slack DN, Keyse SM (2005) Specific inactivation and nuclear anchoring of extracellular signal-regulated kinase 2 by the inducible dual-specificity protein phosphatase DUSP5. Mol Cell Biol 25:1830-1845.

Mantamadiotis T, Lemberger T, Bleckmann SC, Kern H, Kretz O, Martin Villalba A, Tronche F, Kellendonk C, Gau D, Kapfhammer J, Otto C, Schmid W, Schutz G (2002) Disruption of CREB function in brain leads to neurodegeneration. Nat Genet 31:47-54.

Migaud M, Charlesworth P, Dempster M, Webster LC, Watabe AM, Makhinson M, He Y, Ramsay MF, Morris RG, Morrison JH, O'Dell TJ, Grant SG (1998) Enhanced

long-term potentiation and impaired learning in mice with mutant postsynaptic density-95 protein. Nature 396:433-439.

Minematsu K, Fisher M, Li L, Sotak CH (1993a) Diffusion and perfusion magnetic resonance imaging studies to evaluate a noncompetitive N-methyl-D-aspartate antagonist and reperfusion in experimental stroke in rats. Stroke 24:2074-2081.

Minematsu K, Fisher M, Li L, Davis MA, Knapp AG, Cotter RE, McBurney RN, Sotak CH (1993b) Effects of a novel NMDA antagonist on experimental stroke rapidly and quantitatively assessed by diffusion-weighted MRI. Neurology 43:397-403.

Moir RD, Spann TP, Goldman RD (1995) The dynamic properties and possible functions of nuclear lamins. Int Rev Cytol 162B:141-182.

Moir RD, Yoon M, Khuon S, Goldman RD (2000a) Nuclear lamins A and B1: different pathways of assembly during nuclear envelope formation in living cells. J Cell Biol 151:1155-1168.

Moir RD, Spann TP, Herrmann H, Goldman RD (2000b) Disruption of nuclear lamin organization blocks the elongation phase of DNA replication. J Cell Biol 149:1179-1192.

Momiyama A, Feldmeyer D, Cull-Candy SG (1996) Identification of a native low-conductance NMDA channel with reduced sensitivity to Mg2+ in rat central neurones. J Physiol 494 (Pt 2):479-492.

Monyer H, Burnashev N, Laurie DJ, Sakmann B, Seeburg PH (1994) Developmental and regional expression in the rat brain and functional properties of four NMDA receptors. Neuron 12:529-540.

Mori T, Wang X, Jung JC, Sumii T, Singhal AB, Fini ME, Dixon CE, Alessandrini A, Lo EH (2002) Mitogen-activated protein kinase inhibition in traumatic brain injury: in vitro and in vivo effects. J Cereb Blood Flow Metab 22:444-452.

Morris RG (1989) Synaptic plasticity and learning: selective impairment of learning rats and blockade of long-term potentiation in vivo by the N-methyl-D-aspartate receptor antagonist AP5. J Neurosci 9:3040-3057.

Nath R, McGinnis K, Dutta S, Shivers B, Wang KK (2001) Inhibition of p38 kinase mimics survival signal-linked protection against apoptosis in rat cerebellar granule neurons. Cell Mol Biol Lett 6:173-184.

Nicholls DG, Budd SL (2000) Mitochondria and neuronal survival. Physiol Rev 80:315-360.

Nili E, Cojocaru GS, Kalma Y, Ginsberg D, Copeland NG, Gilbert DJ, Jenkins NA, Berger R, Shaklai S, Amariglio N, Brok-Simoni F, Simon AJ, Rechavi G (2001) Nuclear membrane protein LAP2beta mediates transcriptional repression alone

and together with its binding partner GCL (germ-cell-less). J Cell Sci 114:3297-3307.

O'Hare MJ, Hou ST, Morris EJ, Cregan SP, Xu Q, Slack RS, Park DS (2000) Induction and modulation of cerebellar granule neuron death by E2F-1. J Biol Chem 275:25358-25364.

Opitz T, De Lima AD, Voigt T (2002) Spontaneous development of synchronous oscillatory activity during maturation of cortical networks in vitro. J Neurophysiol 88:2196-2206.

Park PC, De Boni U (1992) Nuclear membrane modifications in polytene nuclei of Drosophila melanogaster: serial reconstruction and cytochemistry. Anat Rec 234:15-26.

Paulsen O, Sejnowski TJ (2000) Natural patterns of activity and long-term synaptic plasticity. Curr Opin Neurobiol 10:172-179.

Pawson T, Scott JD (1997) Signaling through scaffold, anchoring, and adaptor proteins. Science 278:2075-2080.

Peng TI, Greenamyre JT (1998) Privileged access to mitochondria of calcium influx through N-methyl-D-aspartate receptors. Mol Pharmacol 53:974-980.

Pickard L, Noel J, Henley JM, Collingridge GL, Molnar E (2000) Developmental changes in synaptic AMPA and NMDA receptor distribution and AMPA receptor subunit composition in living hippocampal neurons. J Neurosci 20:7922-7931.

Pivovarova NB, Nguyen HV, Winters CA, Brantner CA, Smith CL, Andrews SB (2004) Excitotoxic calcium overload in a subpopulation of mitochondria triggers delayed death in hippocampal neurons. J Neurosci 24:5611-5622.

Pokorska A, Vanhoutte P, Arnold FJ, Silvagno F, Hardingham GE, Bading H (2003) Synaptic activity induces signalling to CREB without increasing global levels of cAMP in hippocampal neurons. J Neurochem 84:447-452.

Preger E, Ziv I, Shabtay A, Sher I, Tsang M, Dawid IB, Altuvia Y, Ron D (2004) Alternative splicing generates an isoform of the human Sef gene with altered subcellular localization and specificity. Proc Natl Acad Sci U S A 101:1229-1234.

Rao A, Craig AM (1997) Activity regulates the synaptic localization of the NMDA receptor in hippocampal neurons. Neuron 19:801-812.

Rao A, Kim E, Sheng M, Craig AM (1998) Heterogeneity in the molecular composition of excitatory postsynaptic sites during development of hippocampal neurons in culture. J Neurosci 18:1217-1229.

Rao L, Perez D, White E (1996) Lamin proteolysis facilitates nuclear events during apoptosis. J Cell Biol 135:1441-1455.

Reyes M, Reyes A, Opitz T, Kapin MA, Stanton PK (1998) Eliprodil, a non-competitive, NR2B-selective NMDA antagonist, protects pyramidal neurons in hippocampal slices from hypoxic/ischemic damage. Brain Res 782:212-218.

Reynolds ES (1963) The use of lead citrate at high pH as an electron-opaque stain in electron microscopy. J Cell Biol 17:208-212.

Rivier J, Galyean R, Simon L, Cruz LJ, Olivera BM, Gray WR (1987) Total synthesis and further characterization of the gamma-carboxyglutamate-containing "sleeper" peptide from Conus geographus venom. Biochemistry 26:8508-8512.

Rosenmund C, Feltz A, Westbrook GL (1995) Calcium-dependent inactivation of synaptic NMDA receptors in hippocampal neurons. J Neurophysiol 73:427-430.

Rossi DJ, Oshima T, Attwell D (2000) Glutamate release in severe brain ischaemia is mainly by reversed uptake. Nature 403:316-321.

Rustom A, Saffrich R, Markovic I, Walther P, Gerdes HH (2004) Nanotubular highways for intercellular organelle transport. Science 303:1007-1010.

Sattler R, Charlton MP, Hafner M, Tymianski M (1998) Distinct influx pathways, not calcium load, determine neuronal vulnerability to calcium neurotoxicity. J Neurochem 71:2349-2364.

Sattler R, Xiong Z, Lu WY, Hafner M, MacDonald JF, Tymianski M (1999) Specific coupling of NMDA receptor activation to nitric oxide neurotoxicity by PSD-95 protein. Science 284:1845-1848.

Scaffidi P, Misteli T (2006) Lamin A-dependent nuclear defects in human aging. Science 312:1059-1063.

Schubert P, Morino T, Miyazaki H, Ogata T, Nakamura Y, Marchini C, Ferroni S (2000) Cascading glia reactions: a common pathomechanism and its differentiated control by cyclic nucleotide signaling. Ann N Y Acad Sci 903:24-33.

Schulz S, Siemer H, Krug M, Hollt V (1999) Direct evidence for biphasic cAMP responsive element-binding protein phosphorylation during long-term potentiation in the rat dentate gyrus in vivo. J Neurosci 19:5683-5692.

Sheng M, Pak DT (2000) Ligand-gated ion channel interactions with cytoskeletal and signaling proteins. Annu Rev Physiol 62:755-778.

Sheng M, Kim MJ (2002) Postsynaptic signaling and plasticity mechanisms. Science 298:776-780.

Simon RP, Swan JH, Griffiths T, Meldrum BS (1984) Blockade of N-methyl-D-aspartate receptors may protect against ischemic damage in the brain. Science 226:850-852.

Smith ER, Smedberg JL, Rula ME, Xu XX (2004) Regulation of Ras-MAPK pathway mitogenic activity by restricting nuclear entry of activated MAPK in endoderm differentiation of embryonic carcinoma and stem cells. J Cell Biol 164:689-699.

Smythe C, Jenkins HE, Hutchison CJ (2000) Incorporation of the nuclear pore basket protein nup153 into nuclear pore structures is dependent upon lamina assembly: evidence from cell-free extracts of Xenopus eggs. Embo J 19:3918-3931.

Snider BJ, Tee LY, Canzoniero LM, Babcock DJ, Choi DW (2002) NMDA antagonists exacerbate neuronal death caused by proteasome inhibition in cultured cortical and striatal neurons. Eur J Neurosci 15:419-428.

Spann TP, Goldman AE, Wang C, Huang S, Goldman RD (2002) Alteration of nuclear lamin organization inhibits RNA polymerase II-dependent transcription. J Cell Biol 156:603-608.

Stevens JK, Trogadis J (1986) Reconstructive three-dimensional electron microscopy. A routine biologic tool. Anal Quant Cytol Histol 8:102-107.

Stick R, Hausen P (1985) Changes in the nuclear lamina composition during early development of Xenopus laevis. Cell 41:191-200.

Stocca G, Vicini S (1998) Increased contribution of NR2A subunit to synaptic NMDA receptors in developing rat cortical neurons. J Physiol 507 (Pt 1):13-24.

Stoffel M, Plesnila N, Eriskat J, Furst M, Baethmann A (2002) Release of excitatory amino acids in the penumbra of a focal cortical necrosis. J Neurotrauma 19:467-477.

Stout AK, Raphael HM, Kanterewicz BI, Klann E, Reynolds IJ (1998) Glutamate-induced neuron death requires mitochondrial calcium uptake. Nat Neurosci 1:366-373.

Sugino T, Nozaki K, Takagi Y, Hattori I, Hashimoto N, Moriguchi T, Nishida E (2000) Activation of mitogen-activated protein kinases after transient forebrain ischemia in gerbil hippocampus. J Neurosci 20:4506-4514.

Sullivan T, Escalante-Alcalde D, Bhatt H, Anver M, Bhat N, Nagashima K, Stewart CL, Burke B (1999) Loss of A-type lamin expression compromises nuclear envelope integrity leading to muscular dystrophy. J Cell Biol 147:913-920.

Takahashi A, Alnemri ES, Lazebnik YA, Fernandes-Alnemri T, Litwack G, Moir RD, Goldman RD, Poirier GG, Kaufmann SH, Earnshaw WC (1996) Cleavage of lamin A by Mch2 alpha but not CPP32: multiple interleukin 1 beta-converting

enzyme-related proteases with distinct substrate recognition properties are active in apoptosis. Proc Natl Acad Sci U S A 93:8395-8400.

Takuma K, Baba A, Matsuda T (2004) Astrocyte apoptosis: implications for neuroprotection. Prog Neurobiol 72:111-127.

Tanaka K, Nagata E, Suzuki S, Dembo T, Nogawa S, Fukuuchi Y (1999) Immunohistochemical analysis of cyclic AMP response element binding protein phosphorylation in focal cerebral ischemia in rats. Brain Res 818:520-526.

Tanaka K, Watase K, Manabe T, Yamada K, Watanabe M, Takahashi K, Iwama H, Nishikawa T, Ichihara N, Kikuchi T, Okuyama S, Kawashima N, Hori S, Takimoto M, Wada K (1997) Epilepsy and exacerbation of brain injury in mice lacking the glutamate transporter GLT-1. Science 276:1699-1702.

Taniura H, Glass C, Gerace L (1995) A chromatin binding site in the tail domain of nuclear lamins that interacts with core histones. J Cell Biol 131:33-44.

Torii S, Kusakabe M, Yamamoto T, Maekawa M, Nishida E (2004) Sef is a spatial regulator for Ras/MAP kinase signaling. Dev Cell 7:33-44.

Tovar KR, Westbrook GL (1999) The incorporation of NMDA receptors with a distinct subunit composition at nascent hippocampal synapses in vitro. J Neurosci 19:4180-4188.

Tovar KR, Westbrook GL (2002) Mobile NMDA receptors at hippocampal synapses. Neuron 34:255-264.

Tymianski M, Charlton MP, Carlen PL, Tator CH (1993) Source specificity of early calcium neurotoxicity in cultured embryonic spinal neurons. J Neurosci 13:2085-2104.

Vance JE, Pan D, Campenot RB, Bussiere M, Vance DE (1994) Evidence that the major membrane lipids, except cholesterol, are made in axons of cultured rat sympathetic neurons. J Neurochem 62:329-337.

Vergun O, Sobolevsky AI, Yelshansky MV, Keelan J, Khodorov BI, Duchen MR (2001) Exploration of the role of reactive oxygen species in glutamate neurotoxicity in rat hippocampal neurones in culture. J Physiol 531:147-163.

Vicini S, Wang JF, Li JH, Zhu WJ, Wang YH, Luo JH, Wolfe BB, Grayson DR (1998) Functional and pharmacological differences between recombinant N-methyl-D-aspartate receptors. J Neurophysiol 79:555-566.

Vigouroux C, Auclair M, Dubosclard E, Pouchelet M, Capeau J, Courvalin JC, Buendia B (2001) Nuclear envelope disorganization in fibroblasts from lipodystrophic patients with heterozygous R482Q/W mutations in the lamin A/C gene. J Cell Sci 114:4459-4468.

Walton MR, Dragunow I (2000) Is CREB a key to neuronal survival? Trends Neurosci 23:48-53.

Wang HG, Pathan N, Ethell IM, Krajewski S, Yamaguchi Y, Shibasaki F, McKeon F, Bobo T, Franke TF, Reed JC (1999a) Ca2+-induced apoptosis through calcineurin dephosphorylation of BAD. Science 284:339-343.

Wang S, Nath N, Minden A, Chellappan S (1999b) Regulation of Rb and E2F by signal transduction cascades: divergent effects of JNK1 and p38 kinases. Embo J 18:1559-1570.

Wang Y, MacDonald JI, Kent C (1993) Regulation of CTP:phosphocholine cytidylyltransferase in HeLa cells. Effect of oleate on phosphorylation and intracellular localization. J Biol Chem 268:5512-5518.

Watkins JD, Kent C (1992) Immunolocalization of membrane-associated CTP:phosphocholine cytidylyltransferase in phosphatidylcholine-deficient Chinese hamster ovary cells. J Biol Chem 267:5686-5692.

Westphal RS, Tavalin SJ, Lin JW, Alto NM, Fraser ID, Langeberg LK, Sheng M, Scott JD (1999) Regulation of NMDA receptors by an associated phosphatase-kinase signaling complex. Science 285:93-96.

Williams AJ, Ling G, Berti R, Moffett JR, Yao C, Lu XM, Dave JR, Tortella FC (2003) Treatment with the snail peptide CGX-1007 reduces DNA damage and alters gene expression of c-fos and bcl-2 following focal ischemic brain injury in rats. Exp Brain Res 153:16-26.

Wilson KL, Zastrow MS, Lee KK (2001) Lamins and disease: insights into nuclear infrastructure. Cell 104:647-650.

Wisden W, Errington ML, Williams S, Dunnett SB, Waters C, Hitchcock D, Evan G, Bliss TV, Hunt SP (1990) Differential expression of immediate early genes in the hippocampus and spinal cord. Neuron 4:603-614.

Wittmann M, Bengtson CP, Bading H (2004) Extrasynaptic NMDA receptors: mediators of excitotoxic cell death. In: Pharmacology of Cerebral Ischemia (Krieglstein J, Klumpp S, eds), pp 253-266. Stuttgart: medpharm Scientific.

Wu GY, Deisseroth K, Tsien RW (2001) Activity-dependent CREB phosphorylation: convergence of a fast, sensitive calmodulin kinase pathway and a slow, less sensitive mitogen-activated protein kinase pathway. Proc Natl Acad Sci U S A 98:2808-2813.

Wyllie DJ, Behe P, Colquhoun D (1998) Single-channel activations and concentration jumps: comparison of recombinant NR1a/NR2A and NR1a/NR2D NMDA receptors. J Physiol 510 (Pt 1):1-18.

Xia Z, Dickens M, Raingeaud J, Davis RJ, Greenberg ME (1995) Opposing effects of ERK and JNK-p38 MAP kinases on apoptosis. Science 270:1326-1331.

Xiong S, Zhao Q, Rong Z, Huang G, Huang Y, Chen P, Zhang S, Liu L, Chang Z (2003) hSef inhibits PC-12 cell differentiation by interfering with Ras-mitogen-activated protein kinase MAPK signaling. J Biol Chem 278:50273-50282.

Yang J, Liu X, Bhalla K, Kim CN, Ibrado AM, Cai J, Peng TI, Jones DP, Wang X (1997a) Prevention of apoptosis by Bcl-2: release of cytochrome c from mitochondria blocked. Science 275:1129-1132.

Yang L, Guan T, Gerace L (1997b) Lamin-binding fragment of LAP2 inhibits increase in nuclear volume during the cell cycle and progression into S phase. J Cell Biol 139:1077-1087.

Yano S, Tokumitsu H, Soderling TR (1998) Calcium promotes cell survival through CaM-K kinase activation of the protein-kinase-B pathway. Nature 396:584-587.

Yasuda R, Noji H, Yoshida M, Kinosita K, Jr., Itoh H (2001) Resolution of distinct rotational substeps by submillisecond kinetic analysis of F1-ATPase. Nature 410:898-904.

Yoon WJ, Won SJ, Ryu BR, Gwag BJ (2003) Blockade of ionotropic glutamate receptors produces neuronal apoptosis through the Bax-cytochrome C-caspase pathway: the causative role of Ca2+ deficiency. J Neurochem 85:525-533.

Zeron MM, Chen N, Moshaver A, Lee AT, Wellington CL, Hayden MR, Raymond LA (2001) Mutant huntingtin enhances excitotoxic cell death. Mol Cell Neurosci 17:41-53.

Zhao K, Harel A, Stuurman N, Guedalia D, Gruenbaum Y (1996) Binding of matrix attachment regions to nuclear lamin is mediated by the rod domain and depends on the lamin polymerization state. FEBS Lett 380:161-164.

Zhong J, Carrozza DP, Williams K, Pritchett DB, Molinoff PB (1995) Expression of mRNAs encoding subunits of the NMDA receptor in developing rat brain. J Neurochem 64:531-539.